

MECHANISMS AND MODELING OF ACOUSTIC AIR FILTERING SYSTEM

by

JONG-HYO CHOI

B.A., Chung-Ang University, 2009

M.A., Texas A&M, 2014

A thesis submitted to the  
Faculty of the Graduate School of the  
University of Colorado in partial fulfillment  
of the requirement for the degree of  
Doctor of Philosophy  
Department of Architectural Engineering  
2024

Committee Members:

John Zhai

Moncef Krarti

Wangda Zuo

Jaeyoon Koh

Liangzhu (Leon) Wang

## ABSTRACT

Choi, Jong-Hyo (Ph.D., Architectural Engineering)

Mechanisms and Modeling of Acoustic Air Filtering System

Dissertation directed by Professor John Z. Zhai

This research explores the possibility of an alternative air filtering method through the study of acoustic agglomeration. Acoustic agglomeration is a phenomenon occurring when particles resonate in the presence of sound waves. The mechanisms of acoustic agglomeration are composed of orthokinetic interaction, primary refilling mechanisms, and secondary refilling mechanisms. Orthokinetic interaction, where direct collisions occur between particles due to differences in resonant amplitude and phase angle, is the most essential mechanism. Refilling mechanisms involve shifting particles into the agglomeration volume through repeated vibrations caused by sound waves.

This research developed an OpenFOAM particle agglomeration model, pimAAFoam, by focusing on the key concept of agglomeration volume which is decided by the orthokinetic interaction. The final model consists of acoustic collision, general collision, and wall collision models. Particle collision outcomes are determined by the concept of critical velocity, resulting in either agglomeration or rebound. Model validations were conducted using vertical experimental setups from literature and horizontal laboratory tests from this research. The pimAAFoam model was proven to be valid for both the vertical and horizontal scenarios. The simulation results are within the measurement range from the mixed-air injection in a horizontal duct case. The difference between the measured values and the simulation values for each of the particle sizes was within 25% of the measured values.

With the validated pimAAFoam, sensitivity analysis was performed on variables related to acoustic agglomeration mechanisms. The base-case of the sensitivity test was a 4-liter space with a concentration of 25 parcels per one  $\text{cm}^3$  over a 30-second duration. The simulation time cost for the base-case was approximately 4 days using a 6-core, 3.7 GHz CPU.

Through the sensitivity analysis, it was observed that high sound intensity and initial particle concentration led to an increase in acoustic agglomeration. Unlike bag-filter methods, acoustic agglomeration is valuable in a condition of high initial particle concentration. Additionally, slower air velocity resulted in a higher rate of acoustic agglomeration. Furthermore, the utilization of low-frequency sound waves led to a higher rate of acoustic agglomeration unless altering the frequency significantly affected the entrainment factor difference between particles. Particle removal using acoustic agglomeration mechanisms is focused on small particles with the larger particles acting as collector particles.

The study concludes that the OpenFOAM acoustic agglomeration model, pimAAFoam, offers practical simulation time costs with reliability. Improving accuracy of the model, including primary and secondary refilling mechanisms could be suitable for future study.

## TABLE OF CONTENTS

	Page
Chapter I Introduction .....	1
1.1 Brief Overview .....	1
1.2 Problem Statement and Hypothesis.....	5
1.2.1 Performance Comparison between Fibrous Filter and Acoustic Agglomeration Filtering .....	6
1.3 Research Purposes.....	7
1.4 Tasks of This Study.....	8
1.5 Contributions of Research.....	9
Chapter II Literature Review.....	12
2.1 Fundamentals of Acoustic Agglomeration of Particles.....	12
2.1.1 Process of Acoustic Agglomeration.....	12
2.1.2 Orthokinetic Interaction .....	13
2.1.3 Agglomeration Kernel.....	24
2.1.4 Decide Agglomeration After Collision .....	26
2.2 Fundamentals of Acoustic Agglomeration Modeling.....	28
2.2.1 Methods for Implementing Sound Impact to Particle Movements .....	30
2.2.2 Analysis of Collision.....	30
2.3 Progress in Acoustic Agglomeration Research.....	34
2.3.1 Original Research.....	34
2.3.2 Recent Advances in Acoustic Agglomeration Research.....	42

2.4 Conclusion.....	44
Chapter III Methodology.....	46
3.1 Acoustic Agglomeration CFD Models.....	46
3.1.1 Current OpenFOAM CFD Software .....	47
3.1.2 New Combination of DPMFoam and pimpleFoam .....	48
3.1.3 Composition of the New OpenFOAM - pimAAFoam Model Sets.....	49
3.1.4 Acoustic Collision Model.....	50
3.1.5 General Collision Model .....	55
3.1.6 Wall Collision Model.....	57
3.2 Model Validations .....	58
3.2.1 Mixed-Air Injection in a Vertical Straight Cylinder from Literature.....	59
3.2.2 Mixed-Air Injection in a Horizontal Straight Duct in Laboratory .....	62
3.3 Design of Sensitivity Analysis .....	71
Chapter IV Model Validation Using Reference research.....	73
4.1 Simulation .....	73
4.1.2 Geometry and Grid Study for the CFD Simulation.....	73
4.1.3 Air-Flow and Particle Results Stabilization .....	76
4.2 Model Calibrations Process and Results Comparison.....	79
4.2.1 Simulation Time Intervals and Particle Properties.....	79
4.2.2 Calibration Process and Results Comparison.....	80
4.3 Summary .....	93
Chapter V Model Validation Using Experimental Results .....	95

5.1 Simulation .....	95
5.1.1 Dimensions of Geometry for Simulation .....	95
5.1.2 Geometry .....	96
5.1.3 Mesh .....	97
5.2 Results Comparison.....	100
5.2.1 Results Stabilization.....	100
5.2.2 Impact of Collisional Models .....	103
5.2.3 Comparison of the Simulation Results and Measured Data.....	106
5.3 Summary .....	107
Chapter VI Sensitivity Analysis .....	108
6.1 Information of Sensitivity Analysis .....	108
6.1.1 Geometry .....	108
6.1.2 Grid Study .....	109
6.1.3 Base-Case of the Sensitivity Analysis.....	110
6.1.4 Properties of the Particles.....	112
6.2 Simulation Results.....	113
6.2.1 Results Stabilization.....	113
6.2.2 Results of the Sensitivity Analysis.....	116
6.3 Summary .....	124
Chapter VII Conclusion .....	126
7.1 Summary .....	126
7.2 Discussion .....	129

Nomenclature .....	130
References .....	132

## LIST OF FIGURES

	Page
Figure 1 Principle of HEPA Filter.....	2
Figure 2 Principle of Electrostatic Precipitation .....	3
Figure 3 Principle of Dielectrophoresis .....	4
Figure 4 Principle of Acoustic Agglomeration .....	4
Figure 5 Process of Acoustic Agglomeration (Ref: Shaw, 1978).....	12
Figure 6 Relative Resonance Amplitude Difference to a Larger Particle.....	15
Figure 7 Agglomeration Volumes.....	17
Figure 8 Direction of Force by Flow Line Distortion around a Large Particle (Ref: Mednikov, 1965) .....	19
Figure 9 Hydrodynamic interaction between a pair of particles in a sound field .....	19
Figure 10 Resonance Phase Difference between Particles in an Acoustic Field (Ref: Westervelt, 1950) .....	21
Figure 11 Asymmetry in the Vibration of the Medium in Standing Wave Condition.....	22
Figure 12 Orthokinetic Agglomeration Volume & Extended Agglomeration Volume by Acoustic Wake .....	25
Figure 13 Collision between Identical Particles & Results.....	27
Figure 14 Relationship between Small Particle Diameter and Critical Velocity .....	28
Figure 15 Strategies of Acoustic Agglomeration Process to a Numerical Simulation ....	29
Figure 16 Structure of Spring-Dashpot Collision Model .....	33
Figure 17 Composition of Spring Dashpot Model Forces .....	34

Figure 18 Relative Importance of Acoustic Agglomeration Mechanisms (Ref: Chou, 1981).....	37
Figure 19 Schematic Illustration of Mandralis’s Experiment .....	38
Figure 20 Gravity Issue from DPMFoam .....	49
Figure 21 Structure of the Acoustic Agglomeration Model.....	51
Figure 22 Agglomeration Volume Created by Sound Source and a Pair of Particles .....	52
Figure 23 Distance $w$ in the Sound Wave Direction.....	53
Figure 24 Structure of the General Collision Model.....	56
Figure 25 Structure of the Wall Collision Model.....	57
Figure 26 Particle to Wall Rebound.....	58
Figure 27 Design of Experimental Device in the Reference Research (Ref: Zhang, 2017) .....	60
Figure 28 Whole Experimental Device Configuration in the Laboratory.....	63
Figure 29 Fan Section .....	66
Figure 30 Pre & Post Treatment Measurement Section.....	67
Figure 31 Measurement Devices: Particle Counter and Anemometer .....	68
Figure 32 Geometry and Selected Mesh for Mixed-Air Injection in a Vertical Straight Cylinder from Literature .....	73
Figure 33 Comparison of Velocity Profile from the Three Mesh Settings .....	75
Figure 34 Air Flow Pattern of the Model at 20 Second [m/sec] .....	76
Figure 35 Required Time for Stabilizing Air Flow Results at 10 cm from the Bottom...	77
Figure 36 Dispersion of Particles over Time [m/sec, meter] .....	78

Figure 37 Required Time for Stabilizing Particle Results within 10 cm from the Bottom .....	79
Figure 38 Results Comparison between Stacked Calibration Procedures and Experiments .....	82
Figure 39 Calculated Effective Diameter Difference between Models .....	87
Figure 40 Connection between Four Sections of a Wave and the Time Interval.....	89
Figure 41 Geometry for the Simulation with Dimensions .....	95
Figure 42 Geometry for Mixed-Air Injection in a Horizontal Straight Duct in Laboratory .....	97
Figure 43 Comparison of Air Velocity Profile at Post-Treatment Measurement Section	98
Figure 44 Selected Mesh for Mixed-Air Injection in a Horizontal Straight Duct in Laboratory .....	99
Figure 45 Comparison of Air Velocity from Simulation Results and Measured Data at Post-Treatment Section .....	100
Figure 46 Required Time for Stabilizing Air Flow Results at Post-Treatment Measurement Section .....	101
Figure 47 Dispersion of Particles Over Time.....	103
Figure 48 Required Time for Stabilizing Particle Results Within 10 cm of the Bottom	103
Figure 49 Comparison of Particle Concentration Among Collision Models .....	104
Figure 50 Comparison of the Simulation Results and Measured Data .....	106
Figure 51 Geometry for the Sensitivity Analysis .....	108
Figure 52 Velocity Profile at 5 cm before the Outlet .....	110

Figure 53 Selected Mesh Model.....	110
Figure 54 Entrainment Factors of the Particles Depending on Sound Frequency .....	111
Figure 55 Air Velocity Profile over Time .....	114
Figure 56 Particle Distribution in the Duct over Time.....	115
Figure 57 Total Particle Concentration over Time.....	116
Figure 58 Particle Concentration of the Three Cases of Sound Intensity .....	117
Figure 59 Percentage Reduction of the Three Cases of Sound Intensity .....	118
Figure 60 Particle Concentration of the Five Cases of Air Velocity .....	119
Figure 61 Particle Percentage Reduction of Five Cases with Varying Air Velocity .....	120
Figure 62 Particle Concentration of the Three Cases of Particle Concentration Variations .....	121
Figure 63 Particle Percentage Reduction of the Three Cases of Particle Concentration	122
Figure 64 Particle Concentration of the Six Cases of Sound Frequency .....	122
Figure 65 Particle Percentage Reduction of the Six Cases of Sound Frequency .....	123

## LIST OF TABLES

	Page
Table 1 Comparison of Conventional Air Filtering Methods and Acoustic Agglomeration Method .....	6
Table 2 Particle Properties for Critical Velocity .....	28
Table 3 List of Research Related to Main Theory of the AA Mechanisms .....	40
Table 4 List of Research Related to Application of the AA Mechanisms .....	41
Table 5 List of Research Related to Characteristics of the AA Mechanisms .....	41
Table 6 Particle Injection through the Inlet Surface .....	61
Table 7 Comparison between ASHRAE 52.2 and Experimental Settings.....	64
Table 8 5 Air Flow Profile at Pre-Treatment Measurement.....	69
Table 9 Particle Concentration in Pre-Treatment Measurement [# / Liter] .....	70
Table 10 Test Matrix for the AA Sensitivity Analysis.....	71
Table 11 Meshes for Grid Study .....	74
Table 12 Particle Characteristics.....	80
Table 13 Results Comparison between Stacked Calibration Procedures and Experiments [# / cm <sup>3</sup> ] .....	83
Table 14 Particle Inlet and Extracted Value at the Lower Part of the Experimental Device [# / cm <sup>3</sup> ] .....	84
Table 15 Original Conditions of Simulation .....	85
Table 16 Percentage Difference of Simulation Results Compare to the Measured Data with Sound - A .....	86

Table 17 Percentage Difference of Simulation Results Compare to the Measured Data with Sound - B.....	90
Table 18 Particle Properties for Model Validation Using Experimental Data.....	96
Table 19 Mesh Preparation for Mixed-Air Injection in a Horizontal Straight Duct in Laboratory .....	97
Table 20 Percentage of Particle Concentration at Post-Treatment Measurement Section Compared to Inlet Value .....	105
Table 21 Meshes for Sensitivity Analysis.....	109
Table 22 Particle Properties for Sensitivity Analysis.....	113

# CHAPTER I

## INTRODUCTION

### 1.1 Brief Overview

Air pollution from the burning of fossil fuels is expected in factory areas and densely populated areas. In the process of burning fossil fuels, quite a lot of fine polluting particles are generated in addition to toxic gases. People living in areas with severe air pollution suffer from various respiratory diseases caused by toxic gases and pollutant aerosols. According to Englert (2004), particles larger than 30  $\mu\text{m}$  cannot be suspended in the air for long and are easily deposited on the ground by gravity. On the other hand, there is a possibility that particles smaller than this can be inhaled and affect the human body. In particular, it was revealed that particles of 2.5  $\mu\text{m}$  to 10  $\mu\text{m}$  can affect the respiratory and cardiovascular system of humans. Dockery (1993) also shows that a higher fine particle concentration brings about a higher mortality rate. He compared six US cities regarding the relationship between PM 2.5 (2.5  $\mu\text{m}$ ) concentration and mortality rate. He decided on two cities located in rural areas as standards for comparison, and the cities had about 10  $\mu\text{g}/\text{m}^3$  of PM 2.5 concentration. Other cities had an average of 30  $\mu\text{g}/\text{m}^3$  of PM 2.5 concentration, and had a 1.3 times higher mortality rate than the standard cities. According to Peng (2008), for every 10  $\mu\text{g}/\text{m}^3$  increase in the concentration of PM10-2.5 particles, there was a 0.36% increase in the number of patients admitted for cardiovascular diseases. In addition, the risk of pollutant particles increases as the particle size decreases. According to Schraufnagel (2020), ultrafine particles ( $\text{PM}_{0.1}$ ) have the potential to cause more inflammation in the respiratory system and are more difficult to remove.

To reduce the danger from fine contaminant aerosols, researchers have suggested several strategies to remove pollutant particles from the air. The representative fine particle removal technologies include the following: 1) High Efficiency Particulate Air (HEPA) Filtering, 2) Electrostatic Precipitating, and 3) Dielectrophoresis Technology.

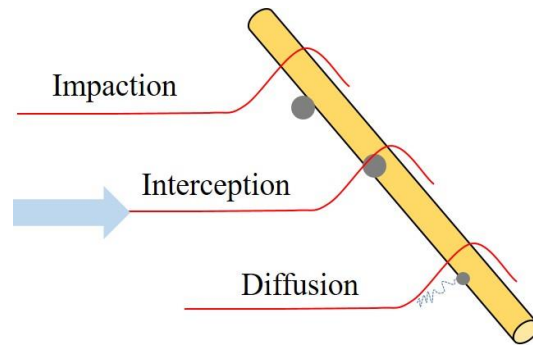


Figure 1 Principle of HEPA Filter

HEPA filtering is the most common strategy to remove fine particles from the air. The filter captures aerosols with three mechanisms (Hosseini and Sahebi, 2023): 1) Impaction, 2) Interception, and 3) Diffusion.

When air passes through a filter, there are streamlines around a filter fiber. High inertia of large particles separates these particles from the main air stream, and they directly collide with and are captured by a filter fiber. The interception mechanisms occur when mid-sized particles move along the air stream. The main air stream carries aerosols, and some portion of aerosols located within one radius of a filter fiber will collide and will be attached to the fiber. Diffusion is caused by the tendency of very small particles to move in random motion. As some fine particles pass through the filter, this random movement causes them to collide with the filter fibers and be removed from the main air flow.

The biggest advantage of HEPA filtering is particle removing ability. By definition, a HEPA filter can remove 99.97% of particles over  $0.3\ \mu\text{m}$ . However, HEPA filtering requires large fan energy consumption compared to conventional air filters. Moreover, filtered fine dust blocks filters, which reduces filter efficiency and increases fan energy consumption drastically. Also, HEPA filtering has limited usability. It cannot be applied to high temperature conditions or very humid conditions.

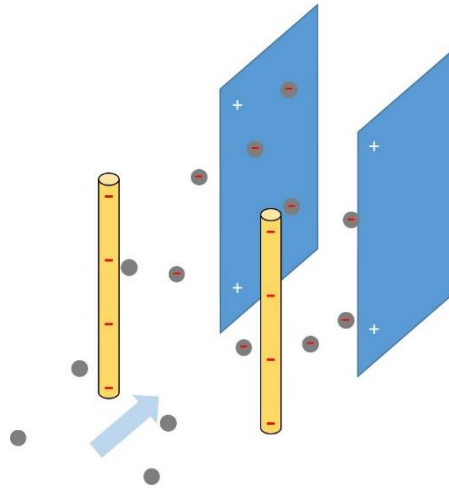


Figure 2 Principle of Electrostatic Precipitation

Electrostatic precipitation (ESP) removes dust particles by using corona dischargers and electrostatic fields. A corona discharge refers to a phenomenon in which fluid molecules around highly charged electrodes become ionized, and an electrically neutral substance becomes positive or negative. Dust particles are passed through two electrodes. First, aerosols meet highly negatively charged electrodes, and the particles become electrically charged by a corona discharger. Then the charged particles are attached to a surface of the positively charged electrodes. This technology can effectively remove dust particles. Moreover, it does not require a significant amount of fan energy. However, this technology has the potential to produce ozone and nitrogen compound gas, which is harmful for humans and the environment (Mizuno, 2000). Furthermore, the electrostatic field must be cleaned regularly.

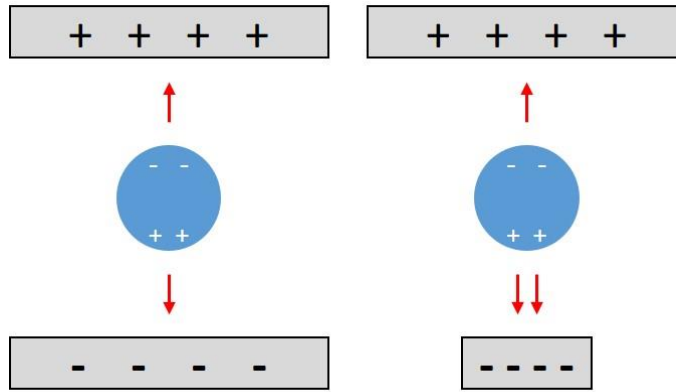


Figure 3 Principle of Dielectrophoresis

Dielectrophoresis also uses electric fields. In contrast to the ESP focusing on modulating target particles, dielectrophoresis mechanisms focus on adjusting electric fields. This technology makes use of dielectric polarization and attracts the dielectric polarized particle using a non-uniform electric field. The disadvantage of this technology is the limited area of non-uniform electric fields, which have sufficient electric magnitude difference (Pethig & Markx, 1997).

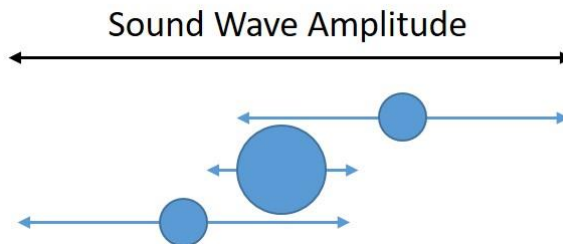


Figure 4 Principle of Acoustic Agglomeration

Acoustic Agglomeration (AA) has the potential to be an alternative particle removal strategy to the three current major particle removal strategies. AA uses particle resonance with acoustic waves and drives particles to collision and agglomeration with each other. AA does not

have the disadvantages of the three fine particle removal strategies mentioned above. First, it can be applied in high-temperature, humid conditions. Moreover, hazardous by-products are not produced during the operation. However, there is a disadvantage in that high energy is required to increase the removal rate of fine particles through AA. Once the efficiency of the AA method is improved, AA can be an alternative fine particle removal strategy when other strategies are not applicable.

## 1.2 Problem Statement and Hypothesis

The first method when considering fine particle removal is using HEPA filters with bigger fans. In general, to remove small particles for HVAC, applying filters that have a high Minimum Efficiency Reporting Value (MERV) is preferred. Montgomery (2012) mentions that for newly installed general filters, required fan pressure was about 400 Pa, and the annual cost for fan operation was about \$134. Thomas (2001) clarified that 1600 Pa and 2000 Pa of pressure was required to flow through a HEPA filter with 3 cm/s and 30 cm/s, respectively. This means using HEPA filters entails four times or five times more fan energy consumption than using general filters. In addition, fine pollutant particles are attached to HEPA filter media during the removal procedure and stay in the filters therefore increasing required fan pressure. Over time, fine particles accumulate in filters, increasing the required fan pressure and reducing the amount of air passing through the filters, which consequently need to be replaced. It is obvious that short filter life is expected in severely contaminated environments.

In 1979 Ariman et al. showed that the higher the initial particle mass concentration in the air, the more the AA mechanism is effective. In contrast to the other filtering methods, the effectiveness of AA is improved in heavily contaminated air conditions. In this case, AA substitutes for the HEPA filtering strategy.

However, the relatively low particle removal rates of the AA strategy are still a challenge. Yuen (2014) researched the possibility of acoustic agglomeration to remove fine particles in the

duct. When air flow velocity was 15 cm/s, fine particle removal rates for 0.3  $\mu\text{m}$  diameter particles from his AA system were about 12%. Removal rates for 6  $\mu\text{m}$  particles was 32%. Compared to particle removal rates of HEPA filtering, the AA method has relatively low removal rates.

The following table summarizes the advantages and disadvantages of each air filtering strategy.

	Fibrous Filter	ESPs	Dielectrophoresis	Acoustic Agglomeration
Pros	High Removal Rate	High Removal Rate Low Pressure Drop	Low Pressure Drop	No Pressure Drop
Cons	High Fan Energy Consumption	Harmful Byproduct (Ozone)	Limited Particle Removal Area	Energy Consumption in Sound Source Low Removal Rate
Special Features	Low Rated Fibrous Filters: Low Fan Energy Consumption but Low Removal Rate  High Rated Fibrous Filters: High Fan Energy Consumption But High Removal Rate	Regular Ventilations are required	-	Better Performance in Highly Contaminated Space

Table 1 Comparison of Conventional Air Filtering Methods and Acoustic Agglomeration Method

### 1.2.1 Performance Comparison between Fibrous Filter and Acoustic Agglomeration Filtering

Noorpoor et al. (2013) conducted acoustic agglomeration experiments to investigate the relationship between energy usage, airflow rate, and particle removal efficiency. They supplied

830 Hz sound at 145 dB, consuming 27 watts of power, to a fluid containing particles ranging from 0.4  $\mu\text{m}$  to 9  $\mu\text{m}$ , and measured the decrease in particle count. When the fluid flowed at rates of 10 liters/min (0.1666 liters/sec) and 50 liters/min (0.8333 liters/sec), the amount of fine particles decreased by 93.35% and 43.2%, respectively.

When supplying 830 Hz ultrasound at flow rates of 30 liters/min (0.5 liters/sec), approximately, 4%, 15%, 70%, and 91% of fine particles were removed by ultrasound corresponding to approximately 3 watts, 6 watts, 11 watts, and 21 watts, respectively. To purify 1  $\text{m}^3$  of air, 6,000 watt-sec, 12,000 watt-sec, 22,000 watt-sec, and 42,000 watt-sec are required, respectively. The fan energy consumption required to move fluid through ducts is excluded.

When utilizing the traditional air purification method with fibrous filter (Nassif, 2012), using a Minimum Efficiency Reporting Value of 8 (MERV 8) in a constant-speed fan 5-ton HVAC system with an airflow of 991 liters/sec results in a pressure drop of 25 Pa due to the filter, requiring 25.23 watt-sec per  $\text{m}^3$ . As the filter becomes dirtier over time, the pressure drop increases to 75 Pa, resulting in a decrease in flow to 779 liters/sec. To purify 1  $\text{m}^3$  of air, 96.28 watt-sec is required.

Using MERV 12 in a variable-speed fan 5-ton HVAC system with an airflow of 991 liters/sec results in a pressure drop of 50 Pa. Using this filter, 50.46 watt-sec is required to purify one  $\text{m}^3$  of air. As the filter becomes contaminated over time, the pressure drop increases to 100 Pa, requiring 100.91 watt-sec to purify 1  $\text{m}^3$  of air.

In addition to this, research related to AA is a minor field in Computational Fluid Dynamics (CFD). Generally, interpreting particle movement following air flow is the only function of CFD software package related to particle motion. Most CFD tools do not equip the function that can model vibrating motion of particles due to sound waves.

### 1.3 Research Purposes

The main purposes of this study are the following:

- 1) Explore the fundamental mechanisms of AA filtering

It is necessary to understand the basic principles of the AA phenomenon for a detailed research plan and in the initial stage of the research. Additionally, the study will support the process of seeking to make contributions to the acoustic agglomeration field.

- 2) Identify AA relationships between systems variables and particle removal performance.

This is a process of collecting data on variables and results. Based on this process, a set of reference values for developing a numerical model can be established. The collected data will also be used in the verification stage of a future AA numerical model.

- 3) Develop proper mathematical and numerical models to predict AA behavior, with experimental validations.

The evaluation of certain phenomena through actual experiments can be limited due to physical, temporal, and financial reasons. Therefore, the numerical approach is required to evaluate the performance of the AA mechanism beyond the actual experimental study. However, current CFD simulation tools are not equipped with the ability to correctly interpret the AA phenomenon. The AA model will be developed based on fundamentals of AA theory.

Moreover, the validity of the developed model will be secured by comparative analysis using data obtained through AA performance evaluation.

#### 1.4 Tasks of This Study

To meet research purposes, the following tasks are required:

- 1) Review the previous studies related to acoustic agglomeration.

In order to determine the background knowledge and starting point for this research, it is necessary to analyze the current status of this research topic.

2) Develop a numerical model that can analyze the AA mechanism.

Currently, detailed implementation of the AA mechanisms are not prepared in most CFD tools. Therefore, it is necessary to develop a CFD solver for the AA phenomenon in order to conduct research on the AA phenomenon through computer simulation.

3) Model validation using data from reference research and experiments.

Accuracy of simulation results produced by numerical models developed solely based on theory are not guaranteed. Therefore, a calibration process for the developed numerical model is required. Calibration was carried out using reference research and experimental data to validate the numerical model.

4) Sensitivity test for the AA phenomenon

Since the actual experiment can only be proceeded in limited conditions, by using the developed CFD solver for the AA, this study plans to evaluate the AA's performance in various conditions.

## 1.5 Contributions of Research

The main contribution of this research was developing a CFD simulation model for particle collisions.

The model consists of three sub-models.

### Direct Particle Pair Collision Model

The main difference in the analysis of collisions from conventional CFD simulation methods is the method used to determine the results of the collision. The conventional collision

model divides the very short time when two particles collide from the moment of collision into detailed analysis. By comparing the inner-particle forces and the repulsive force generated by the collision at the final moment, it determines agglomeration or repulsion. Analyzing the very short collision time in more detail requires a significant amount of simulation time and cost.

However, the method introduced in this study to analyze collisions is the critical velocity method. It predicts the outcome of collisions by comparing the repulsive force generated by the collision and the Van der Waals force. If the velocity at the time of collision is less than a certain speed (the critical velocity), it determines agglomeration. Otherwise, it is expected that the particles will repel each other after the collision.

By introducing the concept of critical velocity into the analysis of collisions, the procedures necessary to analyze collisions have been simplified.

#### Particle-to-wall Collision Model

The existing particle-to-wall collision model determines the outcome of collisions for all particles based on pre-defined results regardless of the physical properties of particles, collision speed, or wall characteristics when particles collide with the wall—whether it be rebound or stick—depending solely on the size and velocity of the particles. However, the model developed in this study applies the concept of critical velocity, where the outcome of collisions for individual particles colliding with the wall is determined based on the physical properties of the particles and the wall, as well as the collision speed.

#### Acoustic Particle Pair Collision Model.

The existing CFD simulation program package lacks a model for acoustic agglomeration analysis. So, for this study, a model for acoustic agglomeration phenomena was developed. The developed model takes into consideration the concept of agglomeration volume, which is a core concept of the acoustic agglomeration mechanism, in order to reduce the simulation time cost required for analysis.

In both the direct collision model and the acoustic particle collision model, when particle-to-particle collisions occur and the collision results in agglomeration, the larger particles are designed to capture the smaller particles, transforming into larger particles, while the smaller particles are removed. In the particle-to-wall collision model, if a particle collides with the wall and sticks to it, it is set to be deleted. Agglomerated particles and particles attached to the wall are excluded from the simulation target, thereby reducing the simulation time cost.

## CHAPTER II LITERATURE REVIEW

### 2.1 Fundamentals of Acoustic Agglomeration of Particles

Due to the differential movement of fine particles in the resonating air caused by ultrasound, collision and agglomeration occur among some particles. The main causes of particle agglomeration are orthokinetic interaction and refilling mechanisms.

#### 2.1.1 Process of Acoustic Agglomeration

Orthokinetic interaction is a phenomenon in which two particles in the air collide directly during the resonating process with ultrasound. Depending on its relative position, the refilling mechanism indirectly induces collisions between particles by decreasing the distance between them. There are two categories of refilling mechanisms. Through the secondary refilling mechanism, the distance between two particles can be closer to a distance where the primary refilling mechanism can take effect. Through the primary refilling mechanism, the distance between two particles is moved to a space where direct collision through orthokinetic interaction is possible. Finally, particle collision and agglomeration occur through orthokinetic interaction.

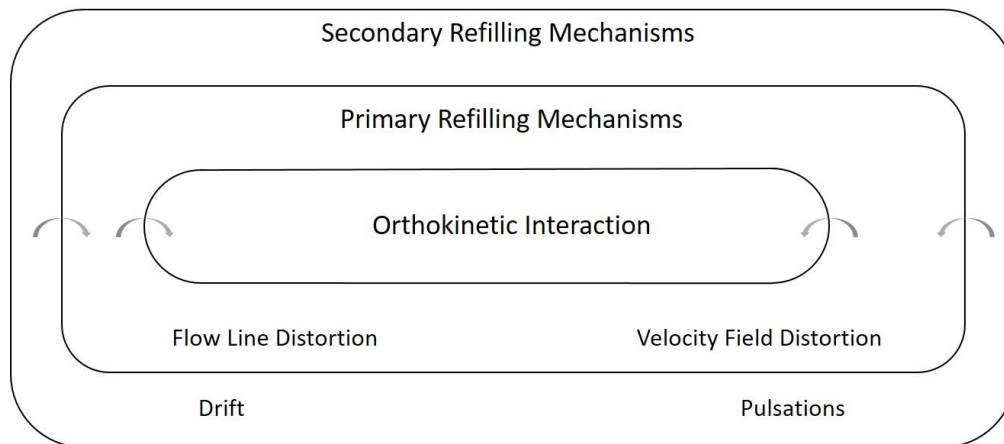


Figure 5 Process of Acoustic Agglomeration (Ref: Shaw, 1978)

### 2.1.2 Orthokinetic Interaction

Orthokinetic interaction is a mechanism that derives direct collisions between particles within the area of sound waves. It represents the phenomenon in which two particles collide with each other during the resonance process. The process happens during the resonating motion of the two particles by sound vibration. When the physical characteristics of the two particles are different especially in size or density each particle has a different resonance amplitude due to the sound wave. The ratio of resonance amplitude formed by the particles influenced in the area of the sound wave to the vibration amplitude of the sound wave is called the entrainment factor. If the particle is small, its inertia is also small, so the entrainment factor is larger than that of larger particles. Therefore, smaller particles have bigger amplitudes. The entrainment factor caused by sound waves in a specific fluid can be calculated using the following equation (Brandt et al., 1936):

$$\mu_p = \frac{U_p}{U_g} = \frac{A_p}{A_g} = \frac{1}{\sqrt{1+\omega^2\tau^2}} = \frac{1}{\sqrt{1+\left(\frac{4\pi\rho_p r^2 f}{9\eta}\right)^2}} \quad (1)$$

$\omega$  is angular frequency as follows:

$$\omega = \pi f \quad (2)$$

$\tau$  is relaxation time as follows:

$$\tau = \frac{2\rho_p r^2}{9\eta} \quad (3)$$

Due to the difference in resonance amplitude between the particles, when two particles are located within a certain area, collisions and coalescence occur between them. Agglomeration volume is the space where collisions can occur between small particles around a larger particle during the resonance process caused by sound waves.

### 2.1.2.1 Agglomeration Volume

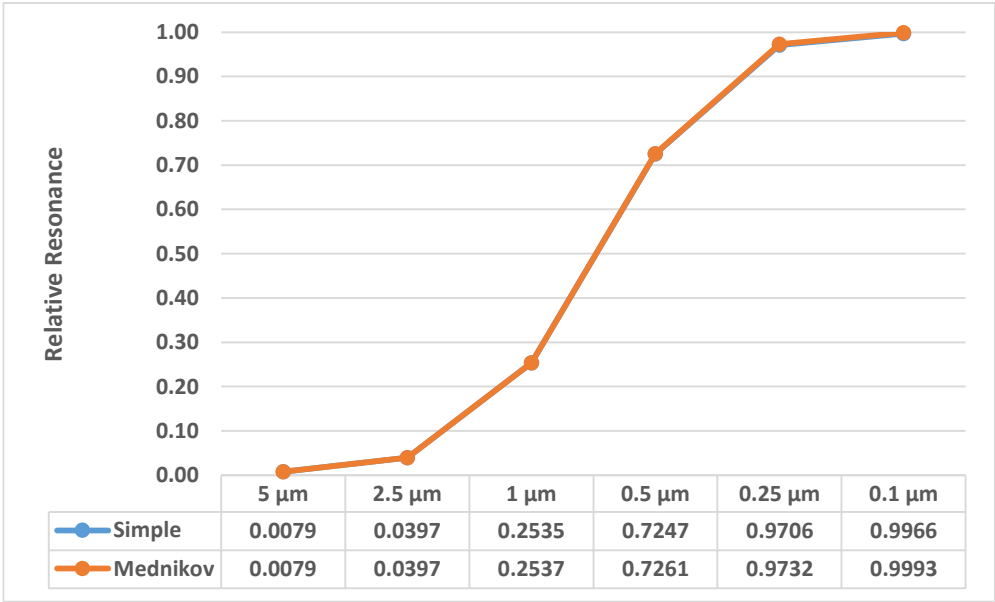
The shape of the agglomeration volume is generally cylindrical, following the direction of sound wave propagation around the larger particle. The length of the cylinder is determined by the intensity and frequency of the sound wave, the viscosity of the fluid, and the size and density of the particles. Referring to the equation provided earlier by Clair, the height of the agglomeration volume is denoted as  $2A_g(\mu_{p2} - \mu_{p1})$ . However, in 1965, Mednikov claimed that to obtain a more accurate height of the agglomeration volume, the phase angle between the two particles should also be considered. The equation proposed by Mednikov (1965) to find the maximum relative distance between particles is as follows.

$$\mu_{12} = \sqrt{\mu_{p1}^2 + \mu_{p2}^2 - 2\mu_{p1}\mu_{p2}(\mu_{p1}\mu_{p2} + \mu_{g1}\mu_{g2})} \quad (4)$$

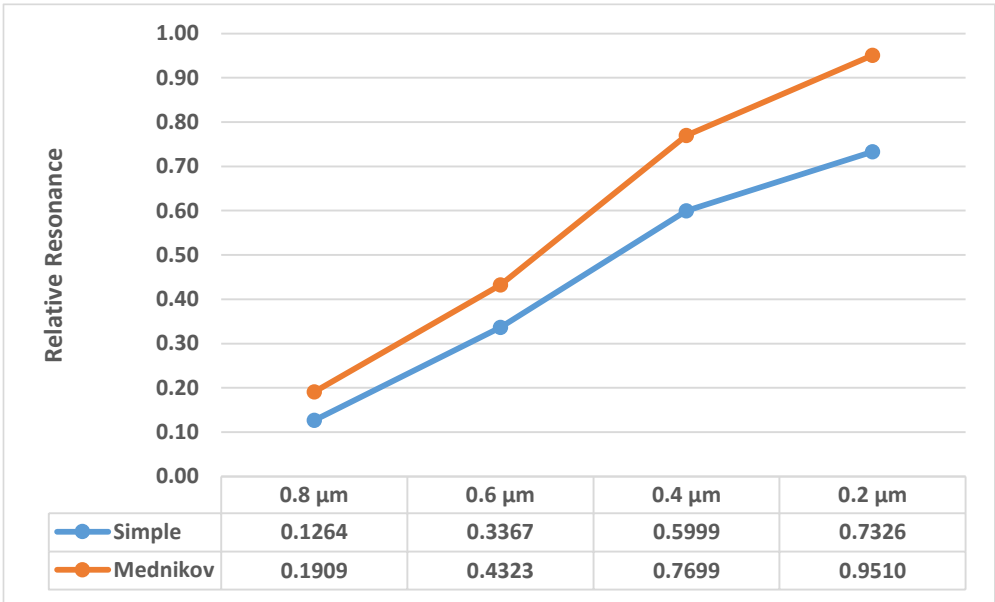
According to the equation proposed by Mednikov, the accurate height of the agglomeration volume is  $2A_g\mu_{12}$ .

The flow around factor,  $\mu_g$ , is given by the following equation:

$$\mu_p^2 + \mu_g^2 = 1 \quad (5)$$



Resonance amplitude difference to 10 μm particle



Resonance amplitude difference to 1.0 μm particle

Figure 6 Relative Resonance Amplitude Difference to a Larger Particle

Figure 4 above represents the estimated maximum fractional displacement of a pair of particles of  $2,500 \text{ kg/m}^3$  to a fluid medium vibration amplitude. The frequency of the sound source is 20 kHz, and the fluid medium viscosity is  $1.849 \times 10^{-5} \text{ kg/ms}$ .

The difference between the two models depends on the entrainment state of the large particle. If the large particle is fully entrained, the difference between the two models is small.

However, as the large particle becomes less entrained, the relative entrainment factor difference between the two models increases.

The radius of the cylindrical agglomeration volume is the sum of the radii of the two particles,  $r_1 + r_2$ . However, at the ends of the agglomeration volume, the interaction between particles must be taken into account to determine the radii. The ratio of the radius of the center of the agglomeration volume to the radius at the ends is called the capture coefficient.

### 2.1.2.2 Capture Coefficient

There are two approaches to determine the capture coefficient (Song, 1990). The first method assumes a capture coefficient of one. The second approach uses the Langmuir formula. According to Langmuir's (1948) formula, the capture coefficient for spherical particles can be expressed as follows:

$$\varepsilon = K^2 / (K + 0.5)^2 \quad (6)$$

$K$  is the ratio of  $\lambda$  to the radius of the collector particle. From the Langmuir, the physical meaning of  $\lambda$  is distance, and a certain particle can move a certain distance when introduced in a stand air with velocity  $U$ . The  $\lambda$  is calculated using the following equation:

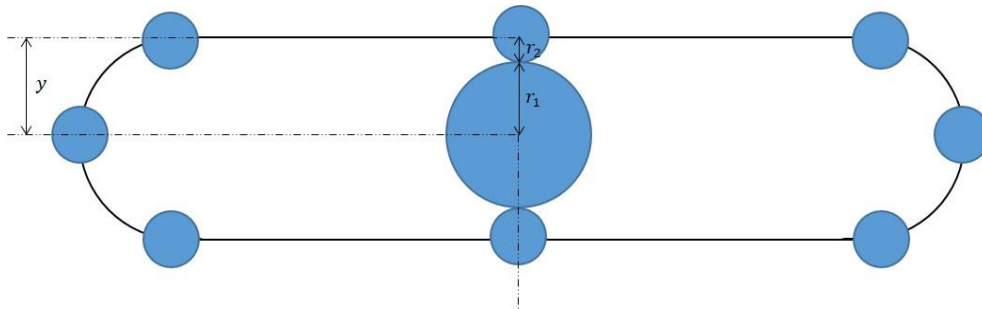
$$\lambda = \frac{2}{9} \rho_p r_2^2 U_0 / \eta \quad (7)$$

Therefore, the  $K$  is as follows:

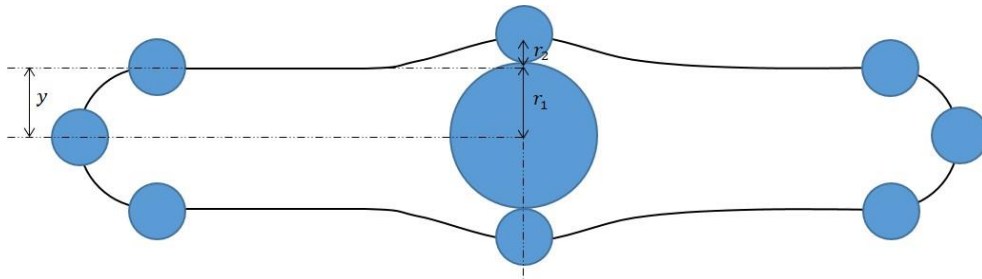
$$K = \lambda / r_1 = \frac{2}{9} \rho_p r_2^2 U_0 / \eta r_1 \quad (8)$$

The shape of the agglomeration volume is modified, depending on the capture coefficient. Without considering mutual interaction between a pair of particles, the shape of

simplified agglomeration volume is a simple cylinder. However, the shape of agglomeration volume considering mutual interaction is similar to the following diagram:



Simple



Detailed

Figure 7 Agglomeration Volumes

The characteristics of the capture coefficient are also related to the factors that determine the entrainment factor. For a shape to closely resemble a cylindrical agglomeration volume, the following conditions can be anticipated:

- When small particles have bigger inertia, causing them to be less influenced by the flow surrounding the larger particle.
- When there is minimal flow line distortion around the larger particle.
- When the viscosity of the medium is low, resulting in gentle flow lines around the larger particle.

These conditions help optimize the capture coefficient and facilitate the formation of agglomerates that resemble a formal cylinder shape.

### 2.1.2.3 Refill Factor

The definition of acoustic agglomeration is the collision and coalescence of particles located within the agglomeration volume, which is determined by the sound wave and particles. However, St Clair (1949) demonstrated that there were additional reductions in particle concentration after one cycle of sound vibration more than the number of small particles in the agglomeration volume. To explain these additional reductions, Mednikov (1965) proposed the concept of refilling mechanisms, which is composed of primary and secondary refilling mechanisms. He explained that there were two primary refilling mechanisms, parakinetic interaction and hydrodynamic interaction. Additionally, he described a secondary refilling mechanism resulting from drift and pulsation. Small particles which are located outside of the agglomeration volume are captured by the large particles when some small particles near the agglomeration volume move toward the volume due to the secondary refilling mechanism. Subsequently, particles near the agglomeration volume move into the volume through the primary refilling mechanism, and they collide and aggregate by orthokinetic interaction.

#### 2.1.2.3.1 Primary Refilling

The phenomenon occurs due to the interaction between the following two principles: 1) Parakinetic interaction (Flow line distortion), and 2) Hydrodynamic interaction (Attractional interaction).

##### 2.1.2.3.1.1 Parakinetic Interaction

Large or high-density particles are relatively less entrained by sound waves compared to small or low-density particles. Large particles, which are entrained less, distort the fluid flow in the sound field. Small particles around the distorted flow are also entrained by the distorted flow and move toward or detach from the agglomeration volume around the larger particles. The movement of small particles approaching or moving away from the agglomeration volume of

larger particles is determined by the relative positions of the large and small particles. The following shows general direction of forces between the particles depending on their positions.

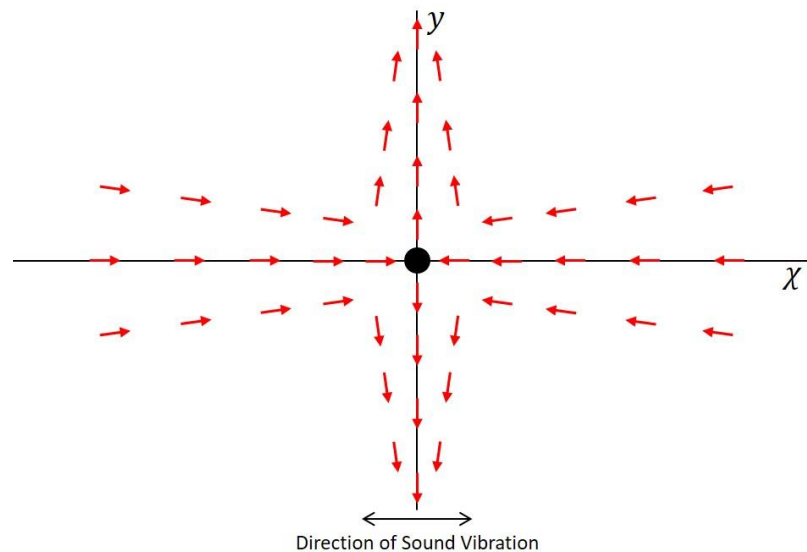


Figure 8 Direction of Force by Flow Line Distortion around a Large Particle (Ref: Mednikov, 1965)

#### 2.1.2.3.1.2 Hydrodynamic interaction

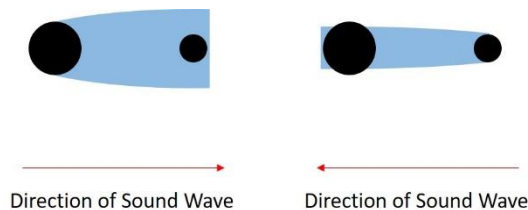


Figure 9 Hydrodynamic interaction between a pair of particles in a sound field

This mechanism is derived by mutual interaction between particles. A particle in the region of an acoustic wave, a parabolic dead zone is created behind the particle. When two adjacent particles are located within a certain distance parallel to the direction of the acoustic wave, the surrounding flow field is distorted due to the influence of the wave, as shown in the diagram above. Every half period of the acoustic wave, the direction of sound force changes consistently. During the first half period, a large particle generates a dead zone behind it, and if a

small particle is located in the dead zone, the force that a small particle receives from the wave is somewhat reduced. Therefore, the distance between the pair is reduced. During the next half period, a dead zone is formed behind a small particle, and a large particle is located in the dead zone. The force from sound source to a large particle is also reduced and the distance between the pair is reduced again. As the vibration of the acoustic wave is repeated, the distance between the two particles gradually decreases.

#### 2.1.2.3.2 Secondary Refilling

Similar to the primary refilling mechanisms, secondary mechanisms can also be divided into two main categories: drift of particles and pulsation of particles.

##### 2.1.2.3.2.1 Drift of Particles

During the vibrational motion in the fluid, a portion of particles conduct modified movements or drift motions. The reasons driving particles in a sound field into drift motion are as follows:

- Radiation pressure
- Periodic change in viscosity of medium
- Difference in phase in the vibrations of the particles in the medium
- Distortion of sound wave
- Asymmetry in the vibration of the medium

#### Radiation Pressure

Obstacles in a sound field absorb a certain amount of the energy from the sound wave and scatter. The points where the obstacles are impacted by the sound source act as secondary

sound sources. The points supplying radiation pressure to the surrounding particles drive the drift motion of other particles (Westervelt 1951).

### Periodic Change in Viscosity of Medium

A sound field is composed of rarefaction and compression, and fluid temperature is related to pressure. These factors affect fluid viscosity. Therefore, temperature changes affect the viscosity of the fluid, which in turn can affect the amount of energy transferred to the fluid particles through vibration.

### Difference in Phase in the Vibrations of the Particles in the Medium

In Westervelt's (1950) study on the resultant or average velocity and pressure of fine particles within the sound wave, the research demonstrated that phenomenon is present in a traveling wave condition and not a standing wave condition.

Figure 1 in his study illustrates this phenomenon, showing the schematic representation of the positions and distances as a pair of particles within the acoustic region.

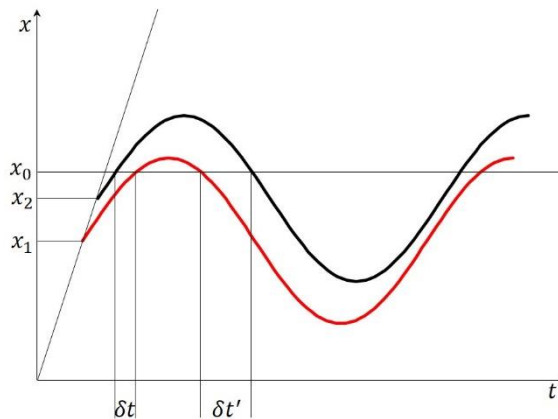


Figure 10 Resonance Phase Difference between Particles in an Acoustic Field (Ref: Westervelt, 1950)

The figure indicates that the time differences between the two particles being at the position  $x_0$  for the first time ( $\delta t$ ) and the position  $x_0$  for the second time ( $\delta t'$ ) are different. Therefore, in the traveling wave condition, the motion of the two particles can be characterized by a phase difference. The time lag in the response of the two particles to the sound wave implies that the pattern of distance in the first half period of vibration is different from that of the next half period of vibration.

### Distortion of Sound Wave

In compressible fluids, the density of the fluid changes depending on rarefaction and compression, and the speed of sound changes depending on the density of the fluid. As the sound wave travels away from the source, the shape of the wave may change due to these variations in density, which can affect the motion of the particles within the sound wave. In a sinusoidal sound wave, aerosols tend to move relatively smoothly with the wave motion. Conversely, in a saw tooth-shaped wave, the sudden changes in fluid motion can cause aerosols to become unable to follow the fluid motion and leave the range of resonance.

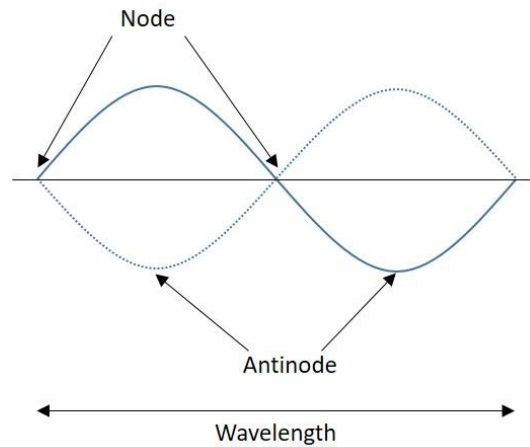


Figure 11 Asymmetry in the Vibration of the Medium in Standing Wave Condition

Standing wave sound fields are composed of nodes and antinodes, as depicted in the figure above. At the nodes there is no amplitude, while at the antinode points the amplitude is at its maximum. This pattern repeats throughout the field. As aerosols position themselves near the nodes, the acceleration due to the sound wave decreases, whereas positioning near the antinodes results in greater acceleration caused by the sound wave. In other words, the node points act as dampers which cause the particles to gather near them as the resonance of the particles repeats.

#### 2.1.2.3.2.2 Pulsation of Particles

##### Diffusional Mechanism

Fine particles exhibit motion along with the fluid while also displaying diffusional movement. The random collisions of particles occur due to Brownian motion and turbulent motion. If the particles are not too large, they can randomly collide with each other through the diffusional movement of the fluid. Collisions resulting from diffusional motion are a consequence of random movement and can occur for particles of the same size or particles of different sizes.

##### Orthokinetic Mechanism

This secondary refilling mechanism occurs due to similar reasons as the orthokinetic interaction between particles. The turbulent motion of the fluid, similar to the influence of sound waves, induces an orthokinetic interaction between particles of different sizes or densities, affecting the distance between them. For this mechanism to affect a pair of particles, their distance should be within the range of the turbulence length scale.

### 2.1.3 Agglomeration Kernel

Acoustic agglomeration is an analysis of the collision phenomenon between two particles. It is crucial that a particle with greater inertia captures another particle and that the number of particles serving as a collector remains constant. According to Madnikov (1965), the acoustic agglomeration rate can be expressed as follows:

$$\frac{dn_2}{dt} = -K_a n_2 \quad (9)$$

If the initial concentration of small particles per unit volume collected by acoustic agglomeration is  $n_{20}$ , the concentration of small particles per unit volume per unit time can be expressed by the following equation:

$$n_2 = n_{20} e^{-K_a t} \quad (10)$$

Agglomeration kernel  $K_a$  is proportional to the number of larger particles present in the system.

$$K_a = K_{a1} n_{10} \quad (11)$$

Similarly, the agglomeration kernel is proportional to the agglomeration volume. According to Shaw (1978), the acoustic agglomeration kernel follows the equation below:

$$K_a = \frac{2\pi(r_1 + r_2)^2 \varepsilon \mu_{12} A_g n_1 \alpha f}{\text{Agglomeration Volume} \quad \text{Refill Frequency}} \quad (12)$$

Agglomeration kernel is composed of agglomeration volume, the number concentration of collector particles, and refill frequency. The total number of agglomeration volumes corresponds to the number concentration of collector particles. The refill frequency represents the additional volume relative to the agglomeration volume supplied to the agglomeration

volumes per unit time. Therefore, the volume filtered per unit volume by collector particles in one unit of time becomes the agglomeration kernel.

### 2.1.3.1 Calculation of Refill Factor

The agglomeration kernel is determined by the sound waves and the agglomeration volume created by a pair of particles within its influence, as well as the frequency, capture coefficient, and refill factor. In general, the refill factor in the classical acoustic agglomeration kernel is set to 1. This means that for each vibration cycle of the sound wave, the same number of particles as the number of particles inside the agglomeration volume is supplied into the agglomeration volume.

Hoffmann (1997) proposed that the refill factor could be controlled by the acoustic wake effect. According to his theory, particles in the external refill volume move or refill into the agglomeration volume every vibration cycle. This suggests that the refill factor is not necessarily equal to 1 in the classic acoustic agglomeration kernel, since external particles continue to refill the agglomeration volume.

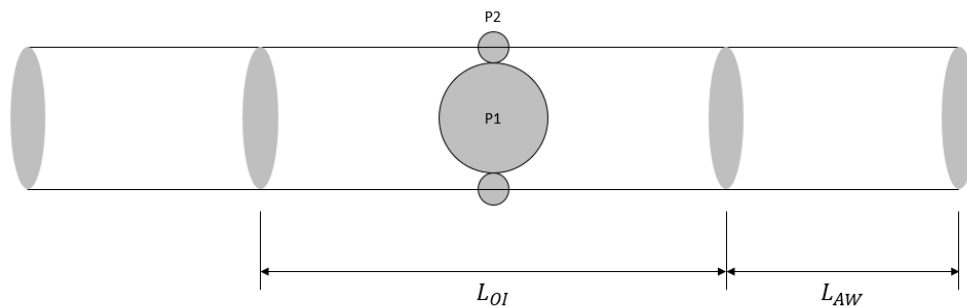


Figure 12 Orthokinetic Agglomeration Volume & Extended Agglomeration Volume by Acoustic Wake

Dianov et al. (1968) derived the time required for particles in the refill volume to move from the outermost position in the refill volume to the outermost position in the agglomeration volume using the relative acoustic wake velocity. Based on this, a modified acoustic agglomeration kernel can be expressed by the following equation:

$$K^* = K \alpha \quad (13)$$

The modified refill factor is expressed by the following equation:

$$\alpha = \frac{2L_{AW}}{A_g \mu_{12}} \quad (14)$$

The additional amplitude due to the acoustic wake effect is calculated by the following equation:

$$L_{AW} = \sqrt{(A_g \mu_{12})^2 + \frac{3U_g(r_1 l_1 + r_2 l_2)}{\pi} \frac{1}{2f} - \frac{1}{2} A_g \mu_{12}} \quad (15)$$

Particle Slip coefficients in the Oseen regime:

$$l_i = \frac{n_i}{\sqrt{1 + 2h_i n_i^2 + h_i^2 n_i^4}} \quad (16)$$

Particle Slip coefficients in the Stokes regime:

$$n_i = \frac{\omega \tau_i}{\sqrt{1 + (\omega \tau_i)^2}} \quad (17)$$

Constants

$$h_i = \frac{9}{2} \frac{U_g}{\pi \omega r_i} \frac{\rho_g}{\rho_p} \quad (18)$$

The movement of particles influenced by ultrasound creates a wake, affecting the motion of neighboring particles either by assisting or hindering their movement. This model considers the additional distance traveled by particles due to this effect. It can be considered an improved model compared to the assumption of particles refilling the existing agglomeration volume. However, according to Figure 6, it does not account for the influence in the direction perpendicular to the direction of ultrasound propagation.

#### 2.1.4 Decide Agglomeration After Collision

The collision between two objects can result in one of three outcomes:

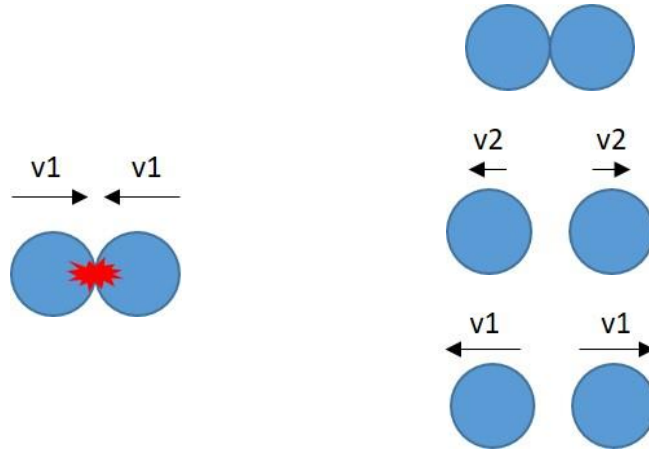


Figure 13 Collision between Identical Particles & Results

In general, collisions between spherical objects do not always result in agglomeration, as depicted in the previous figure. The outcome of particle collisions can be either elastic or non-elastic collisions. Acoustic agglomeration assumes agglomeration as the typical result after collisions. The variation of Van der Waals forces based on particle size can serve as a basis for this phenomenon.

According to Israelachvili (2011), particles possess intermolecular forces, with Van der Waals forces playing a significant role in intermolecular interactions. If the repulsive force between particles after collision is greater than the attractive Van der Waals force, the particles will separate based on energy balance. This phenomenon can be simplified and analyzed using a model called *critical velocity*. If the collision velocity of particles exceeds a certain critical velocity, the adhesive forces between particles are smaller than the repulsive forces after the collision, preventing the particles from staying together. The critical velocity can be determined using the following equation (Ho & Sommerfeld, 2002; Paiva et al, 2010).

$$u_{cr} = \frac{1}{d_{p2}} \frac{(1-e^2)^{0.5}}{e^2} \frac{A}{\pi z_0^2 \sqrt{6} P_p \rho_p} \quad (19)$$

The Figure 11 illustrates the relationship between the size of the smaller particle and the critical velocity when two particles collide, based on the characteristics of the particles used by Ho & Sommerfeld (2002).

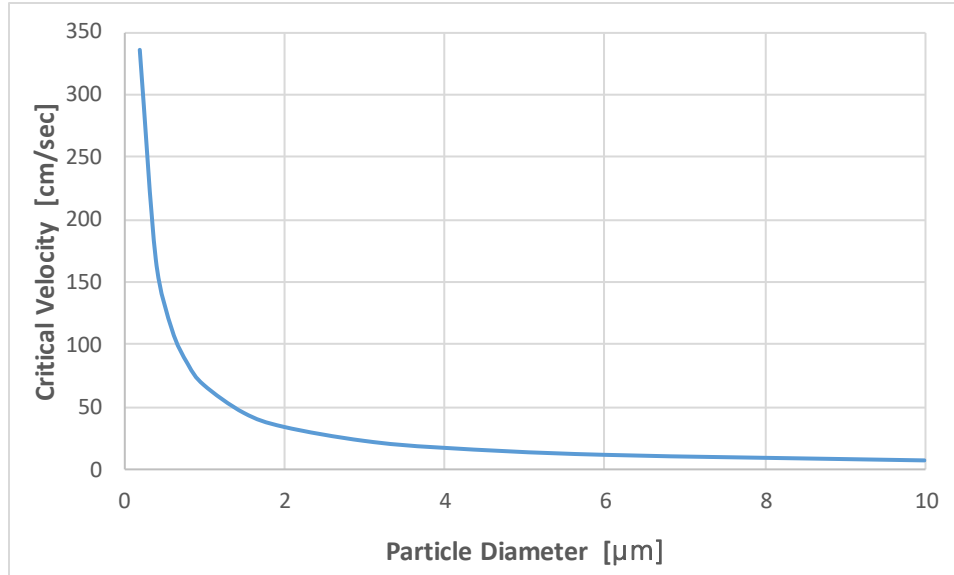


Figure 14 Relationship between Small Particle Diameter and Critical Velocity

Energetic restitution coefficient	0.4
Hamaker constant	5.0e-19 J
Contact distance	4.0e-10 meter
Material limiting pressure	5.0e+9 Pascal
Particle density	2400 kg/m <sup>3</sup>

Table 2 Particle Properties for Critical Velocity

As the particle size decreases, the critical velocity required to form agglomerates increases. Acoustic agglomeration focuses on analyzing small particles that can resonate with sound waves. Therefore, it can be assumed that particle agglomeration happens when a pair of particles collide in the case of small particle analysis.

## 2.2 Fundamentals of Acoustic Agglomeration Modeling

Simulating air flow using numerical techniques such as CFD is sophisticated and time-consuming, especially for cases with fine spatial and temporal resolutions. When particle movements and behaviors are to be tracked, substantial complexity is required in models and

numerical methods as well as computing costs. This is especially true when a large number of particles (as in the real scenarios) are to be simulated. To reduce the time required for particle tracking simulation, the concept of "parcel" is used (Ariyaratne, 2016). A parcel is a group of particles that share the same physical characteristics. By employing the concept of a parcel, a significant reduction of simulation time cost is expected.

This study introduces the approaches that previous researchers attempted to use to analyze the phenomenon of acoustic agglomeration through numerical methods.

Current numerical software lacks a dedicated solver for directly analyzing acoustic agglomeration. However, it is possible to apply the phenomenon of acoustic agglomeration through the following steps:

- Apply sound effects to the particles
- Conduct analysis of the collision: 1) Decide collision, and 2) Results of collision

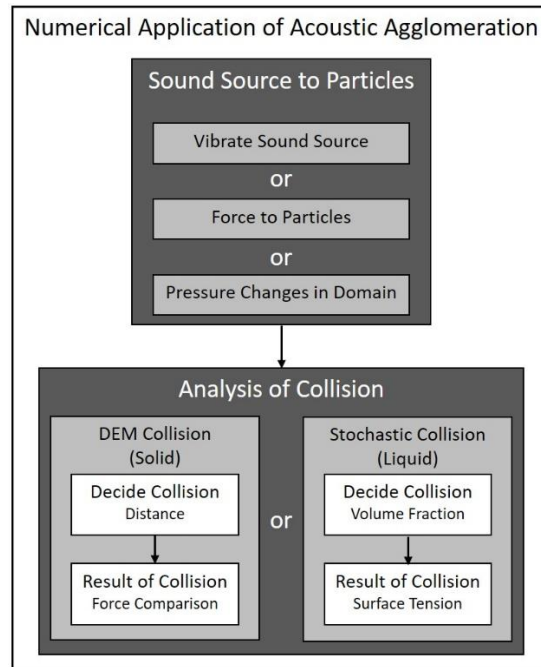


Figure 15 Strategies of Acoustic Agglomeration Process to a Numerical Simulation

### 2.2.1 Methods for Implementing Sound Impact to Particle Movements

Analysis of particle movement induced by sound can be conducted using the following methods:

- **Vibrating the Sound Source (Rahimi et al., 2017):** A method that models the phenomenon as it occurs. Sound constitutes vibrations. The vibrations from a sound source induce corresponding vibrations in the surrounding fluid, consequently causing the particles within the fluid to vibrate.
- **Force Applied to Particles (Shi et al., 2020):** In this method, forces are applied to the particles to simulate their motion. This method involves predicting and directly applying the force transferred from the sound source to the particles in the fluid. This method excludes calculations of the fluid's motion caused by the sound.
- **Applying Pressure Changes in the Domain According to Sound Waves (Flamm, 2017):** This method involves applying pressure changes within the domain based on the characteristics of the sound waves. Fluid medium around the sound source has pressure variation based on both the distance from the sound source and the time. The pressure gradient in the fluid decides the magnitude and direction of the force exerted on the particles in the fluid.

There are aerosol movements caused by the main airstream of the simulation domain. Simultaneously, analysis of acoustic agglomeration begins by examining the positions of particles through the combined effect of aerosol movement and the motion induced by sound waves.

### 2.2.2 Analysis of Collision

The analysis of particle collisions can vary depending on the type of particles involved. For liquid particles, the Stochastic Collision Method can be used, while for solid particles, the Discrete Element Method (DEM) can be employed.

### 2.2.2.1 Analysis of Collision between Liquid Particles

Based on the research of O'Rourke (1981), the family of Stochastic Collision models was developed to analyze collisions between two liquid particles. Rather than interpreting the actual trajectories of two parcels, it predicts collisions through stochastic assumptions. Collisions occur only when a pair of parcels are located in the same cell. The number of particles that collide in a specific cell during one computational time step of simulation can be calculated using the following equation:

Collision frequency is as follows:

$$v = \frac{\delta_2}{v_{ij}} \pi (r_1 + r_2)^2 |U_{p1} - U_{p2}| \varepsilon \quad (20)$$

The number of particles that collide during one simulation time step is as follows:

$$\bar{n} = v \Delta t \quad (21)$$

The probability of no collisions occurring between particles is as follows:

$$P_0 = e^{-\bar{n}} \quad (22)$$

The O'Rourke Stochastic Collision model determines each collision between particles by generating a random number between 0 and 1 and comparing it to the equation (22). If collision occurs, the results of collision will be considered.

Collisions between particles result in rebound or aggregation. If the following conditions are met after a collision, the two particles remain in an aggregated state:

$$b < b_{crit} \quad (23)$$

Critical impact parameter

$$b_{crit} = (r_1 + r_2) \sqrt{\min\left(1.0, \frac{2.4f}{We_L}\right)} \quad (24)$$

Collision impact parameter

$$b = \sqrt{YY}(r_1 + r_2) \quad (25)$$

The function  $f$  is as follows

$$f\left(\frac{r_1}{r_2}\right) = \left(\frac{r_1}{r_2}\right)^3 - 2.4\left(\frac{r_1}{r_2}\right)^2 + 2.7\left(\frac{r_1}{r_2}\right) \quad (26)$$

Weber number

$$We_L = \frac{\rho_l |U_{p1} - U_{p2}|^2 r_2}{\sigma} \quad (27)$$

The randomly generated number  $YY$ ,  $0 < YY < 1$ , decides the result of the collision, whether the collision pair bounces back or generates aggregates.

O'Rourke's model compares the probability of collision by comparing the volume of the target cell to be analyzed with the traveling distance multiplied by the cross-sectional area of the two particles in a unit of time. If a collision event occurs, it then estimates whether agglomeration will be sustained by considering the surface tension of the aggregated fluid particle.

#### 2.2.2.2 Analysis of Collision between Solid Particles

The collision and aggregation of solid particles are typically analyzed through a model contrived based on Cundall & Strack's (1979) Discrete Element Method (DEM). In DEM, the characteristics of parcels, such as size, velocity, torque, material properties, etc., are tracked and observed. There are several DEM models for analyzing particle collisions, including the Spring, Spring-dashpot, Hertzian, and Hertzian-dashpot models. The Spring-dashpot model is commonly used in popular CFD programs such as OpenFOAM, STAR CCM+, and ANSYS Fluent (Kasper, 2017; CD-adapco, 2017; ANSYS, 2020).

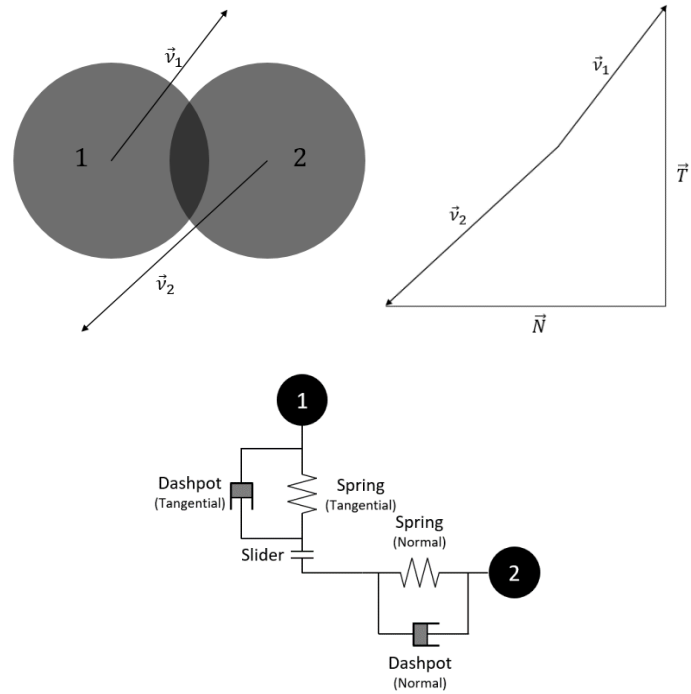


Figure 16 Structure of Spring-Dashpot Collision Model

The Spring-dashpot model analyzes the collision of two particles in 3-D space using three elements: springs, dash-pots, and a slider. The spring model assumes that when a particle is subjected to external forces, its shape changes like a spring before returning to its original form. The Dashpot model incorporates the concept that energy is required to change the shape and restore the particle to its original form. Particle collisions can be divided into normal and tangential components based on the collision angle, as illustrated in the diagram above. The normal collisional force is composed of a spring and dashpot, while the tangential collisional force is also composed of a spring and dashpot, but with the additional consideration of particle rotation in the tangential dash-pot component. Furthermore, if the frictional force between particles, generated by the normal force, is greater compared to the tangential force, then a slider effect is introduced after the collision between particles. According to Tsuji et al. (1992), the force acting on a particle after collisions between solid particles is composed as shown in Figure 17.

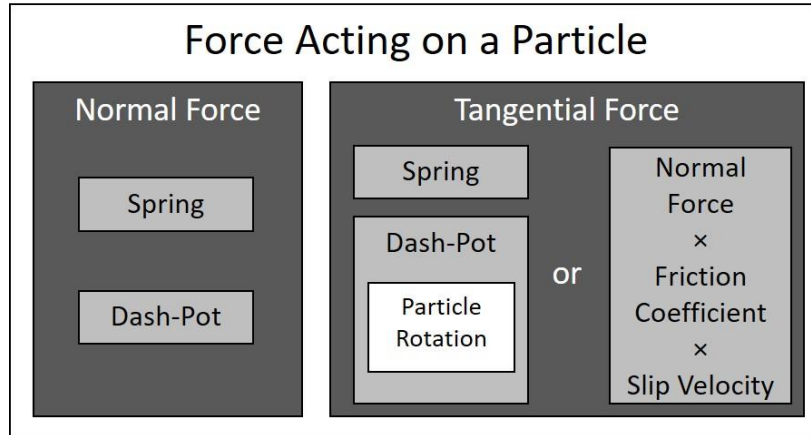


Figure 17 Composition of Spring Dashpot Model Forces

The determination of agglomeration or repulsion following a collision is decided by comparing the magnitude of the force between two particles based on their collision area—known as cohesion energy—and the normal force during the final time step of the collision (OpenFOAM). If the cohesion energy between two particles is greater than the repulsive force, the normal force, the two particles will remain in an agglomerated state even after the collision. Otherwise, collision models are employed to identify collision events between particles and calculate the directions and velocities of their movement after the collision.

## 2.3 Progress in Acoustic Agglomeration Research

### 2.3.1 Original Research

Wood and Loomis (1927) conducted an experiment using ultrasound with high intensity and found interesting physical effects. In 1932, Andrade found relative motion between smaller particles and larger particles. The smaller particles resonated more actively to the sound wave, while the larger particles were less active. He found that if a particle is large enough, the particle remains still while the fluid medium flows around it. Like the fluid medium, smaller particles move around larger particles or collide with them.

Based on the fundamental theory of particle entrainment due to fluid motion (König, 1891), Brandt et al. (1936) established an equation for the entrainment factor. Additionally, they proposed the theory of orthokinetic coagulation, suggesting that collisions can occur due to differences in particle size or density-induced differences in resonance amplitude. In addition to Brandt's team's orthokinetic coagulation theory, Mednikov (1965) introduced the concepts of primary and secondary refill mechanisms. Throughout the book, he reconsiders previous research on acoustic agglomeration.

Parker (1936) tried to provide evidence of sound impact on reduction of particle concentration by using an experimental approach that utilized magnesium oxide particles in ultrasound conditions. From Parker's experiment, the number concentration decreases as the sound exposure time increases. Also, Andrade (1936) attempted to develop a mathematical theory of acoustic agglomeration using smoke.

Parker (1936) attempted to provide evidence of sound impact on the reduction of particle concentration using an experimental approach with magnesium oxide particles under ultrasound conditions. From Parker's experiment, the number concentration keeps decreasing as the sound exposure time increases. Also, Andrade (1936) attempted to develop a mathematical theory of acoustic agglomeration using smoke.

Amy (1934) invented and patented a device using ultrasound to reduce fog that could impair visibility. Shortly thereafter, World War II began, and research on visibility enhancement using ultrasound became very active (Mednikov, 1965). Experiments at Columbia University and Lunken Airport, Ohio (Sinclair, 1950) confirmed the effectiveness of using ultrasound to reduce fog (4 to 16 microns) and improve visibility. The effects were observed at distances ranging from 200 to 400 ft when using ultrasound in the frequency range of 300 to 700 Hz and at the intensity of 130 to 160 dB.

According to results from various experiments ranging from laboratory scale to plant scale done between 1950 and 1960 as collected by Hegarty & Shannon (1976), acoustic agglomeration exhibits the following characteristics:

- The optimal frequency varies depending on the particle size, increasing as the particle size decreases.
- The square root of sound intensity is closely related to the acoustic agglomeration rate.
- Acoustic agglomeration is effective when the particle concentration level is 2 to 5g/cm<sup>3</sup> or higher.
- Acoustic agglomeration is more effective under conditions with a diverse particle size distribution compared to conditions where particle sizes are the same.
- Adding water droplets or seeding can improve the acoustic agglomeration effect, akin to increasing the concentration of collector particles.
- Influences of ultrasound properties and particle concentration on acoustic agglomeration are more significant compared to the influences of physical properties of particles, viscosity, temperature, and pressure of the fluid medium.

Shaw & Tu (1979) conducted research on the relationship between hydrodynamic interaction and acoustic agglomeration. They utilized monodisperse aerosols to minimize hydrodynamic interactions as much as possible. Their research results indicated that for particles larger than 0.5 micrometers, frequencies below 10 kHz played a significant role in hydrodynamic interaction with acoustic agglomeration.

Chou et al. (1981) determined the relative importance of acoustic agglomeration mechanisms based on ultrasound intensity and particle size through experimental and theoretical studies. In their research, they presented the relative importance under each condition, as shown in the figure below:

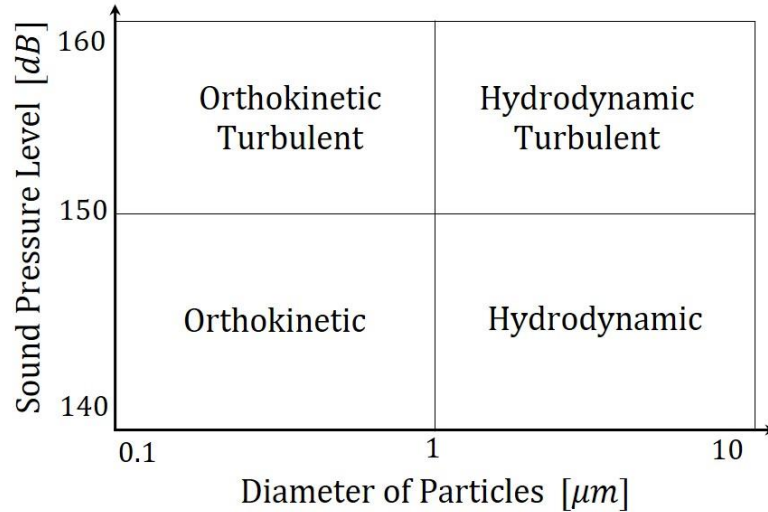


Figure 18 Relative Importance of Acoustic Agglomeration Mechanisms (Ref: Chou, 1981)

Within the range of ultrasound exceeding 150 dB, mechanisms influenced by turbulent flow play a significant role. Acoustic agglomeration among aerosols smaller than 1  $\mu\text{m}$  is induced by the difference in entrainment factors between particles, highlighting the importance of orthokinetic interaction. For aerosols larger than 1  $\mu\text{m}$ , where it is difficult to expect significant resonance amplitude differences between particles, hydrodynamic phenomena are crucial in the acoustic agglomeration process.

Tiwarly & Reethof (1987) developed a numerical model using the acoustic agglomeration kernel. This numerical model predicts changes in particle composition based on particle size after applying ultrasound, compared to the initial particle input. In this study, they demonstrated the reliability of their numerical model by comparing experimental measurements using coal fly-ash aerosol with the results from the numerical model.

Macgill et al. (1989) conducted a study on the removal of hazardous substances that had been released into the air due to accidents through acoustic agglomeration. They assumed a scenario where black soot particles ranging from 0.5 to 10 micrometers were positioned at a concentration of  $1\text{g}/\text{m}^3$  in a chamber of  $4.5\text{m}^3$ . They carried out two experiments for fine

particle removal. The first experiment was carried out by exposing these particles to ultrasound of 21 kHz and 150 dB only. The second experiment used ultrasound with sound of 140 dB and 1 kHz and introduced collector particles of 33  $\mu\text{m}$  at a concentration of 1  $\text{g}/\text{m}^3$ . They confirmed that using collector particles simultaneously with ultrasound was more effective in removing hazardous materials than using ultrasound alone.

Mandralis et al. (1993) conducted a study on separating aerosols from fluid using ultrasound. In their research, they utilized the phenomenon where aerosols concentrate at the nodes of the sound wave by creating a standing sound wave condition. The experimental setup is outlined as shown in the figure below:

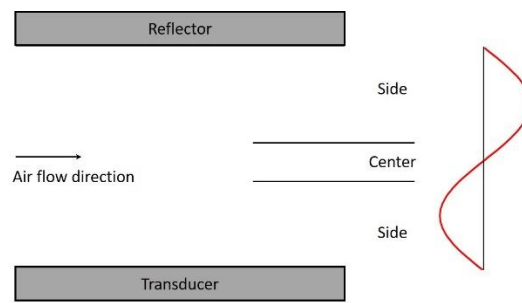


Figure 19 Schematic Illustration of Mandralis's Experiment

The channel thickness was set to half the wavelength of the ultrasound, resulting in a channel thickness of 1.08 mm. The flow rate was maintained at 20  $\text{cm}^3/\text{min}$  throughout the experiment. They observed a decrease in the number of aerosols detected at the sides by increasing the energy supplied to the transducer from 0 watt to 10 watt. The aerosol count reduced from 10.57e5/ $\text{cm}^3$  at 0 Watt to 0.486e5/ $\text{cm}^3$  at 10 Watt, showing a 95.4% reduction compared to 0 watt.

Using acoustic agglomeration, Sarabia et al. (2003) conducted a study on the influence of humidity on the process of removing fine particles generated during the diesel combustion process. They compared fine dust removal efficiency by varying humidity levels during the process of removing particles in the size range of 0.01 to 1  $\mu\text{m}$  by using 21 kHz ultrasound at

151 dB. The total number of fine particles decreased by 25% at a humidity level of 0.01 kg/kg. They observed a 56% fine dust removal efficiency when increasing the humidity to 0.06 kg/kg.

Dong et al. (2006) proposed a new concept called "effective agglomeration length." They presented equations to calculate the effective agglomeration length for two collision cases: orthokinetic interaction and acoustic wake effect. Through theoretical research, they derived these equations and identified the following characteristics of acoustic agglomeration during the process.

- Orthokinetic interaction is significant in the low-frequency range, while the acoustic wake effect is important in the high-frequency range.
- The optimum frequency decreases as the sound pressure level increases.
- Acoustic wake plays a crucial role in collisions between particles of the same size, and its importance increases as the particle sizes grow.
- In the case of low frequencies where orthokinetic interaction is the primary cause of particle collisions, the acoustic wake effect is not significant for the refill mechanism.

Yan et al. (2016) conducted a study to enhance the efficiency of fine dust removal using vapor condensation in the acoustic agglomeration process. They induced the acoustic agglomeration phenomenon with 150 dB and 1800 Hz ultrasound. When using ultrasound alone, the particle removal efficiency ranged from 10% to 23%. By comparison, when using 150 dB ultrasound in conjunction with vapor condensation, the particle removal efficiency increased from 53% to 80%. The super-saturation degree used in this case was 1.2, defined as the ratio of the partial pressure of water vapor to its equilibrium vapor pressure.

Zhou et al. (2016) measured the variation in removal efficiency by integrating the acoustic agglomeration technique with existing fine particle removal methods, namely the bag filter and electrostatic precipitator (ESP). They pre-treated fine particles with ultrasound at 1400 Hz and 148 dB and then measured the final particle removal using either the bag filter or ESP.

When using only the bag filter, the fine dust removal efficiency was 91.29%, whereas after pre-treatment with ultrasound, 99.19% of particles were removed. Similarly, when using ESP alone the fine dust removal efficiency was 89.05% and increased to 99.28% when combined with use of ultrasound.

In this chapter, the long history research on acoustic agglomeration from the discoveries about the substance movement near sound field in the 1920s to the mid-2010s was explored. The following three tables (Table 3-5) summarize the development of key theories of acoustic agglomeration, the application of AA mechanisms, and factors which impact AA mechanisms.

1920 Wood and Loomis	Sound impacts on substance in sound field
1932 Andrade	Oscillation amplitude difference between particles in a sound field
1936 Brandt et al	Proposed the orthokinetic coagulation theory based on König's research
1949 Clair	Deficiency of the orthokinetic coagulation theory
1965 Mednikov	Proposed the primary and secondary refilling mechanisms and organized research works related to the AA mechanisms.
1997 Hoffmann	Refill factor model based on acoustic wake effect

Table 3 List of Research Related to Main Theory of the AA Mechanisms

The oscillation amplitude variance caused by sound due to the difference in inertia of particles was discovered. To theoretically explain this physical phenomenon, the orthokinetic interaction theory was established by applying research results from the late 1800s. Over the past century, there have been numerous studies on the phenomenon of acoustic agglomeration, resulting in significant advancements in understanding the factors that constitute Equation (12). However, the model for the refill factor was developed based solely on the acoustic wake effect, indicating the need for further research to advance Hoffmann's model which can more precisely produce refill factor.

1934 Amy	Patent for defogging
1965 Mednikov	Test for removing fog by using sound during World War II
1950 Sinclair	Test for removing fog by using sound on an airport runway
1989 Macgill et al.	Mock-up test for hazardous substance removal by acoustic agglomeration with adding collector particles
1993 Mandralis et al.	Separate particles from fluid using standing wave
2003 Srabia	Performance of AA and humidity
2016 Yan et al.	Performance of AA and vapor condensation
2016 Zhou et al.	Usage of acoustic agglomeration combined with ESP or bag filter

Table 4 List of Research Related to Application of the AA Mechanisms

Acoustic agglomeration was initially attempted as a means to remove unwanted particles from the air during World War II to achieve better maneuverability. Experimentation initially focused solely on the use of sound waves. However, over time, the purpose of research diversified, exploring methods to improve the performance of acoustic agglomeration, diversify its applications, and combine it with other methods to better remove pollutant particles, aiming for synergistic effects. In the future, exploring the performance of AA in scenarios where other particle removal methods are challenging to apply would be beneficial.

1976 Hegarty & Shannon	Research on characteristics of acoustic agglomeration through lab and plant scale experiments
1979 Shaw & Tu	Relationship between factors and acoustic agglomeration under hydrodynamic interaction dominant condition using mono-dispersed aerosols
1981 Chou et al.	Priority of mechanisms which affect acoustic agglomeration based on particle size and dB
2006 Dong et al.	Found relationships between variables and AA by considering the orthokinetic interaction and acoustic wake effect

Table 5 List of Research Related to Characteristics of the AA Mechanisms

Research in this category was initially focused on determining the relative importance of variables mentioned in the former parts that influence AA phenomenon and finding strategies to

control variables to achieve a higher performance of acoustic agglomeration. Gradually, interest shifted towards investigating the impact of each variable on the agglomeration performance in specific situations.

### 2.3.2 Recent Advances in Acoustic Agglomeration Research

There are experimental and numerical approaches to acoustic agglomeration research. Recent studies related to AA have been mainly conducted using numerical methods. Experiments were mainly conducted with numerical studies to secure the validity of their numerical models. Most studies related to acoustic agglomeration have been focused on the analysis of the motion between two particles in the region of sound waves. The main focus of the studies aims to establish a more accurate numerical simulation model.

In 2018, Kacianauskas et al., Zhang et al., and Shang et al. did numerical acoustic agglomeration research focused on improving simulation results accuracy.

Kacianauskas et al. (2018) applied the Oseen effect to their discrete element method (DEM) based on the acoustic agglomeration model and analyzed two particles of the same size. They compared results from their previous model with CFD simulation, then conducted CFD simulations and DEM simulations under the condition of a 3-D space incompressible viscous flow. The mutual effects of micrometer sized particles on each other in the sound wave region of 3 kHz were investigated. In the CFD simulation, it took 18 milliseconds for the distance between two particles to decrease from approximately 95  $\mu\text{m}$  to 20  $\mu\text{m}$ , whereas their previous model took approximately 25 milliseconds. They found the cause was from setting the slip conditions between the particles and the fluid medium that occurred in the boundary layer of the particles. As a result of their three-step calibration, the results from their new DEM model had similar results to the CFD simulation.

Zhang et al. (2018) performed CFD simulations with two particles of 500  $\mu\text{m}$ . Domain size was carried out in a two-dimensional square space of 500 times the particle size, 25  $\text{cm} \times 25$

cm. The particle density was  $2500 \text{ kg/m}^3$  and the simulation was performed in the region of 2 kHz. Zhang found that the perturbation velocity of particles differed by 50% compared to Dianov's model, which was developed in 1968 and the CFD simulation. By improving Dianov's model, Zhang's team developed a more accurate DEM model.

Shang et al. (2018) applied the sound attenuation effect to a one-dimensional spatial sectional model to obtain an agglomeration kernel for different locations. They conducted an experiment by placing a 150 dB speaker in the direction of a long tube with a length of 2.75 meters and a diameter of 15 cm. As a result of his experiment, it was found that it matched well with the experimental result derived from his model to which the sound attenuation effect was applied. They found that the particle number concentration differed approximately twice between the model with sound attenuation effect and without sound attenuation effect.

Lu et al. (2019) used a software called COMSOL to investigate the interaction between two solid particles. Additionally, their acoustic agglomeration model decides whether particle aggregates separate or remain aggregated, based on the Van der Waals force. They found that as the sound intensity increased, the maximum size that could hold the aggregates became smaller.

Shi et al. (2020) also conducted a study on acoustic agglomeration using a break-up model. With the break-up model, the simulation results showed a closer resemblance to the measured data. Simulation results without the break-up model exhibited a higher number concentration in larger aggregates and a lower number concentration in smaller aggregates. In real-life scenarios, strong sound waves can cause larger particles to break apart. Their research indicated that when comparing smaller and larger aggregates, smaller aggregates could maintain their cohesion even under relatively high acoustic intensity.

The former numerical studies on AA generally focused on improving simulation accuracy between only two particles. However, these studies are difficult to apply on a larger scale that contains many particles spread in a relatively wide space. For example, in the study of Kacianauskas et al., approximately 1 hour of simulation time was required to analyze the mutual interaction between one pair of particles in a space of 1 mm by 1 mm by 1 mm during only one cycle of oscillation of sound waves. Therefore, in order to analyze the interactions between large

numbers of particles in a larger space, simplification of the acoustic agglomeration phenomenon is required.

## 2.4 Conclusion

Research on acoustic agglomeration, which began in the 1920s, has a rich legacy due to its history of extensive exploration. Studies have covered practical applications, numerical interpretations of the phenomenon, and more. Research focused on practical applications began during the era of World War II, with the goal of enhancing visibility for efficient operation of aircraft or ships. Currently, research is ongoing for efficient removal of aerosol pollutants in an effort to reduce air pollution.

Energy-intensive acoustic agglomeration technology is being investigated in conjunction with other scientific technologies, rather than using it alone to remove pollutants. This combined approach aims to achieve a synergistic effect. Theoretical research initially focused on establishing the fundamentals of the acoustic agglomeration mechanism. Subsequently, research attention then shifted towards understanding trends for the efficient use of acoustic agglomeration technology.

Over time, there has been a growing trend to apply acoustic agglomeration mechanisms to simulation programs, alongside efforts to improve the accuracy of acoustic agglomeration models. Many researchers have made efforts to incorporate fundamental concepts from various recent acoustic agglomeration theories into existing simulation programs or even create new simulation programs. This study introduces methodologies for interpreting acoustic agglomeration phenomena through CFD simulation.

However, when analyzing acoustic agglomeration using CFD simulation programs, there are noticeable constraints. While it's possible to analyze agglomeration between a small number of particles influenced by sound, analyzing acoustic agglomeration among a large number of particles requires a significant amount of computation time. To analyze large-scale acoustic agglomeration through CFD simulation, we need to consider the main factors that drive substantial calculation time, including:

- Simulation time step settings: The time steps should be short enough to accurately predict the precise movement of particles influenced by sound, necessitating the division of one sound wave cycle into several segments for analysis.
- Number of pairs of particles for potential collision: With a greater number of particles, the number of pairs of particles that might collide increases, thereby increasing time costs. Introducing the concept of "parcels" helps manage this, but if a single parcel contains too many particles, accuracy may be compromised. Therefore, a judicious choice of the number of particles is crucial between simulation time cost and accuracy.
- Mechanisms affecting particle movement: The acoustic agglomeration process considers the precise movement of particles due to sound and the various effects it imparts on surrounding particles. While incorporating all mechanisms into the simulation process could enable precise predictions, it would also require additional computation time. Thus, a pragmatic approach is needed to select and apply mechanisms in order of importance, balancing simulation time cost and accuracy.

## CHAPTER III

### METHODOLOGY

This study developed an acoustic agglomeration CFD model capable of transient simulations by selecting and applying key mechanisms of acoustic agglomeration. The created AA CFD model was validated for reliability through experiments and reference studies. Additionally, sensitivity analysis allowed us to discern the trends in how AA mechanisms impact particle removal efficiency.

#### 3.1 Acoustic Agglomeration CFD Models

The general CFD simulations require an extensive time cost, even more so when analyzing acoustic agglomeration using CFD simulation. This is because in order to analyze acoustic agglomeration, two additional factors need to be considered: the number of particles to be analyzed, and the frequency of the acoustic waves.

##### Number of Particles to Be Analyzed

Particle collisions occur when the distance between two particles is equal to or smaller than the sum of their radii. To analyze these collisions, all pairs of particles in the objective space need to be considered. Even a slight increase in the number of particles can cause a significant increase in the number of particle pairs to consider for deciding pair collision. As a result, increasing the number of particles requires a substantial increase in simulation time cost.

##### Frequency of the Acoustic Waves

Acoustic waves cause pressure changes in the surrounding fluid, affecting the movement of particles in the fluid. When analyzing the movement of particles, dividing the time taken for pressure changes by a shorter time interval allows for a more accurate prediction of particle movement. A higher frequency of acoustic waves means more frequent pressure changes. As a result, analyzing the movement of particles influenced by acoustic waves takes more time with increasing frequency of the sound waves.

Due to the reasons listed above, as stated in the later part of the literature review chapter, there are limitations to analyzing acoustic agglomeration phenomena using CFD simulations. Therefore, this study has attempted to explore the method of analyzing acoustic agglomeration phenomena through CFD simulations focusing on simulation time cost.

This study contrived an acoustic agglomeration CFD model by following features.

Rather than meticulously implementing the actual movements of particles induced by acoustic waves, this study predicts the “agglomeration volume” formed by the movement of particles induced by the sound waves within one cycle of sound vibration. If a pair of particles are located in the volume, the pair of particles will collide with each other.

Since the only the very small particles can be moved by the waves, it is common to consider agglomeration occurring when collisions happen. However, collisions result in either agglomeration or repulsion. Therefore, to classify the results of collisions into two categories, the concept of critical velocity was applied for determining agglomeration or repulsion.

In this study, coalescences formed after collisions are considered to be a single, larger particle. Smaller particles are captured by larger particles and removed. This reduces the number of particles to be analyzed due to agglomeration phenomena, thus saving simulation time costs.

In addition, the commonly used concept of parcels were utilized.

### 3.1.1 Current OpenFOAM CFD Software

In this study, a CFD simulation program called Open Field Operation and Manipulation (OpenFOAM) was selected. The CFD software was chosen for two reasons.

First, as the name says, OpenFOAM is a program that allows the user to directly access the source code and modify the program based on the user’s intention. However, in the case of general commercial software, it usually does not allow users to modify their programs. From an open-source code, users get fundamentals behind the software operation and find a way to modify the solver. Therefore, using OpenFOAM is a more accessible way than using other software to create a new CFD solver.

Second, because it is free software, there are many users, meaning there is an abundant amount of simulation software code modifying works. The previous users’ work on software

coding could be stepping stones for developing a new AA CFD solver. This factor serves as a huge pool of sources for a literature review. Using software that has many users is similar to studying a famous research topic.

In general, CFD simulation process is as follows:

#### Pre-processing

##### Geometry and Meshing

A model including mesh information that serves as an object to CFD simulation is produced in the pre-processing stage. In this study, it was produced using a program called Salome.

#### Data Input

Users input the simulation variables in the form of a text file in the C++ style.

#### Processing

The CFD calculation procedure is conducted under the selected CFD solver and calculation settings. In this process, the geometry, mesh information, and boundary conditions of the model created in the pre-processing step are applied.

#### Post-processing

The simulation results are presented in tables such as vector plots, contour plots, data curves and streamlines. In this study, a software called ParaView is used as a post-processing tool.

### 3.1.2 New Combination of *DPMFoam* and *pimpleFoam*

For the preparation of the main stage of numerical research, it was decided to test a standard solver in the OpenFOAM CFD simulation package. This study had to consider the flow of the fluid medium and the flow of the fine particles simultaneously. Therefore, *DPMFoam* a basic solver equipped with a particle tracking function of a single type of particle was selected.

The solver is a transient solver, meaning users can verify motions of particles and fluid medium by user-specified time intervals.

However, problems were discovered during a simple test of the solver. When gravitational force was applied, the solver did not show correct results.



Figure 20 Gravity Issue from DPMFoam

The experimental device design was applied to the CFD simulation. As noted from the image above, it was confirmed that outside air was taken in from the upper part of the outlet and discharged to the lower part. In addition, the laminar flow was expected due to the very slow air velocity of 0.9 cm/sec at the inlet. However, for unknown reasons strong turbulence was observed throughout the experimental device.

To resolve these problems, this study decided to transplant the particle-tracking function of DPMFoam to another solver. Another OpenFOAM standard solver that can simulate the flow of a general fluid called pimpleFoam was selected. This is a transient solver which can calculate the flow of an incompressible fluid.

### 3.1.3 Composition of the New OpenFOAM - *pimAAFoam* Model Sets

This study created a model for the study of AA mechanisms' performance when transporting a fluid containing solid aerosols to a specific space. As the positions of aerosols change with the fluid flow, the repetitive vibration-induced refilling mechanisms have minimal impact on acoustic agglomeration. Consequently, the most crucial mechanism of acoustic agglomeration, orthokinetic interaction, was placed at the forefront.

Particle collision and agglomeration can occur not only due to sound waves but also due to fluid flow and interactions with walls. Therefore, the developed model consisted of three main parts:

- 1) Acoustic collision between aerosol particles
- 2) General collision between aerosol particles
- 3) Wall collision between particles and walls

The Acoustic Collision Model and the General Collision Model, responsible for analyzing particle collisions, was implemented in one file, while the Wall Collision Model was implemented in a separate file.

#### 3.1.4 Acoustic Collision Model

Figure 5 illustrates the mechanisms constituting the phenomenon of acoustic agglomeration. Acoustic agglomeration refers to the phenomenon where particle collisions occur due to ultrasound, leading to the formation of aggregates. Acoustic agglomeration mechanisms consist of the core mechanisms orthokinetic interaction and refilling mechanisms. Through the core mechanism of orthokinetic interaction, particles undergo direct collisions, forming aggregates. Refilling mechanisms serve as auxiliary mechanisms that move some particles beyond the distance where direct collisions occur, induced by repetitive ultrasound vibrations, within the range where direct collisions between particles can occur through orthokinetic interaction. The CFD acoustic agglomeration model developed in this study incorporates the mechanism of orthokinetic interaction where direct collisions occur between particles to develop the model.

Orthokinetic interaction is a phenomenon in which two particles, located in an agglomeration volume driven by an acoustic wave, form an aggregate. An agglomeration volume is determined by the characteristics of sound waves and the properties of two particles. This study developed a CFD solver that determines the collision and aggregation between particles by directly

calculating the agglomeration volume using physical characteristics of sound waves and the two particles. The AA results prediction process is shown in figure below:

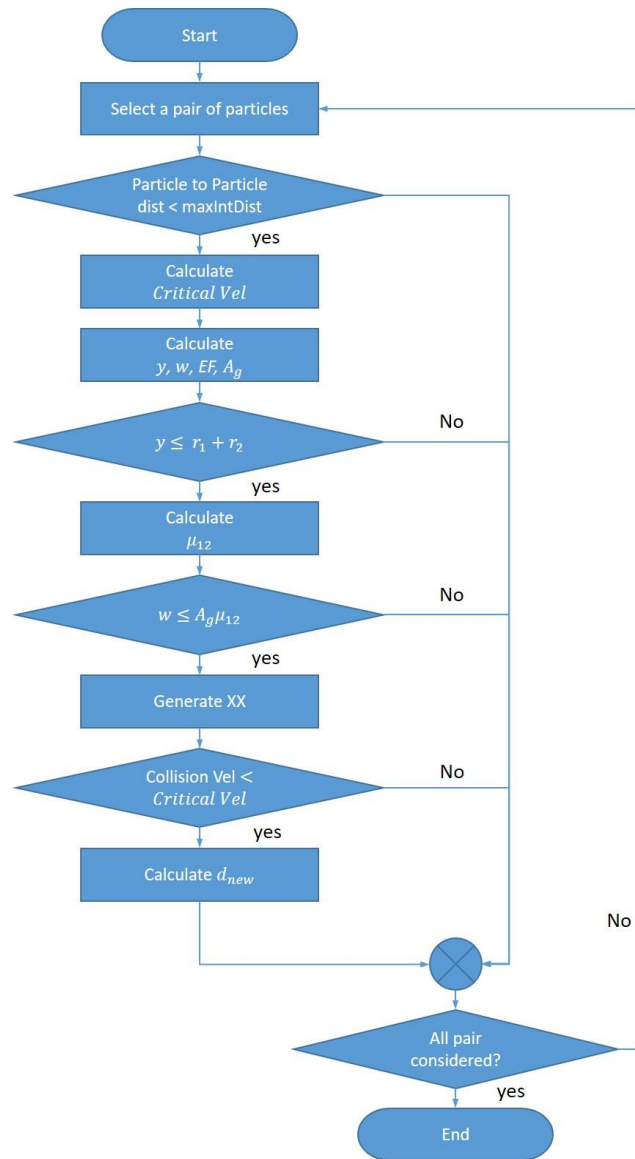


Figure 21 Structure of the Acoustic Agglomeration Model

If the selected pair of particles exceeds the specified maximum inter-particle distance, it is considered that there is no possibility of collision. Subsequently, the analysis begins for another pair. This is a process to save time in the simulation by skipping subsequent calculations for

pairs with no collision possibility. The particle to particle distance is calculated using equation 28.

$$d = \sqrt{(x_1 - x_2)^2 + (y_1 - y_2)^2 + (z_1 - z_2)^2} \quad (28)$$

Collisions between particles result in either rebound or agglomeration. The outcome of the collision can be determined by comparing it to the Van der Waals force. In this study, we have decided to apply the concept of critical velocity. The properties of the particles and their velocities at the time of collision are compared to determine the collision outcome. Detailed information regarding the "decide agglomeration after collision" can be found in the literature review section.

For two particles to collide through the orthokinetic interaction mechanism of acoustic agglomeration, they must exist within the agglomeration volume. To determine whether two particles are inside the agglomeration volume, information about the following is needed: 1) the perpendicular distance between the two particles, 2) the distance along the component of the ultrasound vibration direction between the two particles, 3) the entrainment factor of the two particles, and 4) the fluid displacement amplitude driven by sound vibration.

The below figure compares the perpendicular distance between the small particle and the line connecting a speaker and a large particle.

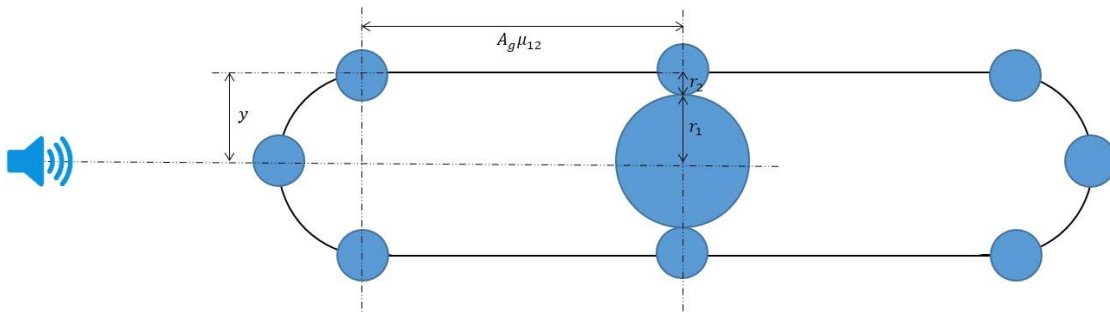


Figure 22 Agglomeration Volume Created by Sound Source and a Pair of Particles

If the shortest distance ( $y$ ) from the small particle to the straight line connecting the speaker and the large particle is greater than the sum of the radii of the two particles, the large

particle and small particle cannot contact each other during resonant motion caused by sound waves. Therefore, for acoustic agglomeration to occur,  $y$  must be less than the sum of the radii of the two particles. The magnitude of  $y$  in 3-D space can be obtained by the following equation. (“X” represents a cross product between vectors):

$$y = \frac{|\overrightarrow{SP_2} \times \overrightarrow{SP_1}|}{|\overrightarrow{SP_1}|}$$

( 29 )

Where,

$\overrightarrow{SP_1}$  : A vector from a speaker to the large particle

$\overrightarrow{SP_2}$  : A vector from a speaker to the small particle

Distance  $w$

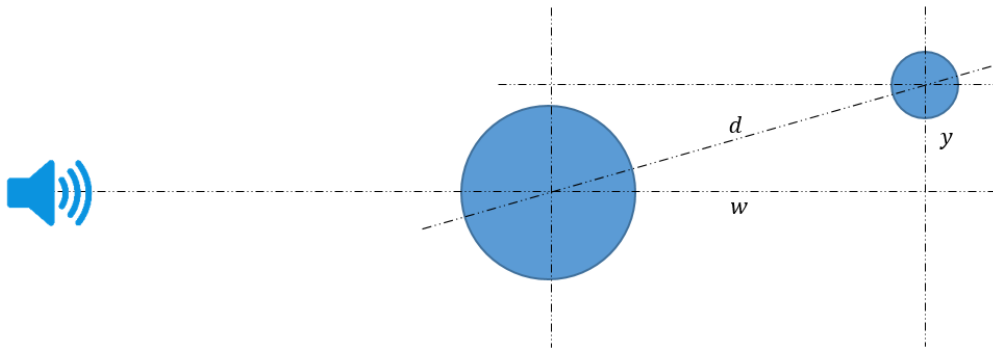


Figure 23 Distance  $w$  in the Sound Wave Direction

The difference in resonance amplitude between the two particles, due to the difference in the entrainment factor, is  $A_g(\mu_{p_2} - \mu_{p_1})$ . Additionally, due to the phase angle difference between the two particles, half height of the agglomeration volume is  $A_g\mu_{12}$ . The combined distance of the  $x$  and the resonance amplitude difference is the maximum distance at which a collision between two particles can occur according to the  $y$  distance. The distance between two

particles in the sound wave direction ( $w$ ) can also be calculated in a similar manner. If the  $w$  distance is within the combined distance of amplitude difference and the distance  $x$ , acoustic agglomeration can be expected.

#### Calculate Displacement of Fluid Medium by Sound Source

According to Eargle (2003), the intensity and decibel of a sound wave generated by a speaker at a specific point can be obtained by the following equation:

$$\text{SPL} = \varphi + 10 \times \log(\text{watt}) - 20 \times \log(x) \quad (30)$$

The dB value of the target location can be converted into a pressure value (Pascal) using the following relational equation. The reference pressure is  $2 \times 10^{-5}$  Pascal.

$$\text{dB} = 20 \log_{10} \left( \frac{P_{\text{rms}}}{P_{\text{ref}}} \right) \quad (31)$$

Finally, the actual displacement of fluid medium by the speaker at the target position is calculated by the following equation according to Carley (2001):

$$A_g = \Delta P / \rho_f c \omega \quad (32)$$

#### New Physical Properties of Particle Aggregates

When two particles combine into one larger particle through acoustic agglomeration, the properties of the particle are changed. In addition, if the two particles have different velocities before they merge, the velocity of the aggregates will have a different value.

Assuming that the volume of the existing two particles is conserved, the new radius value of the aggregate is as follows:

$$r_{\text{new}} = \sqrt[3]{\frac{3}{4}(V_1 + V_2)}$$

( 33 )

The size of the larger particle is adjusted as mentioned above in one pair of particles. The size of the smaller particle is set to 1.0e-37 meters, OpenFOAM “*VSMALL*” value.

Once the analysis of all pairs is completed within the current simulation time step, the analysis for the next time step begins. Before proceeding to the next time step, particles with a diameter of less than 1.0e-18 meters, OpenFOAM “*ROOTVSMALL*” value, are removed.

### 3.1.5 General Collision Model

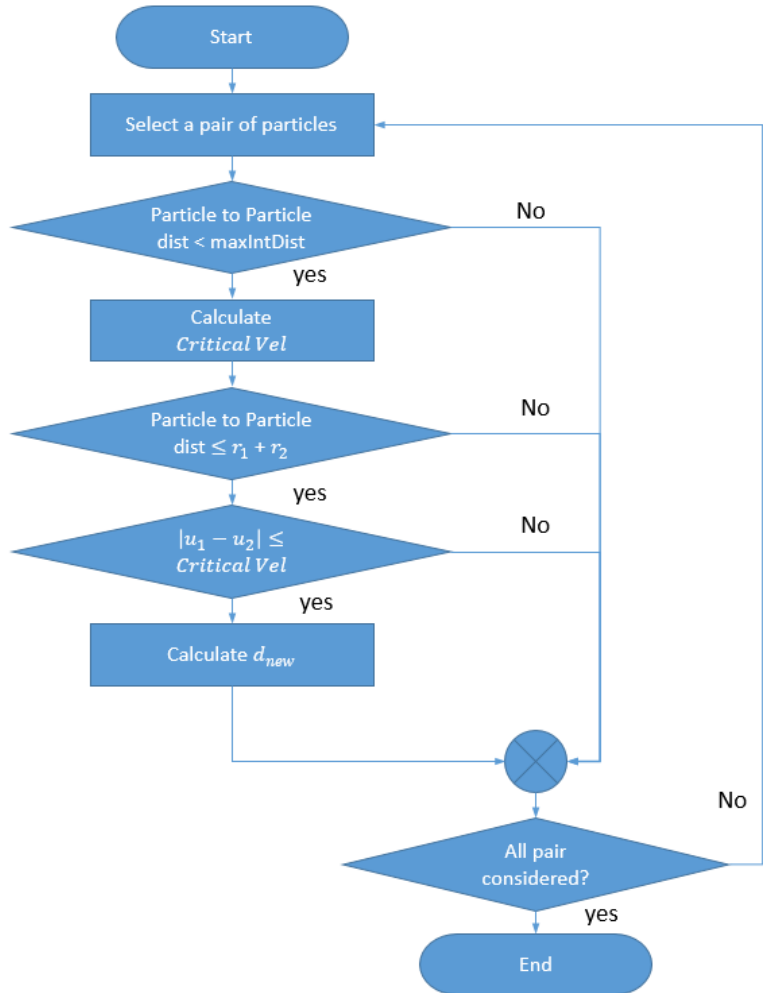


Figure 24 Structure of the General Collision Model

Collision analysis is performed in a manner similar to the Acoustic Agglomeration (AA) model. As aerosols move with the fluid flow, collisions between particles can occur due to differences in particle inertia, turbulent motion of the fluid, and other factors. Collisions occur when the distance between two particles becomes less than or equal to the sum of their radii. Similar to the AA model, critical velocity is used to predict the outcomes of collisions. If the velocity difference between two particles during a collision is greater than the critical velocity, they rebound and continue their individual motion.

In cases where agglomeration occurs, the size of the larger particle in one pair of particles is adjusted as per the equation mentioned above (33). The size of the smaller particle is set to  $1.0e-37$  meters.

Once the analysis of all pairs is completed within the current simulation time step, the analysis for the next time step begins. Before proceeding to the next time step, particles with a diameter of less than  $1.0e-18$  meters are removed.

### 3.1.6 Wall Collision Model

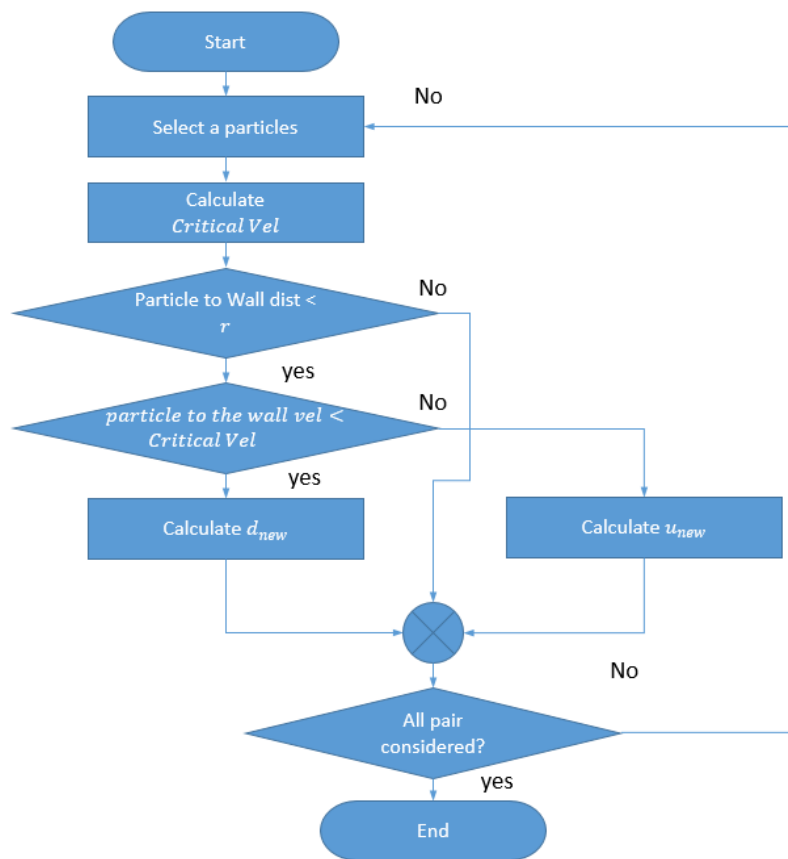


Figure 25 Structure of the Wall Collision Model

First, like the two models mentioned previously, we calculate the critical velocity for each particle. Collisions are determined based on the distance between particles and the wall.

After a collision, we compare the critical velocity with the collision velocity to decide whether the particles will adhere to the wall or rebound. If the particles bounce back after the collision, we consider the restitution coefficient of the particles to determine the rebound velocity, as shown in Figure 26.

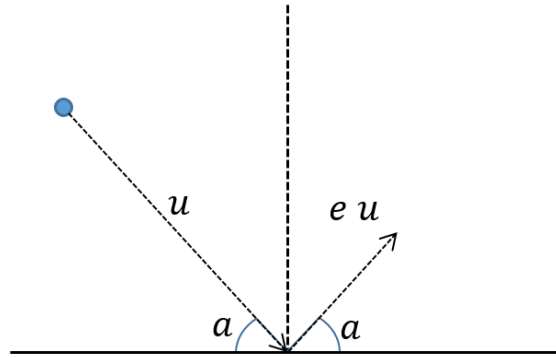


Figure 26 Particle to Wall Rebound

After a collision, when particles adhere to the wall, their velocity becomes zero. Subsequently, particles with zero velocity are removed from the simulation. If particles attached to the walls are not removed from the simulation domain, the time cost required for analyzing particle to particle collisions and collisions between particles and walls will continue to increase. As the number of particles attached to the walls or between particles increases, the number of particle pairs to be analyzed increases drastically, leading to a selection to suppress the increase in simulation time cost.

Detailed information regarding the Acoustic Collision model, General Collision model, and Wall Collision model codes can be found in the appendix section.

### 3.2 Model Validations

This is a process aimed at ensuring the reliability of the developed Acoustic Agglomeration CFD model. To secure the model's reliability, changes in the number concentration of aerosol particles based on their size due to the acoustic agglomeration phenomenon were compared. The comparison was made as aerosols traveled along a duct,

influenced by sound waves, in two distinct scenarios: 1) vertical movement and 2) horizontal movement.

For situations involving vertical fluid flow, we utilized experimental data from other researchers to evaluate reliability. Aerosol-laden fluids moved through a cylindrical duct installed vertically on the ground, and any changes in number concentration resulting from the influence of sound waves were measured. These measurements were then compared with the results obtained from the AA CFD model.

In addition to the reliability assessment under vertical conditions, a calibration process was conducted for the AA CFD model. This process involved analyzing the application of formulas that could potentially affect the results of the acoustic agglomeration simulation, as well as the approach for inputting simulation data.

To assess the reliability regarding horizontal movement, experiments were conducted that were specifically designed for this study and compared the measured values obtained with the data from the CFD simulation. Unlike the vertical reliability test, a different type of duct was used. The reliability was evaluated by comparing measurements from Section 1 taken before entering the sound section, and measurements from Section 2 that were collected before the exit. These measurements were then compared with the results from the CFD simulation.

In summary, reliability tests through reference studies included model calibration and the analysis of the simulation approach, while reliability tests through experimental studies involved analyzing the individual impacts of general collision, wall collision, and acoustic collision.

### 3.2.1 Mixed-Air Injection in a Vertical Straight Cylinder from Literature

Research conducted by Zhang et al. (2017) was selected as a reference study. In this study, particles move horizontally through a circular duct from top to bottom. A sound source is positioned in the upper part of the circular duct.

#### 3.2.1.1 Introduction of the Experiment from the Literature

In the reference research, the analysis of particle number concentration reduction was conducted under three conditions: 1) the influence of sound waves, 2) fine water mist, and 3)

sound waves with a fine water mist. However, it was the results from the first condition—the sound only case—that were chosen for the acoustic agglomeration model validation.

This setup involved fluid moving vertically through a circular duct with a speaker installed at the upper part of the duct. A mixture of air fluid and aerosols was supplied through the upper part of the duct and discharged through the lower part of the duct. Before the acoustically treated aerosol-laden fluid discharge, a measurement device was installed to measure the final particle concentration.

The duct had a diameter of 9.9 cm, and there is a measurement point 150 cm from the duct's entrance where particle concentration is measured. The intensity of the sound was measured at the center of the device, 75 cm from the entrance. The sound frequency was 1400 Hz and the sound pressure level was 144 dB.

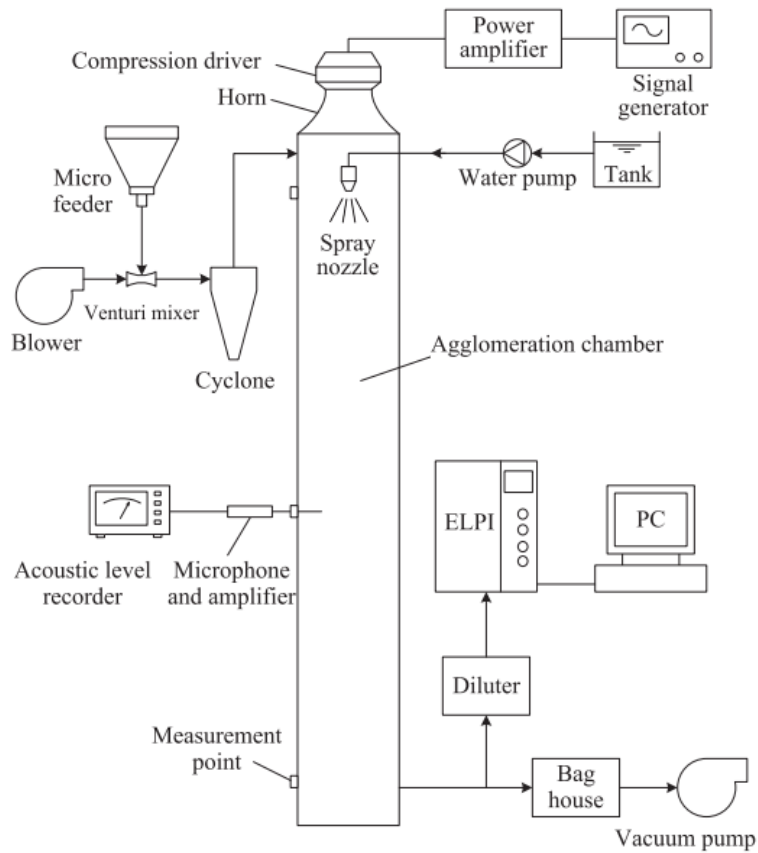


Figure 27 Design of Experimental Device in the Reference Research (Ref: Zhang, 2017)

### 3.2.1.1.1 Air Flow

The reference research established the residence time of the injected particles at 4 seconds as the baseline. The height of the device used in the experiment is 150 cm, and every 4 seconds, all fluid within the experimental equipment needs to be exchanged. This is equivalent to a constant flow of 37.5 cm/sec being supplied into the device through the upper surface of the cylindrical duct with a diameter of 9.9 cm. This corresponded to an airflow rate of 2.887 liters per second.

### 3.2.1.1.2 Particle Injection

In the experiments, fine particles were injected through the entrance of the device in 12 size-range, as indicated in Table 6 below.

$\mu\text{m}$	$\#/\text{cm}^3$	$\#/\text{sec}$	$\mu\text{m}$	$\#/\text{cm}^3$	$\#/\text{sec}$
0.021	2,288	6,604,125	0.483	73,308	211,612,121
0.04	3,622	10,456,798	0.76	61,983	178,921,236
0.071	5,666	16,356,210	1.226	87,756	253,318,307
0.119	16,315	47,093,970	1.945	43,953	126,875,073
0.201	24,027	69,356,375	3.078	32,354	93,394,954
0.315	47,932	138,361,822	6.274	23,718	68,465,762

Table 6 Particle Injection through the Inlet Surface

### 3.2.1.2 Calibration of the pimAAFoam Prototype Model

The CFD simulation model was developed by incorporating the critical concept of acoustic agglomeration “orthokinetic interaction”. However, during the process of validating the CFD model, a discrepancy between the measured results from the reference study and the CFD

simulation results was identified. This is evidence that the simulation does not accurately reflect reality. Therefore, it necessitates the need for CFD model calibration and potential changes in the modeling approach. In this study, a sequential process of model calibration and alterations in the modeling approach were carried out to progressively achieve similar results with the actual data.

There are various models available for explaining the phenomenon of acoustic agglomeration, and these models have continued to evolve to achieve higher levels of accuracy compared to their predecessors.

In the process of applying variables to interpret acoustic agglomeration, there can be instances where the actual influences of specific variables are either overestimated or underestimated. Consequently, the process of applying these variables to the model was re-evaluated. During this review process, issues were identified in determining the effective diameter. Furthermore, while revalidating the model for the acoustic agglomeration phenomenon, it was discovered that there are models with accuracy. As a result, the model for determining the height of the agglomeration volume was replaced by considering more factors.

### 3.2.2 Mixed-Air Injection in a Horizontal Straight Duct in Laboratory

Particles generated by burning an incense stick and fan generates main air flow through the straight horizontal duct. Two measurement sections, pre-treatment measurement and post-treatment measurement, are prepared. The pre-treatment measurement was prepared for by deciding initial particle concentration depending on particle size. After being treated by sound, which is located at the top of the duct, the post-measurement section measured particle concentration which was affected by acoustic agglomeration phenomenon.

#### 3.2.2.1 Introduction of the Experiment in the Laboratory

The overall configuration of the experimental apparatus is depicted in the following Figure 28. It spans a total length of 234 cm (92.13 inches).



Figure 28 Whole Experimental Device Configuration in the Laboratory

In contrast to the previous validation process that used a cylindrical duct, a rectangular duct was employed this time. At the starting point of the experimental setup, an incense stick was ignited to generate particulate matter. A fan was positioned at the subsequent point to induce airflow throughout the experimental apparatus. A speaker was placed at the upper center of the duct to induce the acoustic agglomeration phenomenon. The outlet at the endpoint allowed the expulsion of particles to the outside.

The experimental set-up is structured in the following sequence:

1. Particle Generation
2. Fan
3. Pre-Treatment Measurement
4. Sound Generation
5. Post-Treatment Measurement

#### 3.2.2.1.1 Main difference between ASHRAE 52.2 and Experiment in the Laboratory

The experimental setup conducted in this study aims to explore the phenomenon of acoustic agglomeration. Therefore, it differs significantly from the configuration for rating air filtering products. The following table summarizes the main differences between the test facility standards presented in ASHRAE 52.2-2017 Method of Testing General Ventilation Air-Cleaning Devices for Removal Efficiency by Particle Size and the experiments used in this study.

	ASHRAE 52.2	Experiment
Face Area	61 × 61 cm (Rectangular)	15 × 15 cm (Rectangular)
Airflow Rate	0.22, 0.93, 1.4 $m^3/sec$	0.00045 $m^3/sec$
Particles	Potassium Chloride (KCl) A2 Arizona Test Dust, Powdered Carbon, Milled Cotton linters	Burning Incense Stick
Particle Counter	12 Channel (0.3 $\mu m$ ~ 10 $\mu m$ )	6 Channel (0.3 $\mu m$ ~ 10 $\mu m$ )
Inlet Filter	HEPA	None
Measuring Points	9	4
Pressure Measurement	O	X

Table 7 Comparison between ASHRAE 52.2 and Experimental Settings

#### Face Area

Both ASHRAE 52.2 and the experimental setup used in this study employed rectangular-shaped ducts. However, the face area of the duct used in this study, approximately  $225\text{ cm}^2$ , is roughly 6% compared to the ASHRAE standard of  $3721\text{ cm}^2$ .

#### Airflow Rate

In contrast to the recommended airflow rates by ASHRAE, ranging from  $0.22\text{ m}^3/sec$  to  $1.4\text{ m}^3/sec$ , the study used a significantly lower airflow rate of  $0.00045\text{ m}^3/sec$ , which is approximately 0.048% of  $0.93\text{ m}^3/sec$ .

#### Particles

While ASHRAE standards use Potassium Chloride (KCl), A2 Arizona Test Duct, Powdered Carbon, and Milled Cotton Linters, this study employed a simpler method to generate particles compared to ASHRAE. For the experiments, particles were generated by burning incense sticks.

#### Particle Counter

Both ASHRAE and the study used optical aerosol particle counters capable of measuring particles ranging from 0.3  $\mu\text{m}$  to 10  $\mu\text{m}$ . However, while ASHRAE employs a particle counter with 12 channels corresponding to 12 size ranges, this study used a particle counter with 6 channels.

#### Inlet Filter

The inlet filter prevents particles other than those generated for measurement from entering the duct. While ASHRAE standards recommend its installation, this was not done in the experiments conducted for this study. Despite the absence of an inlet filter, relatively consistent particle concentrations were observed across multiple measurements.

#### Measurement Points

ASHRAE standards divide the duct's cross-sectional area into 9 zones to measure fluid velocity and particle concentration. In the experiments conducted in this study, measurements were taken at 4 points located at regular intervals along the vertical direction of the duct.

#### Pressure Measurement

ASHRAE standards include pressure measurement primarily because ASHRAE Standard 52.2 mainly focuses on rating fibrous air filters. Evaluation criteria include not only particle removal efficiency but also pressure drop through the filter and pressure drop changes, which are essential for assessing the filter's grade and performance rating. However, since acoustic agglomeration-based air filtering methods do not cause pressure drop through the filter, pressure measurement is unnecessary.

### 3.2.2.1.2 Particle Generation

Fine particles are generated by burning incense sticks in this study. From Ji (2010), Cheng (1995), Cohen (2013), and Vu (2017), the average density of smoke particles from burning incense sticks is  $1.08 \text{ mg/mm}^3$ .

### 3.2.2.1.3 Fan

A variable air flow fan of 8 cm by 8 cm (3.15 inches by 3.15 inches) was located at the center of the duct to produce the air stream in the device. The fan produced an air flow with a cross-sectional area average velocity of 2 cm/sec to 14.5 cm/sec. As shown in the figure below, a square tube and additional planes were installed around the fan as a guide to stabilize air flow.

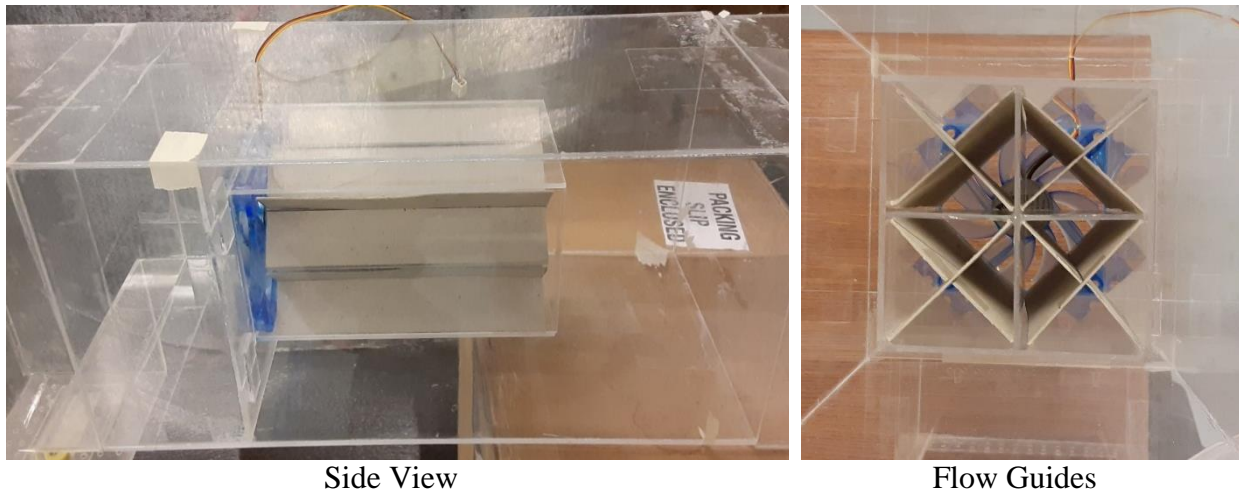


Figure 29 Fan Section

### 3.2.2.2.4 Measurement

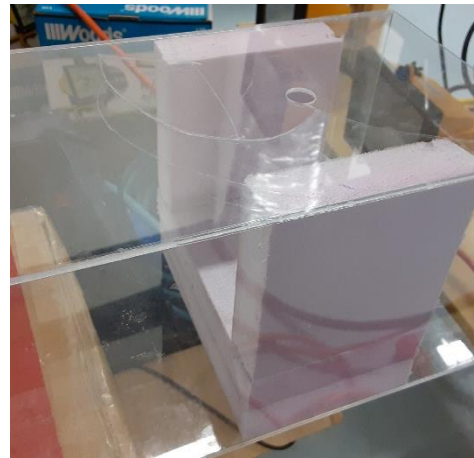
Air velocities and particle number concentration per unit volume were measured at two specific positions. The initial measurement took place in the pre-treatment measurement section,

situated before the sound treatment was administered. The subsequent measurement was conducted in the post-treatment measurement section, located after the sound treatment. At each measurement position, obstacles were installed to create channels with a cross-sectional area of 10 cm by 10 cm and a length of 10 cm.

This study collected air velocity and particle number concentration data at 4 points along a vertical axis at each measurement section. Measurements were obtained at intervals of 2 cm, 4 cm, 6 cm, and 8 cm from the top of the duct. The first measurement section was located 62 cm (24.41 inches) away from the fan, while the second measurement section was 10cm (3.94 inches) before the end of the experimental device.



Pre-Treatment Measurements



Post-Treatment Measurements

Figure 30 Pre & Post Treatment Measurement Section

### 3.2.2.2.5 Sound Generation

The speaker was located 45 cm (17.72 inches) away from the first measurement position and installed at the top of the device. The sound signal generated by a PC was amplified through an audio amplifier, converted into sound waves through the speaker, and propagated inside the experimental device.

To maximize the impact of sound waves on aerosols, the channel where the speaker was located was set to be narrower than the rest of the duct. The cross-sectional area of the narrow

channel was 4 cm by 4 cm. This allowed the aerosols to flow closer to the speaker, thus enhancing the impact from the sound source.

The sensitivity of the Pyle Dryver PDBT 58 speaker used is 109 dB/watt meter. This speaker is suitable for producing sound in the frequency range of 2-25 kHz. The experiment and simulation were conducted under conditions where the characteristics of the sound wave were 2500 Hz with 500 watts of electricity being supplied to the speaker. Pyle Pro PT6000CH was used as an amplifier to receive signals from the PC and transmit the signal in the form of electricity to the speaker. The maximum power from the amplifier to the speaker is 700 watts with a sound-to-noise ratio of 81 dB.

### 3.2.2.2.6 Measurement Device and Pre-Treatment Measurements



Particle Counter



Anemometer

Figure 31 Measurement Devices: Particle Counter and Anemometer

To collect air velocity data, this study chose a TSI 9545 Air Velocity meter with a measurement error of  $\pm 3\%$  of reading or  $\pm 3$  ft/min ( $\pm 0.015$  m/s), whichever is greater. When

measuring wind speed, it had an average value of 2 cm/sec. The measuring accuracy could be approximately 75%. According to the measured data, the average values and uncertainties for air flow speed were  $2.23 \pm 0.12$  cm/sec,  $2.03 \pm 0.16$  cm/sec,  $1.83 \pm 0.12$  cm/sec, and  $1.42 \pm 0.19$  cm/sec at distances of 2 cm, 4 cm, 6 cm, and 8 cm from the top of the duct, respectively.

A Fluke Particle Counter 983 was selected to measure the concentrations of fine particles by size. The counter is equipped with 6 channels, and each channel counts the number of particles of different sizes. The particle diameter sizes covered by the counter are 0.3  $\mu\text{m}$ , 0.5  $\mu\text{m}$ , 1.0  $\mu\text{m}$ , 2  $\mu\text{m}$ , 5  $\mu\text{m}$ , and 10  $\mu\text{m}$ . The counting efficiency for 0.3  $\mu\text{m}$  particles is 50%, and the efficiency for particles of 0.5  $\mu\text{m}$  or bigger is 100%. The measured average values with uncertainty for the particle concentrations were  $527086.25 \pm 1098.05$ ,  $491050.50 \pm 272.47$ ,  $240638.13 \pm 462.77$ , and  $80764.63 \pm 520.31$  for 0.3  $\mu\text{m}$ , 0.5 $\mu\text{m}$ , 1.0  $\mu\text{m}$ , and 2  $\mu\text{m}$  particles, respectively.

The particles ranging from 0.3  $\mu\text{m}$  to 2.0  $\mu\text{m}$  used in the experiment are distributed uniformly within the measurement locations of the duct, regardless of height. This is similar to the results of Figure 55 of the subsequent sensitivity analysis. The sensitivity analysis and this case analyze particles with similar density. It can be visually confirmed in Figure 56 that particles smaller than 2.5  $\mu\text{m}$  are evenly distributed in the duct. Therefore, it can be expected that the particles analyzed in the case of mixed-air injection in a horizontal straight duct are also evenly distributed. This could also be confirmed from the measurement results below.

#### Pre-Treatment Measured Data

##### Air Flow

cm from the top	1	2	3	4	5
2	2.03	2.54	2.54	2.03	2.03
4	2.03	2.03	2.03	1.52	2.54
6	1.52	2.03	1.52	2.03	2.03
8	1.02	1.52	2.03	1.02	1.52

Table 8 5 Air Flow Profile at Pre-Treatment Measurement

The measured air velocity at 2 cm intervals in the pre-treatment location was as depicted in Table 8. The average wind speed from the 5 measurements in the measured area of 10 by 10 cm was 1.878 cm/sec.

In order to measure the flow velocity, an anemometer with a resolution of 1.0 ft/min, which is approximately equivalent to 0.5 cm/sec, was used. This is on the condition that even a small fluctuation of measurement can greatly affect the stability of experimental conditions which use a slow air flow. The measurement error is  $\pm 3\%$ , which can also affect the measured values. Therefore, measurements were taken multiple times. The average values of the measured data were selected as the input values for the simulation to conduct the research.

### Particle Distribution

In the pre-treatment measurement, two data sets for four points in the location were produced. This simulation inputs the average values for each size particle. However, input values for sizes of 5  $\mu\text{m}$  and 10  $\mu\text{m}$  particles were excluded for the analysis because their number concentrations were too small to be considered.

$\mu\text{m}$	cm from Top								Average
	Data set #1				Data set #2				
	2	4	6	8	2	4	6	8	
0.3	528687	528196	526902	527654	519645	528765	531654	525187	527086.25
0.5	492028	491450	490142	491623	492013	490354	489760	491034	491050.50
1.0	238096	241355	240915	240764	239056	241034	240873	243012	240638.13
2.0	77592	81994	82690	80587	79532	80364	81037	82321	80764.63
5.0	2	3	0	2	1	2	1	2	1.63
10.0	0	0	0	0	1	0	0	1	0.25

Table 9 Particle Concentration in Pre-Treatment Measurement [# / Liter]

Particle concentrations were measured using a handheld particle counter. The number of particles by size per liter was measured, and it took 21 seconds for each measurement at each point. It took at least 90 seconds or more to complete one data set of particle concentration. As

shown in Table 9, the particle concentration generally remained constant during the measurements.

### 3.2.2.2 Comparison between Measured Data and Simulation Results.

By comparing the measured data with the values obtained from simulations in the case of the mixed-air injection in a horizontal duct, the validity of the simulation model, pimAAFoam, is confirmed. This ensures the model's validity in both horizontal and vertical scenarios.

In addition, under experimental conditions, investigation of impact of each collision model on the reduction of particles caused by collision and agglomeration effect was conducted.

### 3.3 Design of Sensitivity Analysis

Using the reliable AA CFD model, a sensitivity analysis of the acoustic agglomeration phenomenon under horizontal movement conditions is conducted. Through sensitivity analysis, the priority and trends of various factors influencing the acoustic agglomeration phenomenon are examined.

	Cases					
dB	145 dB		150 dB		155 dB	
Air Flow	3 cm/sec	4 cm/sec	5 cm/sec	6 cm/sec	7 cm/sec	
Initial Concentration	200,000 /cm <sup>3</sup>		250,000 /cm <sup>3</sup>		300,000 /cm <sup>3</sup>	
Sound Frequency	500 Hz	1000 Hz	1500 Hz	2000 Hz	2500 Hz	3500 Hz

Table 10 Test Matrix for the AA Sensitivity Analysis

As depicted in Table 10, simulations were carried out for each variable type, resulting in three cases for each. A total of 17 simulations were performed. The base-case employs input values corresponds to the following values for the variable.

- Sound intensity: 150 dB
- Air flow: 5 cm/s
- Initial particle concentration: 250,000/cm<sup>3</sup> (for each 0.3, 0.5, 2.5, 10.0 μm particles)
- Sound frequency: 2,000 Hz

CHAPTER IV  
MODEL VALIDATION USING REFERENCE RESEARCH

4.1 Simulation

4.1.2 Geometry and Grid Study for the CFD Simulation

The experimental setup used in the reference research was implemented for CFD simulation as follows:

4.1.2.1 Geometry

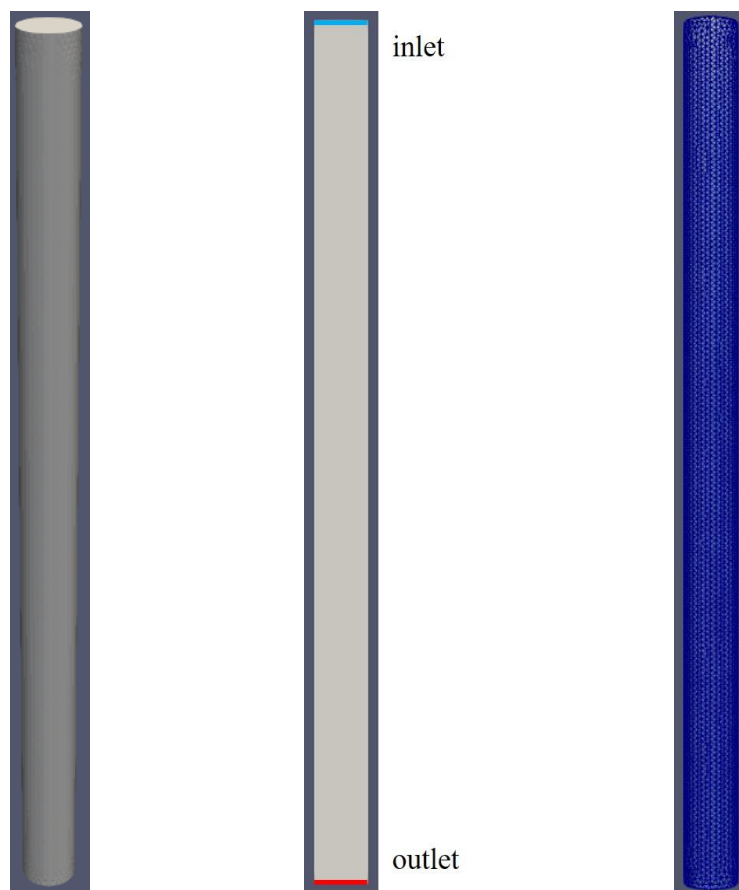


Figure 32 Geometry and Selected Mesh for Mixed-Air Injection in a Vertical Straight Cylinder from Literature

Based on the information presented in the reference research, geometry was created as shown in Figure 32. The duct diameter was set to 9.9 to match the actual experimental equipment. However, geometry for the CFD simulation set the height of the duct to 160 cm, which included an additional 10 cm compared to the actual length of 150 cm. The particle number concentration in this additional 10 cm section was counted and compared to the experimental results. The rightmost picture in the Figure 32 represents the mesh model selected after grid study for the model calibration procedure in this chapter.

Fine particles were introduced through a particle inlet surface with the same diameter as the duct at the top, 1 mm from the top of the cylindrical duct.

#### 4.1.2.2 Grid Study

To ensure the accuracy of the fluid flow analysis, a grid study was conducted. Information about the three mesh settings used is documented in Table 11.

	Minimum Length	Maximum Length	Growth Rate	Total Cells
Coarse	2	2	NA	6,532
Mid	1	2	0.3	36,974
Fine	1	1	NA	47,296

Table 11 Meshes for Grid Study

After conducting simulations corresponding to a 20-second scenario—equivalent to the reference research’s experiment—a comparison of flow profiles was made for three different mesh settings. The fluid passing through the experimental device had a velocity of 37.5 cm/sec, and every 4 seconds, the all of the fluid was exchanged. The analysis of air velocity at five evenly spaced locations of 5 cm above the bottom part of the device is shown in Figure 33 below.

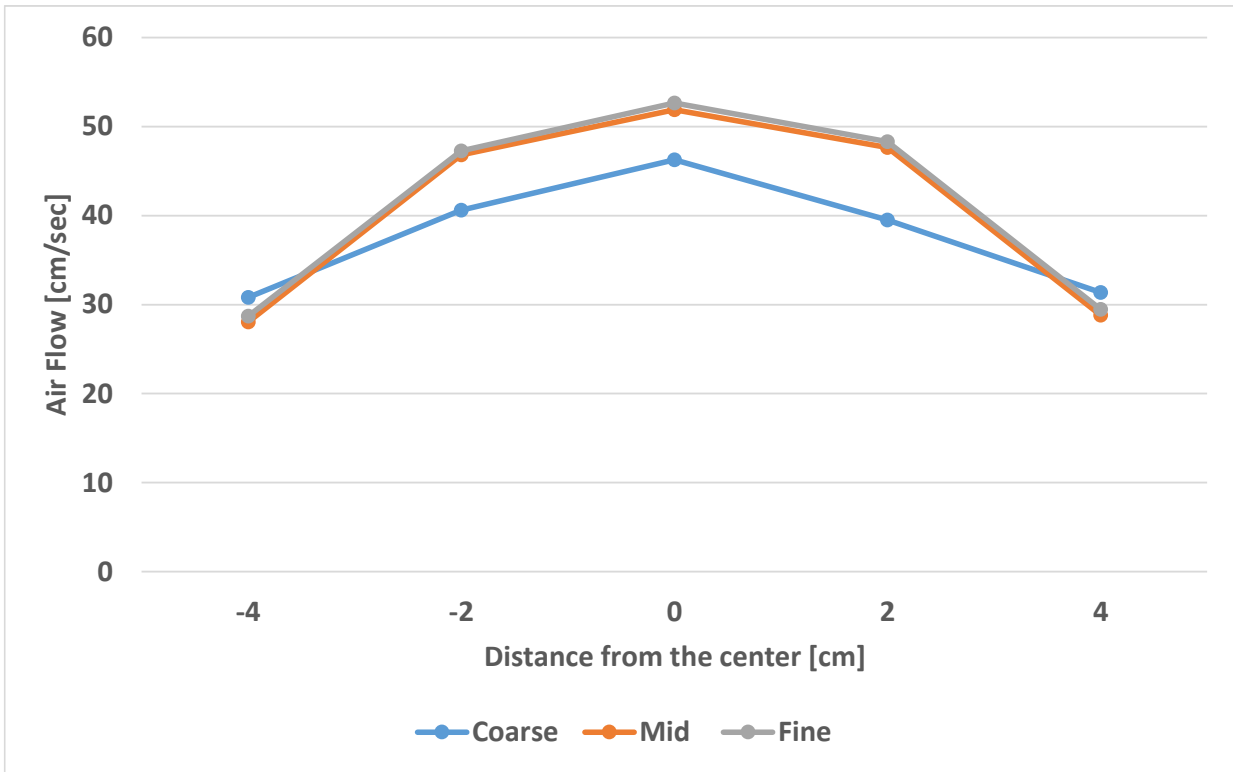


Figure 33 Comparison of Velocity Profile from the Three Mesh Settings

The analysis of flow profiles through simulations with the three different mesh settings showed significant differences when compared to the coarse mesh setting in relation to both mid and fine mesh settings. The reliability of simulation results with coarse mesh settings cannot be ensured. However, there was no significant difference between mid-mesh and fine-mesh settings. Therefore, to ensure an appropriate level of reliability for this study relative to the time cost by simulations, the mid-mesh setting was selected.

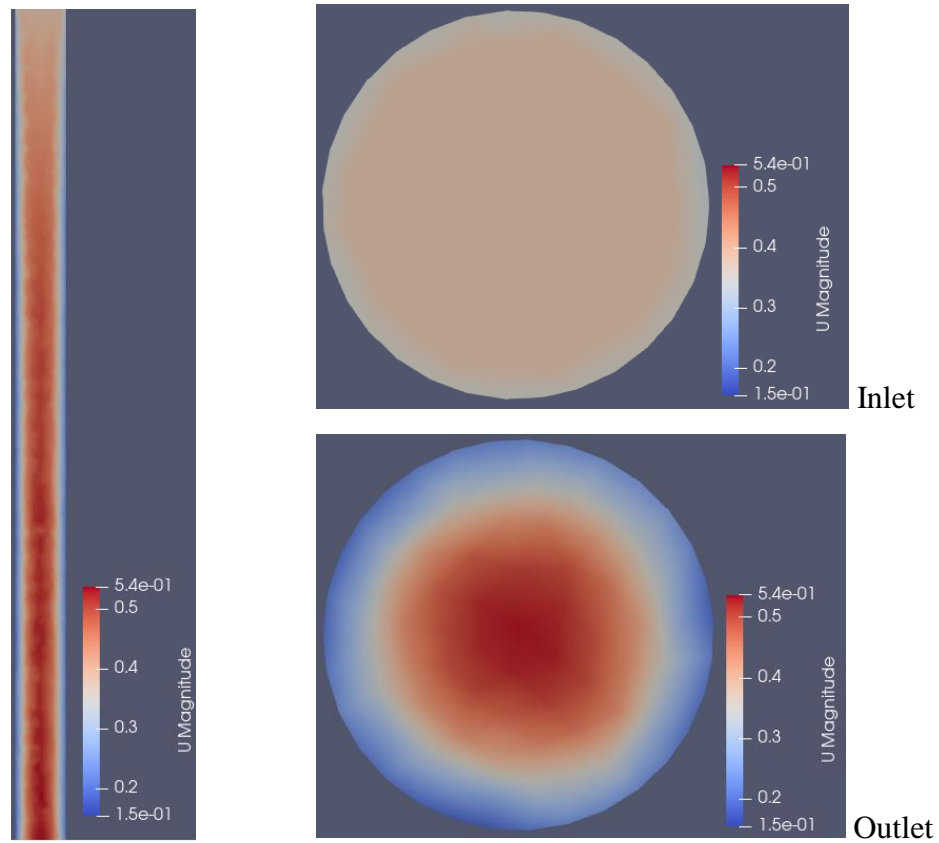


Figure 34 Air Flow Pattern of the Model at 20 Second [m/sec]

#### 4.1.3 Air-Flow and Particle Results Stabilization

In order to get the stabilized results of fluid flow and the entrained particles, a certain amount of time is required. Figures below contain information on the time required for the stabilized results under the conditions used in the reference research.

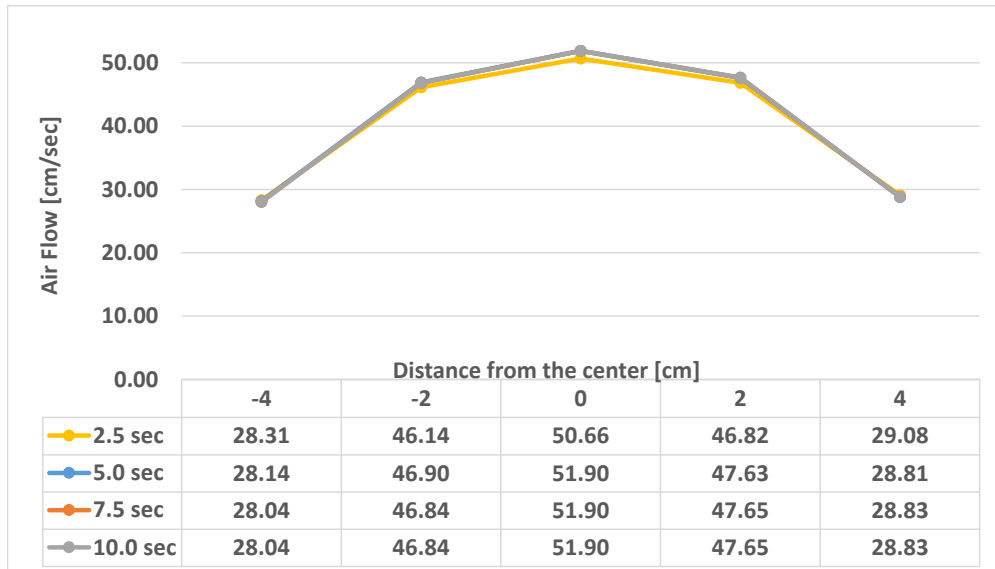


Figure 35 Required Time for Stabilizing Air Flow Results at 10 cm from the Bottom

Figure 35 represents the changes in the velocity profile over time at a distance of 10 cm from the bottom of the experimental apparatus. The air velocities at five points spaced every 2 cm apart from the center of the cylindrical duct are schematically described. According to the figure, the air flow almost stabilized between 2.5 seconds and 5 seconds.

Particles were introduced into the experimental device at a constant rate starting at 4 seconds. As shown in the visual results in Figure 36, after 3.5 seconds of particle injection, the aerosols reached the bottom. At the points corresponding to 19 seconds and 20 seconds, the particles exhibited a uniform distribution.

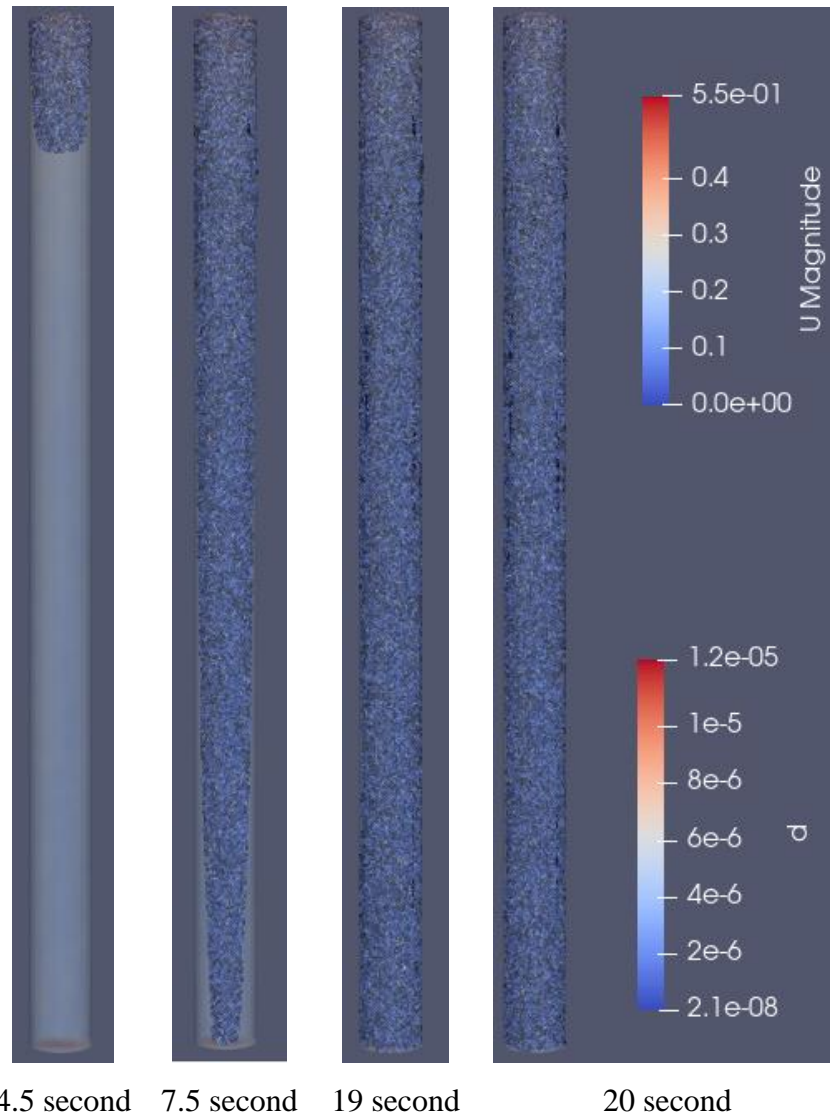


Figure 36 Dispersion of Particles over Time [m/sec, meter]

Figure 37 represents the concentration of particles in the space corresponding to the bottom 10 cm of the CFD simulation domain, showing results for the total number of particles regardless of their size. The results for the particles stabilized after approximately 17 seconds. After this, minor fluctuations were still observed. Therefore, the average value of the results for the three time steps was used in the following research process:

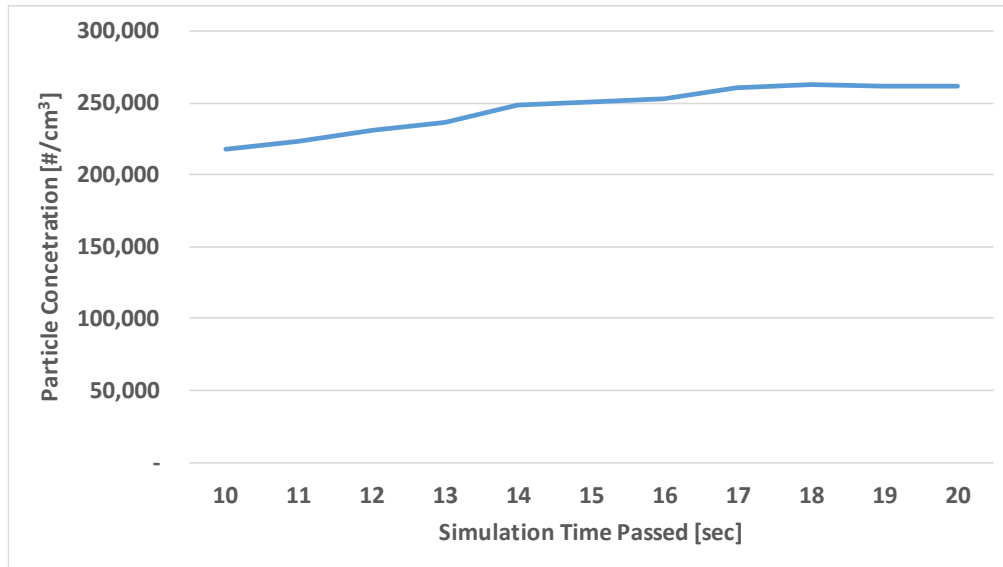


Figure 37 Required Time for Stabilizing Particle Results within 10 cm from the Bottom

## 4.2 Model Calibrations Process and Results Comparison

In this study, the calibration process adopted a step-by-step approach, adding individual elements incrementally. At each step, the goal was to reduce the differences between the experimental data and the simulation results.

### 4.2.1 Simulation Time Intervals and Particle Properties

#### 4.2.1.1 Simulation Time Interval

The initial simulation employed two different time step settings, one with a maximum Courant number of 0.35, and the other with a maximum of 0.0009 seconds. Setting the CFD simulation with a maximum Courant number ensures that the fluid velocity in each cell is calculated to be below a specified value concerning the characteristic length of each cell in the simulation domain. While there are minor fluctuations in the fluid flow through the whole simulation domain at every time step, the time step varies slightly. The OpenFOAM program selects the smaller time step value of the two time step settings for the simulation. In this study,

the time step used was maintained at approximately 0.000872 seconds throughout the simulation, except exact time step calibration stages.

#### 4.2.1.2 Particle Properties

The particles used in the simulation was fly ash, and its characteristics, as shown in Table 12, were input.

Particle Restitution Coefficient	0.01
Hamaker Constant	1.24e-19 Joule
Material Limiting Contact Pressure	0.41e+9 Pascal
Minimal Contact Distance	0.0004 $\mu\text{m}$
Particle Density	2500 $\text{kg}/\text{m}^3$

Table 12 Particle Characteristics

Initially, each parcel contained 50,000 particles. The simulation began with particles being introduced after 4 seconds to match the residence time used in the experiments. Since the 4-second particles were continuously injected with a constant amount for 11 seconds until reaching 15 seconds. The simulation reports were generated at 0.5-second time intervals, and the averaged values of the results corresponding to the last three time steps (19, 19.5, and 20 seconds) were used for analysis.

#### 4.2.2 Calibration Process and Results Comparison

The red solid line and red dotted line represent the input and measured values specified in the reference research, respectively. The red solid line indicates the quantity of particles introduced through the inlet surface based on the particle size. The red dotted line represents the measured values after inducing acoustic agglomeration by operating the speaker located at the top of the experimental setup.

Except the two red lines, the remaining lines depict the results generated by the developed model. Particularly, the black dashed line represents the final result of CFD simulation that went through the whole stage of calibration procedure.

All the results in the simulation are extracted from the 10cm of the bottom part of the cylindrical duct.

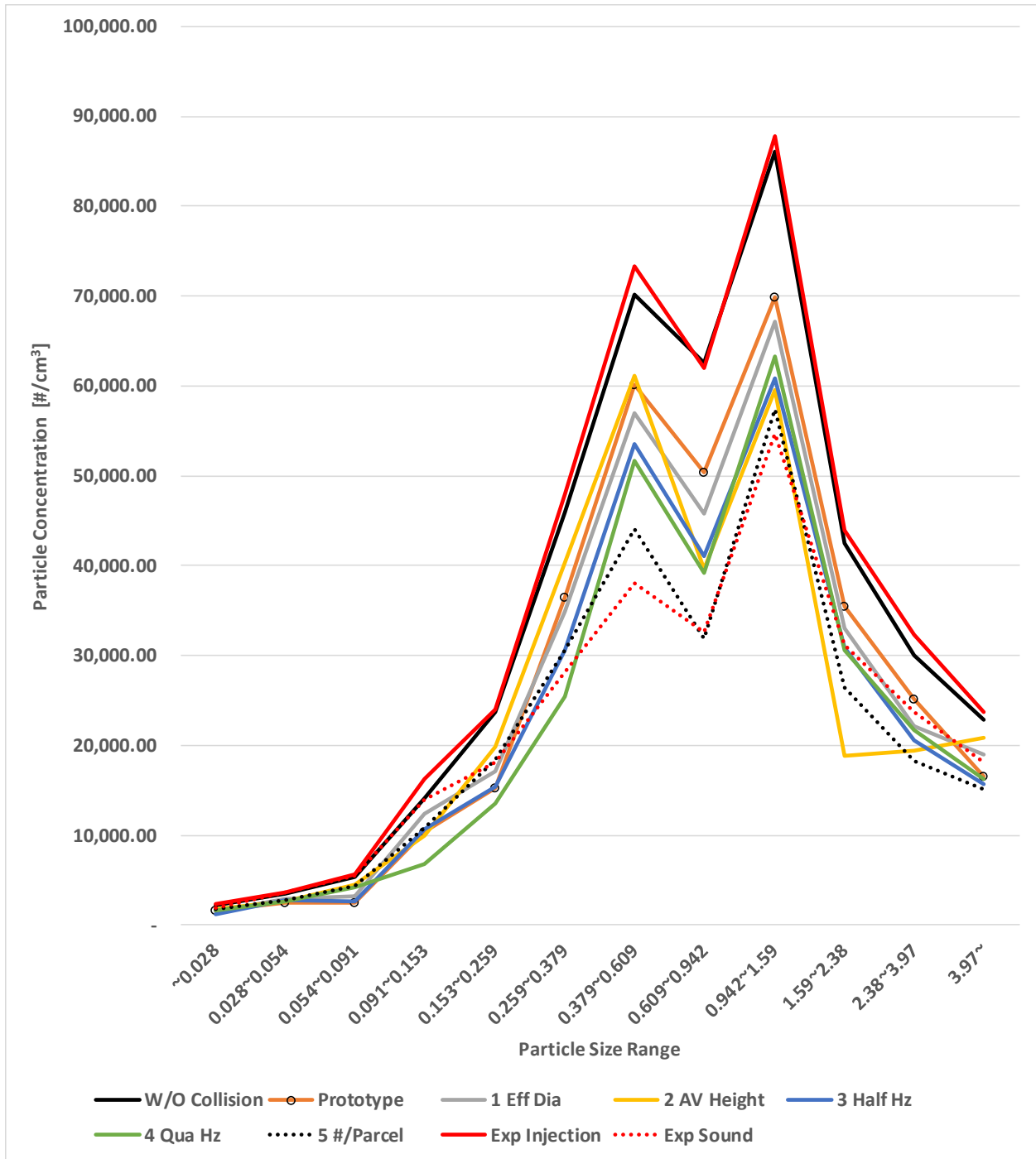


Figure 38 Results Comparison between Stacked Calibration Procedures and Experiments

$\mu\text{m}$	W/O Collision	Prototype	1 Eff Dia	2 AV Height	3 Half Hz	4 Qua Hz	5 #/Parcel	Exp Injection	Exp Sound
~0.028	2,195.78	1,697.48	1,454.98	1,753.77	1,204.91	1,625.49	1,826.31	2,287.83	1,866.39
0.028~0.054	3,446.92	2,447.70	2,849.34	2,684.79	2,796.29	2,568.95	2,712.94	3,622.49	3,651.02
0.054~0.091	5,377.84	2,531.06	3,235.82	4,481.87	2,614.42	4,205.81	4,372.53	5,666.19	5,530.20
0.091~0.153	14,108.73	10,306.13	12,420.40	9,981.35	10,616.82	6,774.76	10,874.48	16,314.50	13,922.61
0.153~0.259	23,678.11	15,224.27	17,073.31	19,811.14	15,345.52	13,583.63	18,376.73	24,026.74	18,082.92
0.259~0.379	45,862.86	36,503.39	34,896.84	40,401.74	30,577.37	25,496.29	30,622.83	47,931.91	28,140.77
0.379~0.609	70,095.55	60,048.34	56,979.23	61,165.56	53,470.60	51,674.61	44,013.22	73,307.60	38,105.95
0.609~0.942	62,551.25	50,424.24	45,763.74	39,578.99	41,035.05	39,193.59	31,873.21	61,982.68	32,639.41
0.942~1.59	86,054.84	69,907.36	67,194.42	59,498.39	60,768.25	63,303.10	57,426.34	87,755.64	54,722.24
1.59~2.38	42,446.25	35,427.31	33,002.34	18,815.17	30,895.64	30,634.20	26,394.29	43,952.62	31,182.01
2.38~3.97	30,013.94	25,196.96	22,067.23	19,334.81	20,528.89	21,745.17	18,308.53	32,354.29	23,776.85
3.97~	22,902.98	16,520.11	19,036.02	20,872.07	15,641.06	16,288.98	15,034.82	23,718.21	18,153.70
total	408,735.05	326,234.34	315,973.69	298,379.66	285,494.84	277,094.59	261,836.22	422,920.69	269,774.06

Table 13 Results Comparison between Stacked Calibration Procedures and Experiments [ $\#/cm^3$ ]

#### 4.2.2.1 W/O Collision

"Exp Injection" represents the initial value of particle injection. "CFD Tracking" corresponds to values extracted when particles are introduced through the inlet surface without activating the speaker in the CFD simulation.

The experimental initial (Exp Injection) values were used for the injection of particles. The collected values of particle concentration from those located within 10 cm of the bottom of the cylindrical duct are presented in the Table 14 below.

The overall particle count decreased by 3.35% compared to the input value. The segment with the most significant difference is the range from 0.091  $\mu\text{m}$  to 0.153  $\mu\text{m}$ , which was measured to be 13.52% less than the input value.

$\mu\text{m}$	Exp Injection	W/O Collision	% Difference
~0.028	2287.83	2195.78	-4.02%
0.028~0.054	3622.49	3446.92	-4.85%
0.054~0.091	5666.19	5377.84	-5.09%
0.091~0.153	16314.50	14108.73	-13.52%
0.153~0.259	24026.74	23678.11	-1.45%
0.259~0.379	47931.91	45862.86	-4.32%
0.379~0.609	73307.60	70095.55	-4.38%
0.609~0.942	61982.68	62551.25	0.92%
0.942~1.59	87755.64	86054.84	-1.94%
1.59~2.38	43952.62	42446.25	-3.43%
2.38~3.97	32354.29	30013.94	-7.23%
3.97~	23718.21	22902.98	-3.44%
Total	422920.69	408735.05	-3.35%

Table 14 Particle Inlet and Extracted Value at the Lower Part of the Experimental Device  
[ $\#/cm^3$ ]

#### 4.2.2.2 Prototype Model

These are the analysis results for the acoustic agglomeration phenomenon using the first prototype model without conducting the calibration process. In simulation using the prototype model, factors corresponding to Table 15 were applied. Subsequently, through the step-by-step stacking of factors in the calibration process, this study was able to reach the final results.

	Original Condition
Effective diameter model	$d \times \sqrt[3]{n\text{Particle}}$
Height of the agglomeration volume	$2A_g(\mu_{p2} - \mu_{p1})$
Number of particles per parcel	50,000 particles/parcel
Time interval	0.000872 sec

Table 15 Original Conditions of Simulation

Table 17 represents the percentage difference compared to the measured values with sound, indicating the differences between the initial simulation and the values obtained after two stages of calibration.

In the simulation using the prototype model, there was on average 20.93% more particles compared to the measured values. Additionally, there was a segment showing a maximum difference of 57.58% compared to the measured values.

$\mu\text{m}$	Prototype Model	1 Effective Diameter	2 Height of the Agglomeration Volume
~0.028	-9.05%	-22.04%	-6.03%
0.028~0.054	-32.96%	-21.96%	-26.46%
0.054~0.091	-54.23%	-41.49%	-18.96%
0.091~0.153	-25.98%	-10.79%	-28.31%

0.153~0.259	-15.81%	-5.58%	9.56%
0.259~0.379	29.72%	24.01%	43.57%
0.379~0.609	57.58%	49.53%	60.51%
0.609~0.942	54.49%	40.21%	21.26%
0.942~1.59	27.75%	22.79%	8.73%
1.59~2.38	13.61%	5.84%	-39.66%
2.38~3.97	5.97%	-7.19%	-18.68%
3.97~	-9.00%	4.86%	14.97%
Total	20.93%	17.13%	10.60%

Table 16 Percentage Difference of Simulation Results Compare to the Measured Data with Sound - A

#### 4.2.2.3 Effective Diameter

CFD simulation employs the concept of parcels to reduce the significant simulation time cost incurred during the analysis of tracking aerosol particles and inter-particle collisions. Typically, to enable collisions between parcels, it's necessary to determine the collision distance based on the effective diameter of a pair of parcels. The initial model used in this study employed the equation ( 34 ) below to determine the effective diameter. However, following the calibration process, the principle of equation ( 20 ) described in the literature review was adopted for effective diameter determination. Therefore, the calibrated model for effective diameter is equation ( 35 )

$$d \times \sqrt[3]{n\text{Particle}} \quad ( 34 )$$

$$d \times \sqrt{n\text{Particle}} \quad ( 35 )$$

Particles within the agglomeration volume undergo collisions due to the acoustic effects. The total agglomeration volume generated by the acoustic action is “ $\mu_{12} \times 2A_g(r_1 + r_2) \times$  the number of large particles.” Therefore, when analyzing collisions between parcels after converting particles into parcels, it is reasonable to use the effective diameter corresponding to equation ( 35 ) rather than the equation ( 34 ).

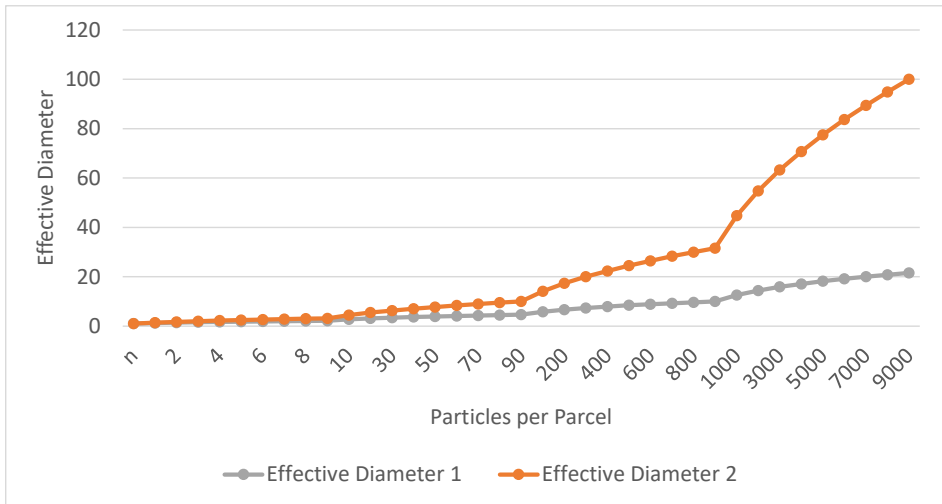


Figure 39 Calculated Effective Diameter Difference between Models

Figure 39 illustrates the differences of effective diameter between the two models. Effective diameter 1 represents the results calculated using equation ( 34 ), while Effective diameter 2 corresponds to the results generated using equation ( 35 ). It can be observed that the difference in effective diameter between the two models becomes bigger when the number of particles are accommodated per parcel.

To predict the movement of parcels, the size of individual particles representing the parcels was utilized.

Through the first calibration, the total percentage difference between the measured value and simulation value was reduced to 17.13%. This was achieved by replacing the formula used to calculate the effective diameter with the equation ( 35 ).

#### 4.3.2.4 Height of the Agglomeration Volume

As highlighted in the literature review chapter, there are two models that can be used to estimate the height of the agglomeration volume. The first model employs a method that considers the displacement amplitude of the fluid medium due to ultrasound and the difference in

entrainment factor between the two particles. The second model, in addition to the factors mentioned earlier, also considers the phase angle difference between the two particles, as depicted in Figure 10.

There are existing concerns regarding the simple model potentially underestimating the actual height of the agglomeration volume, as shown in Figure 6. In this study, the simple model was initially used to calculate the height of the agglomeration volume, but during the calibration process, it was replaced with the Mednikov's model.

The initial simulation showed a difference of 20.93% compared to the measured values, and was reduced more than 10% to become 10.60%.

#### 4.2.2.5 Simulation Time Interval

In the process of analyzing particle collisions, having a large time interval could lead to a probability of missing collisions that actually occur, as the analysis may move to the next time step without considering certain collisions. This approach involves calculating agglomeration volume and determining collisions only at each time step, excluding the possibility of collisions occurring in the brief moments between time intervals.

To find the appropriate time interval for the acoustic agglomeration model developed in this study for CFD simulation, a calibration process was carried out. Setting the time interval to one-quarter of the sound vibration period resulted in the CFD simulation's output approximating the experimental values from the reference study.

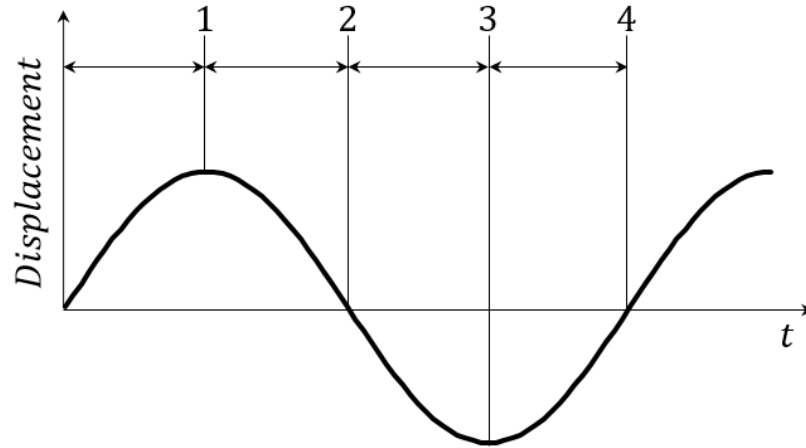


Figure 40 Connection between Four Sections of a Wave and the Time Interval

The reason for the approximation to the measurement values when using a time step of one-quarter of the sound vibration period is believed to be related to the nature of sound. Over one vibration period, the movement of the medium can be divided into the following four phases: 1) movement from the neutral position to the crest point, 2) movement from the crest to the neutral position, 3) movement from the neutral to the trough point, and 4) movement from the trough to the neutral. Since collisions can occur in each of these phases at every simulation time step, setting the simulation time step to one-quarter of a vibration period is expected to yield results that closely approximate actual measurement values.

The additional calibration process was motivated by the concern that the time step set in the simulation might be insufficient to capture all of the collisions between the particles.

Around the sound source, the fluid medium oscillated back and forth during the period of the vibration. Each motion has acceleration and deceleration phases. Therefore, one cycle of a sound wave can be divided into four section and can then be set as the simulation time step.

Table 17 below illustrates the gap between the simulation results obtained through the remaining calibration steps and the measured values.

$\mu\text{m}$	3 Half Hz	4 Quarter Hz	5 #/Parcel
~0.028	-35.44%	-12.91%	-2.15%
0.028~0.054	-23.41%	-29.64%	-25.69%
0.054~0.091	-52.72%	-23.95%	-20.93%
0.091~0.153	-23.74%	-51.34%	-21.89%
0.153~0.259	-15.14%	-24.88%	1.62%
0.259~0.379	8.66%	-9.40%	8.82%
0.379~0.609	40.32%	35.61%	15.50%
0.609~0.942	25.72%	20.08%	-2.35%
0.942~1.59	11.05%	15.68%	4.94%
1.59~2.38	-0.92%	-1.76%	-15.35%
2.38~3.97	-13.66%	-8.54%	-23.00%
3.97~	-13.84%	-10.27%	-17.18%
Total	5.83%	2.71%	-2.94%

Table 17 Percentage Difference of Simulation Results Compare to the Measured Data with Sound - B

Initially, the simulation was run with a time step set to 0.000872 seconds and was subsequently adjusted to 0.000357 seconds, corresponding to half a period of the sound wave, and then the simulation was executed. Following that, the time step was set to 0.000178 seconds, corresponding to a quarter period of the sound wave, and the simulation was run.

When the time step was initially adjusted, the difference compared to the measured values decreased to 5.83%, bringing the simulation closer to the actual values. Through the second adjustment, a mere 2.71% increase in particles was achieved, producing results even closer to the measured values.

#### 4.2.2.6 Number of Particles per Parcel

Similar to the grid refinement, setting the parcel more finely can yield results that are closer to reality. At this stage, the number of particles included by a single parcel which had been set at 50,000 was adjusted to 17,500. Proceeding with this adjustment, an overall reduction of 2.94% was observed. Compared to the previous calculation of a 2.71% difference, the gap was slightly enlarged. While the overall count was less accurately predicted, the differences with the measured values at individual sizes were generally closer to the experimental data.

#### 4.2.2.7 Simulation Time Cost Saving through Maximum Interaction Distance

As the simulation progresses after the initial particles are introduced into the simulation domain, their numbers gradually increase. The more particles present in the simulation domain, the more time is required for the analysis of particle movement. The time required for analyzing particle collisions increases even more steeply since it involves an analysis of all pairs of particles, which grows significantly. One approach to mitigate the steep increase in simulation time cost is to set a maximum interaction distance. For particle collisions to occur, the distance between particles must be equal to or smaller than the sum of their radii. The maximum interaction distance for collisions due to the resonant motion of particles caused by sound waves is determined by the displacement amplitude of the fluid due to the sound wave. To ensure accurate simulations, the maximum interaction distance should be greater than the fluid's displacement amplitude. If the distance between a selected pair of parcels is greater than the maximum interaction distance setting, a series of calculations that is necessary for the subsequent analysis of the acoustic agglomeration phenomenon is omitted. Instead, the analysis continues with the next pair, reducing simulation time cost.

In this study, the consideration of the max interaction distance was carried out during the calibration process to confirm a slight reduction in simulation time cost.

Subsequently, simulations were conducted under the condition of introducing particles for 5 seconds with the max interaction distance set to approximately 10 cm, similar to the duct diameter. The simulation for 5 seconds with the max interaction distance settings required a total time of 403,023 seconds (approximately 4 days and 16 hours). In contrast, conducting the simulation without the max interaction distance setting took 424,241 seconds (approximately 4

days and 22 hours). The max interaction distance setting reduced the simulation time by approximately 5%.

#### 4.2.3 Application of Calibration Parameters

During the calibration process, five parameters were addressed:

- Simulation Time Interval
- Effective Diameter
- Height of the Agglomeration Volume
- Number of Particles per Parcel
- Maximum Interaction Distance

Through the calibration process, adjustments were made to the following parameters, which can be categorized into two levels: code level and user input level.

At the code level, calibration parameters such as Effective Diameter and Height of the Acoustic Agglomeration Volume were already completed during the development process of the CFD simulation model and do not require user adjustment. On the other hand, at the user input level, parameters such as simulation time interval, maximum interaction distance, and Number of Particles per Parcel need to be inputted by users for each simulation case.

The Effective Diameter applies to the concept of parcels, representing the virtual parcel diameter applied to a collection of particles with similar characteristics. The Height of the Acoustic Agglomeration Volume refers to the resonance amplitude difference between particles formed due to sound waves.

The simulation time interval is the minimum time interval necessary for precise analysis of particle collisions and is associated with the sound frequency. It is recommended to input a simulation time interval of less than 1/2 Hz based on comparisons between simulation and measurement results.

The maximum interaction distance is an additional input considered to reduce simulation time cost. It is recommended to input the Maximum Height of the Acoustic Agglomeration

Volume after obtaining the minimum distance between large particles from sound frequency, dB, and expected sound source.

The number of particles per parcel indicates the number of particles composing one parcel, similar to setting up a mesh in conventional CFD simulations. A denser mesh increases accuracy but also increases simulation time cost. Similarly, representing a small number of particles per parcel may enhance the accuracy of collision analysis but significantly increases simulation time cost. Finding a balance between the accuracy of collisional analysis and saving simulation time costs requires a process similar to grid study. In order to find a suitable consensus point, we should compare the results based on the number of particles per parcel. In this study, obtaining reasonably accurate simulation results required including fewer than 17,500 particles per parcel when there were approximately 1,339,541 particles per liter.

#### 4.3 Summary

The first prototype model was developed with a focus on the key concept of the acoustic agglomeration theory, orthokinetic interaction. However, there was a significant discrepancy between the simulation results from the prototype model and the experimental measurements from the reference research. The particle number concentration estimated through simulation using the prototype model was 20.93% higher than the reference research. This indicates that there are factors which were ignored in the simulation using the prototype model.

Factors affecting the accuracy of the simulation include the accuracy of the model itself and the lack of expertise in the simulation data input process. Therefore, a step-by-step calibration process was carried out for both the existing prototype acoustic agglomeration CFD model and the simulation data input process.

Firstly, various principles found in the orthokinetic interaction phenomenon and identified during the literature review were analyzed. The model calibration process was conducted by re-selecting equations, explaining element principles for the orthokinetic interaction. The modifications made in this study involved replacing equations applied to the effective diameter and height of the acoustic agglomeration volume.

In addition to the model, the configurations of the environment for computer simulation also influences the accuracy of the results. Therefore, settings associated with the accuracy of particle collision analysis were investigated. Simulation settings related to the accuracy of particle collision analysis revealed in this study include simulation time interval and particle number per parcel.

CFD simulation is generally a time-consuming task, especially when analyzing particles. To reduce the additional time spent on particle analysis, a feature was implemented to exclude particle pairs located beyond the user-defined maximum distance from additional collision analysis. This function saved approximately 5% of the time under the conditions used in this study.

As a result of all calibration processes, the total particle number concentration from the simulation had a difference of 2.94% compared to the experimental data. The number of concentration values for each particle size range generally showed a difference within 25%.

CHAPTER V  
MODEL VALIDATION USING EXPERIMENTAL RESULTS

To assess the reliability of the acoustic agglomeration model when fluid motion is in the vertical direction relative to the ground, reference research was utilized. To validate the model under conditions where the fluid undergoes horizontal motion, experimental equipment was prepared and was implemented through CFD simulation to generate results. The reliability of the acoustic agglomeration model was evaluated by comparing these results with experimental data.

5.1 Simulation

To reduce the time cost for CFD simulation, the actual experimental conditions were minimized. The final portion of the first measurement point was designated as the inlet surface. The inlet surface to the final outlet section constituted the second measurement, and was set as the simulation domain. The total length of the experimental apparatus is 234 cm. However, the total length for the simulation domain is 128 cm.

5.1.1 Dimensions of Geometry for Simulation

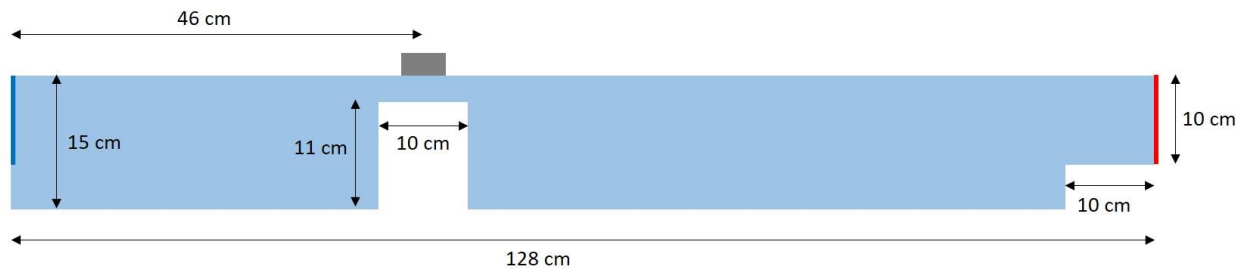


Figure 41 Geometry for the Simulation with Dimensions

5.1.1.1 Sound

A sinusoidal pattern of sound waves was used in the experiment. The intensity of the sound was set to 170 dB at the center of the narrow channel. The frequency of the sound was 2500 Hz.

#### 5.1.1.2 Simulation Time Interval

Based on the finding during the model validation process, the time interval was set at four times the frequency of the sound, which was 0.0001 seconds. The report frequency was 0.5 seconds.

#### 5.1.1.2 Particle Properties

Aerosols generated by burning incense sticks were used for the experiment. The following input values in Table 18 were used for the simulation:

Particle Restitution Coefficient	0.01
Hamaker Constant	1.24e-19 Joules
Material Limiting Contact Pressure	0.41e+9 Pascal
Minimal Contact Distance	0.0004 $\mu\text{m}$
Particle Density	1080 $\text{kg}/\text{m}^3$

Table 18 Particle Properties for Model Validation Using Experimental Data

#### 5.1.2 Geometry

The experimental setup was implemented as depicted in the Figure below.

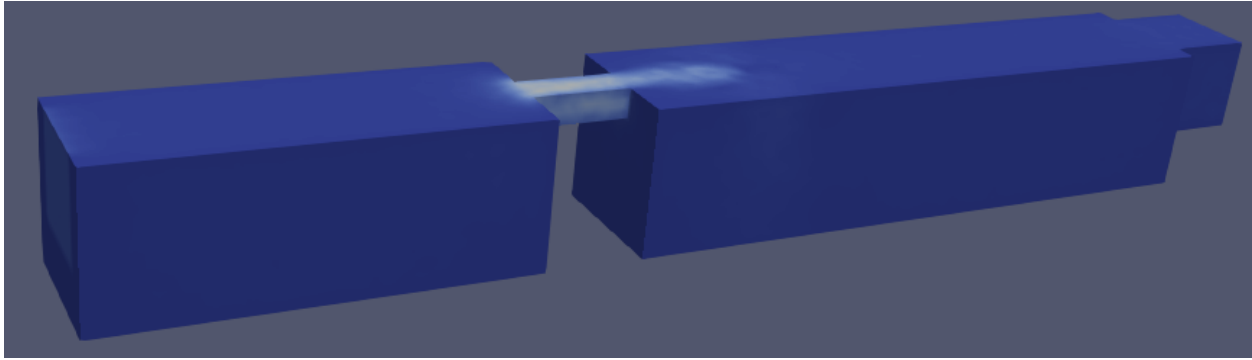


Figure 42 Geometry for Mixed-Air Injection in a Horizontal Straight Duct in Laboratory

### 5.1.3 Mesh

To analyze the geometry represented above through CFD simulation, the following five mesh settings were prepared.

	Max. Length	Min. Length	Growth Rate	Total Cells
1	2 cm	1 cm	0.2	112,023
2	2 cm	1 cm	0.1	167,729
3	1 cm	1 cm	NA	221,511
4	0.85 cm	0.65 cm	0.1	407,872
5	0.8 cm	0.6 cm	0.1	510,377

Table 19 Mesh Preparation for Mixed-Air Injection in a Horizontal Straight Duct in Laboratory

After applying the average wind speed of 1.878 cm/sec at the inlet surface, the simulation results at the post-treatment measurement section were compared.

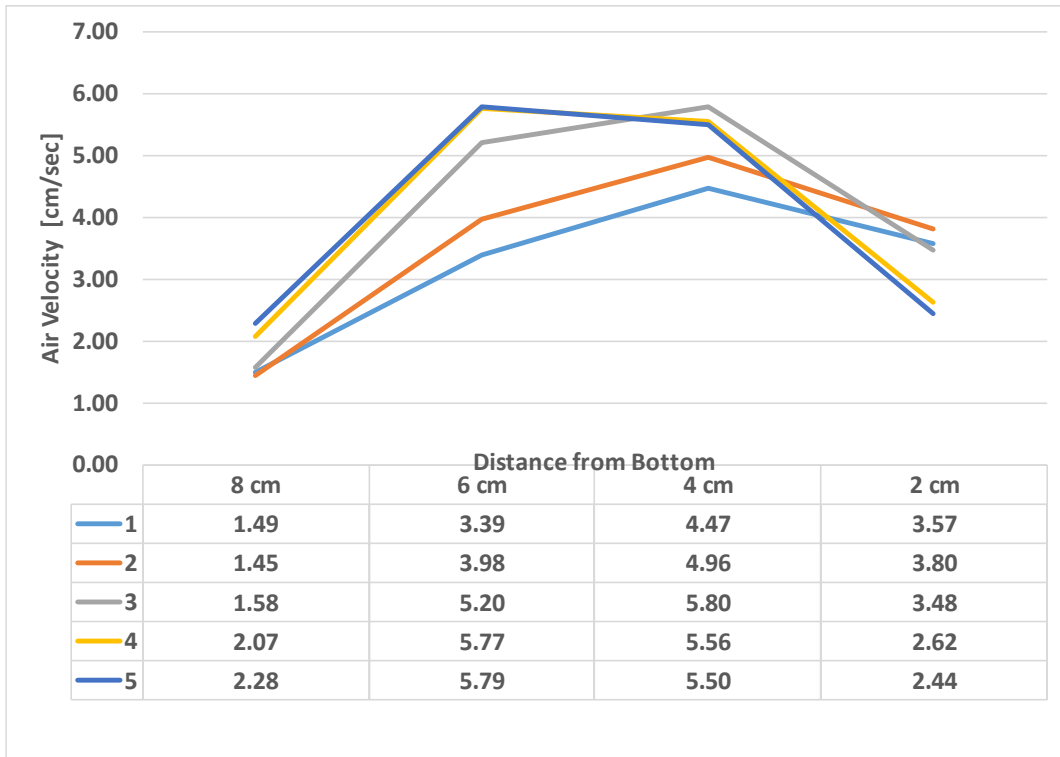
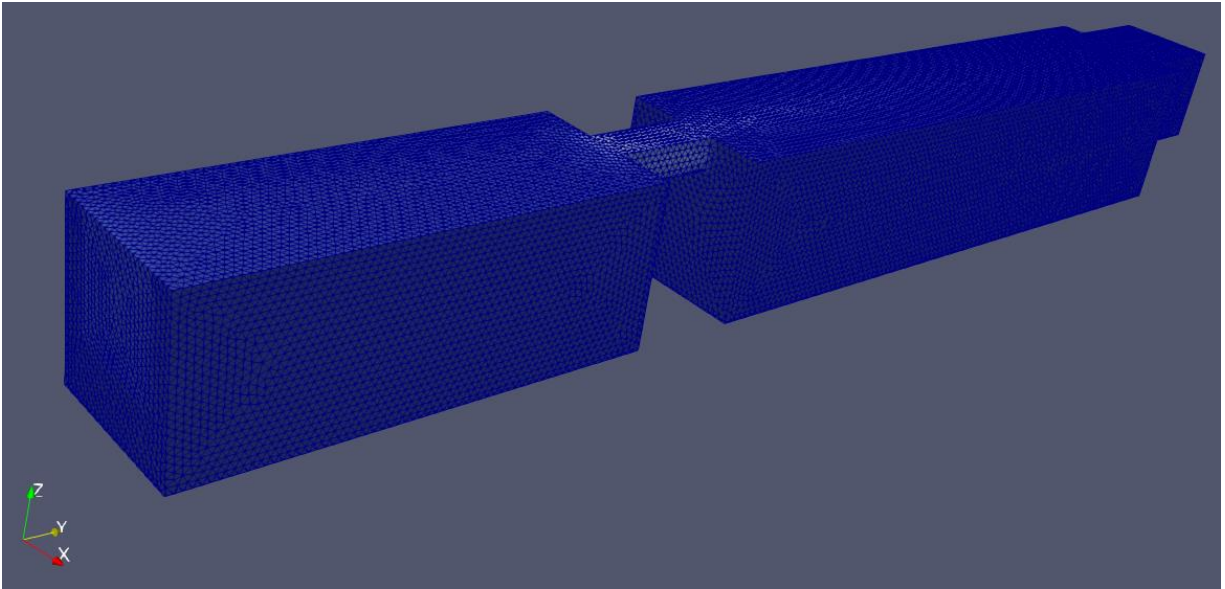


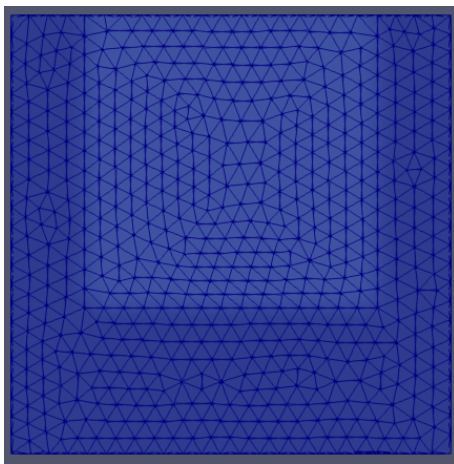
Figure 43 Comparison of Air Velocity Profile at Post-Treatment Measurement Section

The fourth mesh was used for the validation process. This choice was made to reduce simulation time and because it showed minimal differences in velocity profiles compared to the most detailed mesh.

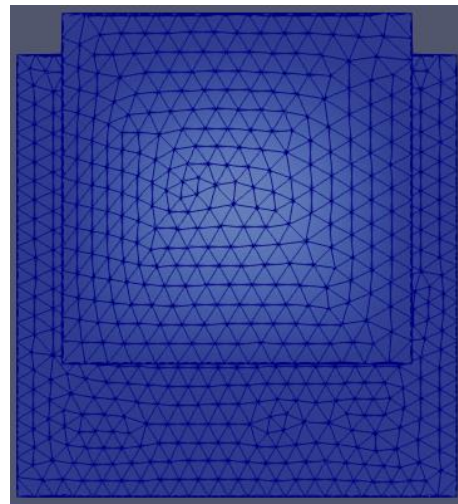
The selected mesh is shown in Figure 44. The shaded regions at the inlet and outlet represent the contours of air velocity after the simulation results stabilized.



Isometric View



Inlet



Outlet

Figure 44 Selected Mesh for Mixed-Air Injection in a Horizontal Straight Duct in Laboratory

The Box-and-Whisker plot in Figure 45 represents the measured air velocity values from five measurements taken at four spots spaced 2 cm apart and 2 cm from the top of the duct in the post-treatment measurement section. The blue line represents the results generated through simulation. Although the match between the simulation simulation results and the measured values is not perfect, it can be observed that the simulation results are within the range indicated by the Box-and-Whisker plot.

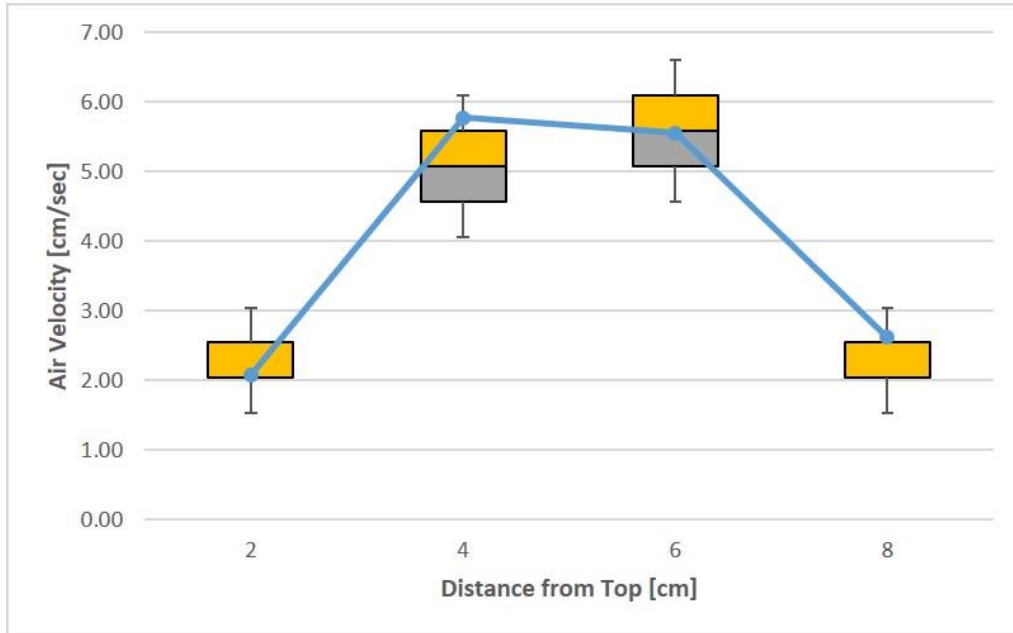


Figure 45 Comparison of Air Velocity from Simulation Results and Measured Data at Post-Treatment Section

## 5.2 Results Comparison

The object of analysis was the results for particle concentration in the post-treatment measurement section. In this study, the collisional analysis for particles consists of three components: 1) General collision between particles, 2) Particle-to-wall collision, and 3) Acoustic collision between particles. The analysis starts with the results for the changes in particle concentration in the post-treatment measurement section, excluding all collision components. Then, the effects of each collision model mentioned above are considered by analyzing the changes in result values.

### 5.2.1 Results Stabilization

To demonstrate constant results in transient CFD simulations, it is necessary for the simulation to have had sufficient time. Information about the required time was determined by

analyzing the simulation report files according to the progression of time. Afterward, the average values of the results corresponding to three simulation time steps are compared to the actual measured data.

### 5.2.1.1 Air-Flow

To obtain the stabilized results of fluid flow and the entrained particles, a certain time is required. Figures below contain information on flow-pattern changes over time.

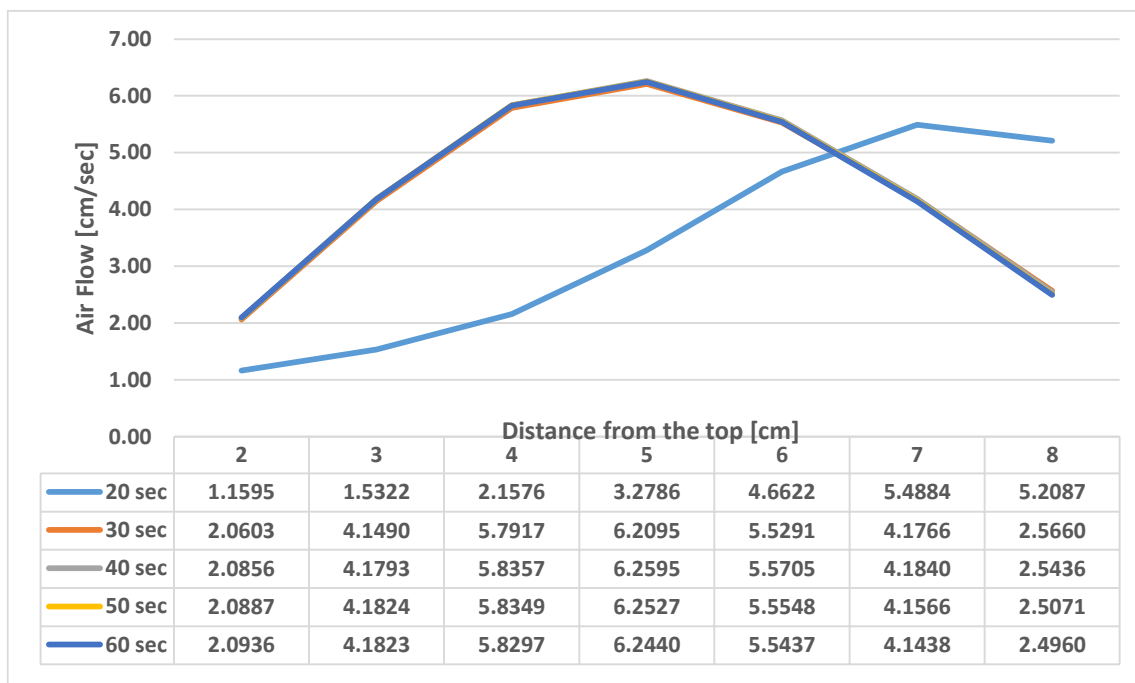


Figure 46 Required Time for Stabilizing Air Flow Results at Post-Treatment Measurement Section

Figure 46 shows the vertical velocity profile at the central point of the post-treatment measurement. Velocity profiles are shown at intervals of 10 seconds from the 20 second mark. It can be observed that the results have sufficiently stabilized between the 20 second and 30 second points. After that, only nominal changes were observed, which can be ignored.

### 5.2.1.2 Dispersion of Particles

The particles were uniformly introduced 50 seconds after the flow had already sufficiently stabilized. Figure 47 visualizes the dispersion of the particles over time. It is expected that the results related to the particles will have stabilized between the 220-second and 225-second marks.

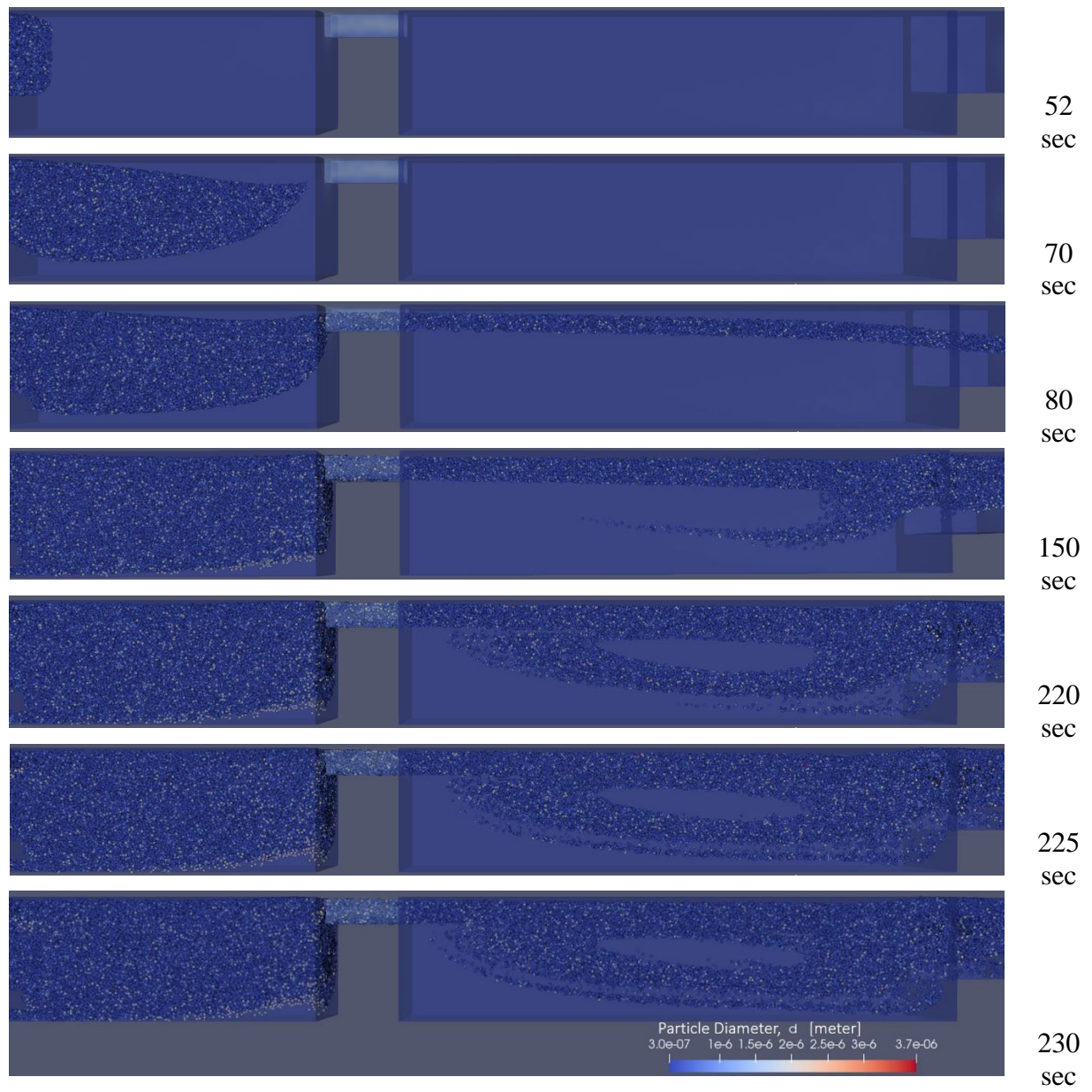


Figure 47 Dispersion of Particles Over Time

Figure 48 represents the concentration of particles in the space corresponding to the post-treatment measurement section (one liter). It shows the results for the total number of particles, regardless of size. The results for the particles stabilized near the 210-second mark. After this moment, minor fluctuations were still observed. Therefore, the average value of the results for the three time steps was used in the subsequent research process. In this research, the three result sets from the last three time steps were used.

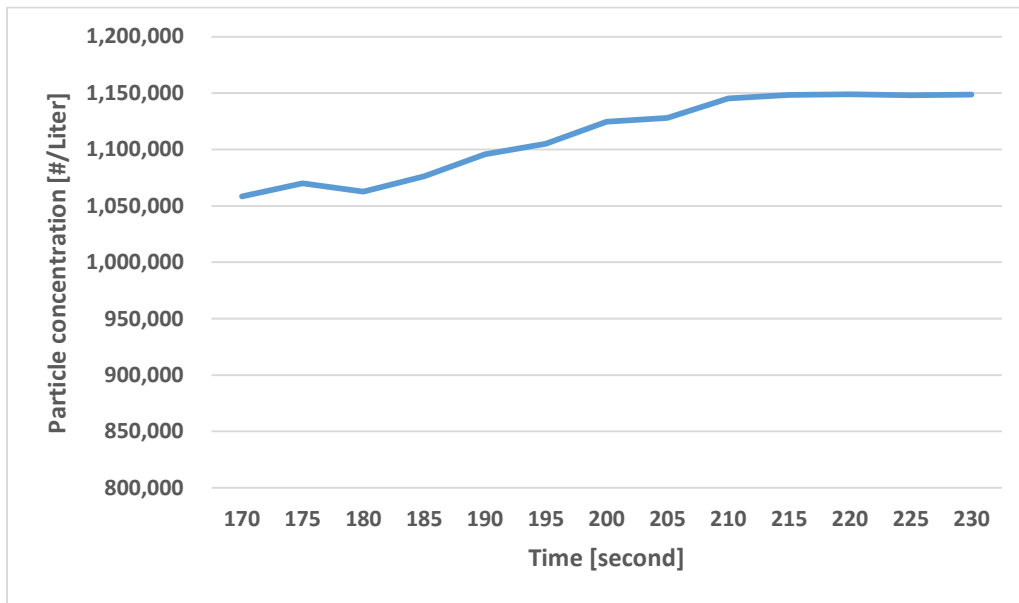


Figure 48 Required Time for Stabilizing Particle Results Within 10 cm of the Bottom

### 5.2.2 Impact of Collisional Models

Figure 49 illustrates the composition of particles inputted into the simulation and the results obtained from applying three collision models in the post-treatment measurement section.

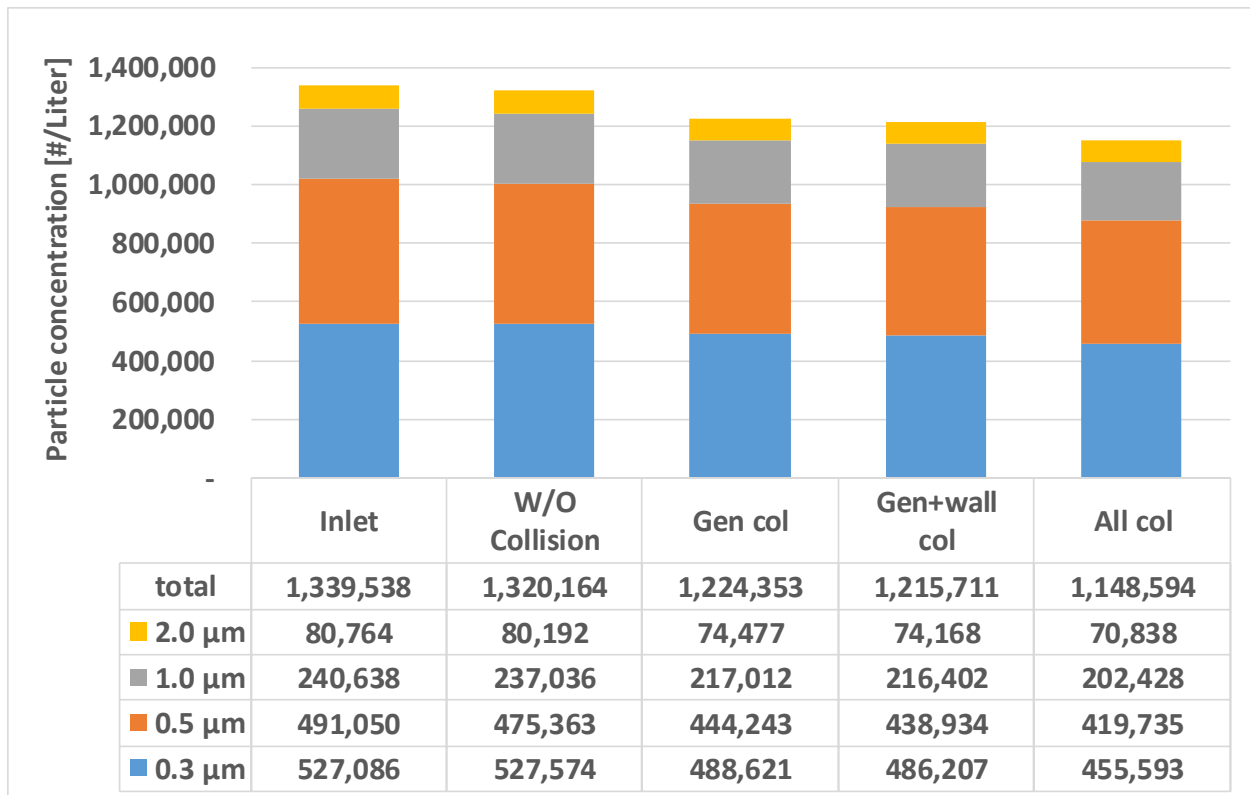


Figure 49 Comparison of Particle Concentration Among Collision Models

The leftmost bar shows the concentration of particles per liter of induced fluid and air, categorized by size. The second bar represents predicted results, excluding all collision models. The third bar displays outcomes when solely utilizing the general collision model. Changes in concentration occur as smaller particles are captured by larger ones through collisions, and the larger particles increase in size while moving with the fluid flow.

The fourth bar indicates particle concentration under test conditions, excluding the acoustic agglomeration phenomenon. This can be compared to actual measurement data. The last bar depicts results considering all collision models, general, wall, and acoustic collision. The results can also be compared to actual experiments by introducing particles and operating the speaker.

General collisions led to a noticeable decrease in particle concentration. Acoustic agglomeration mechanisms also resulted in decreased particle concentration.

Particle Size	W/O Collision	Gen col	Gen + wall col	All col
0.3 $\mu\text{m}$	0.093%	-7.298%	-7.756%	-13.564%
0.5 $\mu\text{m}$	-3.195%	-9.532%	-10.613%	-14.523%
1.0 $\mu\text{m}$	-1.497%	-9.818%	-10.072%	-15.878%
2.0 $\mu\text{m}$	-0.709%	-7.784%	-8.167%	-12.291%
total	-1.446%	-8.599%	-9.244%	-14.254%

Table 20 Percentage of Particle Concentration at Post-Treatment Measurement Section Compared to Inlet Value

It was expected that the amount of particles injected and the amount of particles measured at the post-treatment measurement point would be the same when the collision model was not applied; however, there was a slight decrease in the number of particles, likely due to the air flow profile. The outermost part of the duct has a fluid velocity of near zero, while the fluid velocity is highest at the center. This exerts a force that pulls particles located at the outer edges of the duct toward the center. Therefore, the number of particles at the outermost part of the post-measurement area is reduced. It is speculated that the method of deriving simulation results also led to a slight difference by counting the number of particles in one liter in the post-measurement area.

The general collision model reduced the overall particle concentration by 8.6%. The concentration decrease exhibited variations of up to 2% between particle sizes. Additionally, the wall collision contributed to a decrease of about 0.65% in particle concentration compared to the reduction caused by general collisions. This difference is negligible. Furthermore, the acoustic agglomeration phenomenon resulted in an additional decrease of approximately 5% in particle concentration. It was confirmed that both the general collisions and acoustic collisions significantly impacted the decrease in particle concentration under the experimental conditions.

Wall collisions did not decrease particle concentration for two possible reasons. First, with 2  $\mu\text{m}$  particles being the largest introduced into the test facility, natural deposition down to

the bottom of the duct was hard to predict. Second, the structure of the experiment did not tend to cause wall collisions.

### 5.2.3 Comparison of the Simulation Results and Measured Data

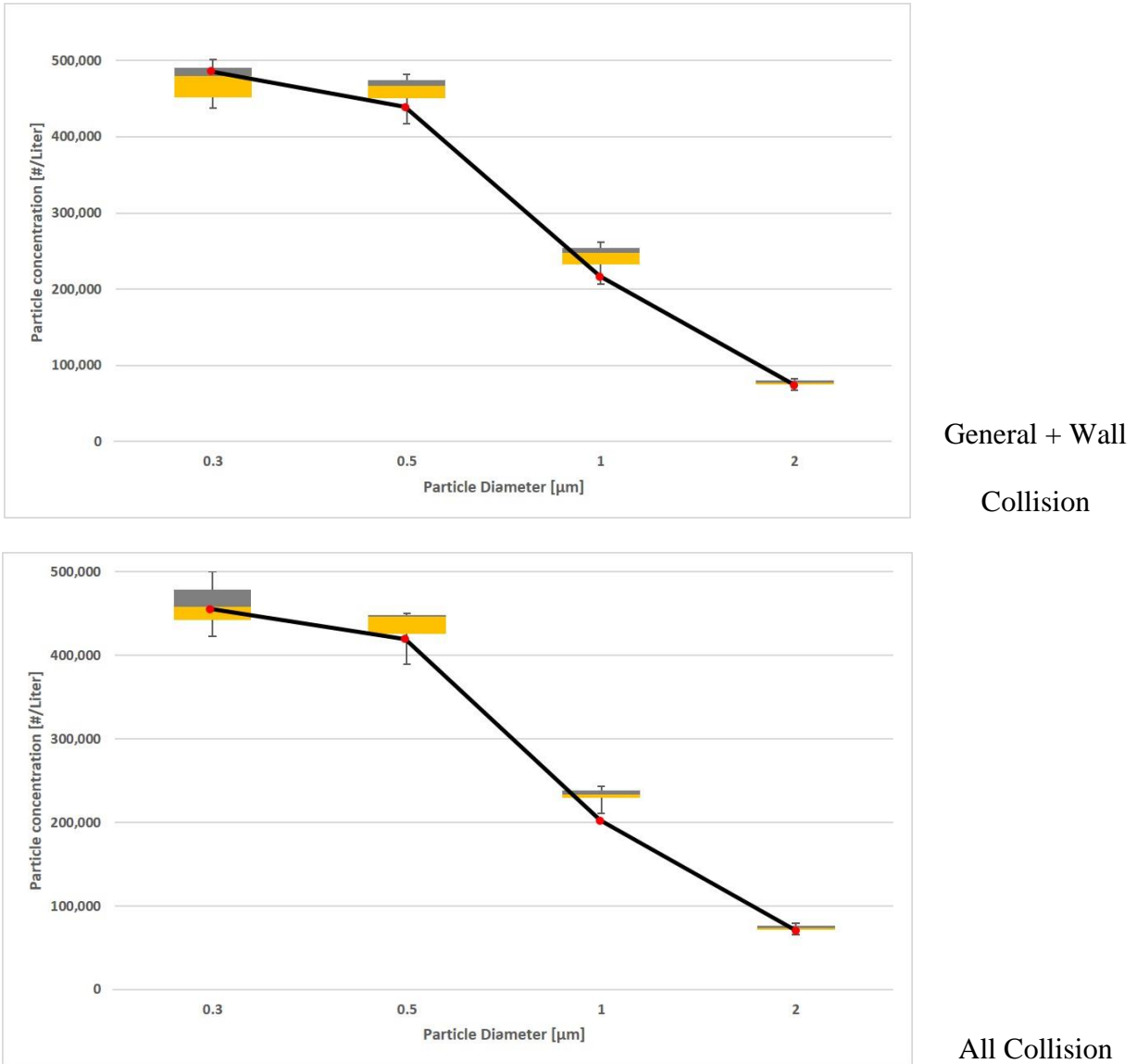


Figure 50 Comparison of the Simulation Results and Measured Data

A comparison was conducted between the post-treatment measurement data from the experimental setup and the simulation results using the general and wall collision models.

Although the simulation outcomes do not precisely match the median value of the measured data, they fall within the fluctuation observed in the measurements.

When contrasting the measured values with the simulation outcomes obtained by employing all collision models (general, wall, and acoustic collision) in conjunction with the generation of sound waves, the patterns were akin to those observed when using only the general + wall collision model. Within the experimental conditions, only the results associated with particles in the 1  $\mu\text{m}$  category exceeded the range of measured values, yet the distribution and trend of particle concentration were predicted to be similar to the actual values.

### 5.3 Summary

The general collision and acoustic collision significantly contributed to the decrease in particle concentration under the experimental conditions. However, there was no notable decrease in particle count through wall collision. This limitation could be attributed to the simplicity of the experimental setup and the constraint of particle sizes. The conclusion was drawn based on model validation using mixed injection of air and particles in a horizontal straight duct test.

The new acoustic agglomeration CFD model does not ensure highly precise results, but it provides approximate outcomes and demonstrates a particle concentration distribution by size that closely resembles the measured values from experiments. Thus, the developed AA CFD model for OpenFOAM can be considered reliable. Building upon the model's reliability, the next chapter conducts a sensitivity test considering four factors that impact particle agglomeration.

## CHAPTER VI

### SENSITIVITY ANALYSIS

Evaluation of acoustic agglomeration was conducted concerning the changes in sound intensity, airflow, initial particle concentration, and the frequency of sound waves.

#### 6.1 Information of Sensitivity Analysis

The setup involves airflow that includes aerosols which move horizontally through a square duct. The aerosols are affected by a speaker positioned at the center's top. Particles are introduced through the left inlet surface. Their concentration is observed at the portion of the duct on the right side, allowing for a comparison of concentration changes concerning the particle input.

##### 6.1.1 Geometry

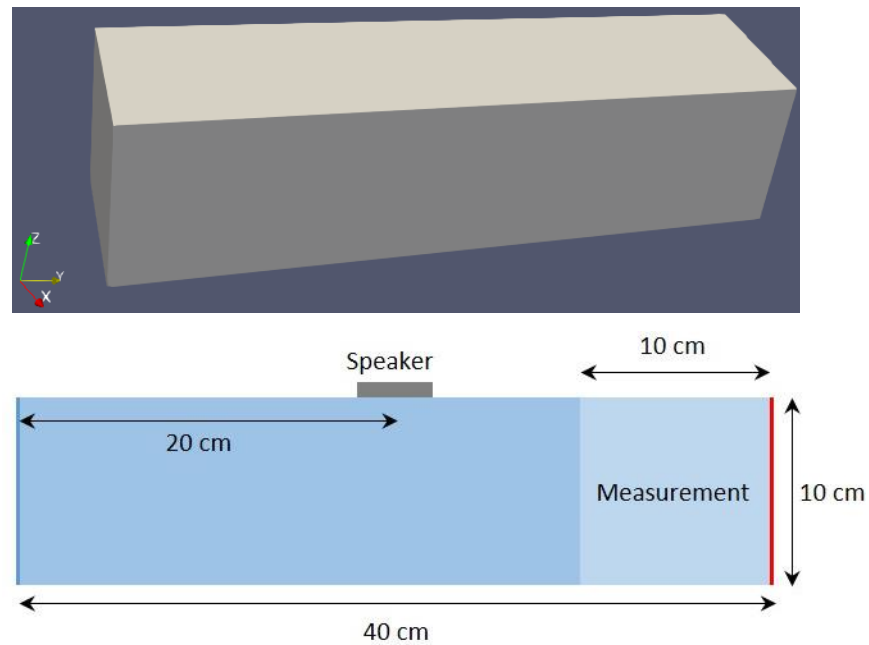


Figure 51 Geometry for the Sensitivity Analysis

Air carrying particles flowed through a square duct from the left side to the right side. The square duct measured 40 cm in length and had a cross-sectional area of 10 cm × 10 cm. As illustrated in Figure 51, the airflow mixed with the particles progressed through the left blue line (the inlet surface) and exits through the right red line (the outlet surface). The particle concentration within a 1-liter segment, located up to 10 cm from the outlet surface on the right. That measured concentration was compared to the particle concentration at the inlet surface based on particle size.

### 6.1.2 Grid Study

	Max. Length	Min. Length	Growth Rate	Total Cells
Coarse	1 cm	1 cm	NA	17,976
Mid	1 cm	0.5 cm	0.3	78,286
Fine	0.5 cm	0.5 cm	NA	137,292

Table 21 Meshes for Sensitivity Analysis

Following this configuration, three different meshes were prepared to compare velocity profiles. The entire length of the duct is 40 cm, and the air velocities were compared at seven points 5 cm away from the outlet. Air velocity values at the 10-second mark were used for comparison.

There weren't significant differences among the three mesh models. Whichever mesh was used among the three, did not significantly affect the accuracy of the results. There was not a significant simulation time cost difference for obtaining results at the 10-second mark. To ensure higher accuracy, the finest mesh model was selected.

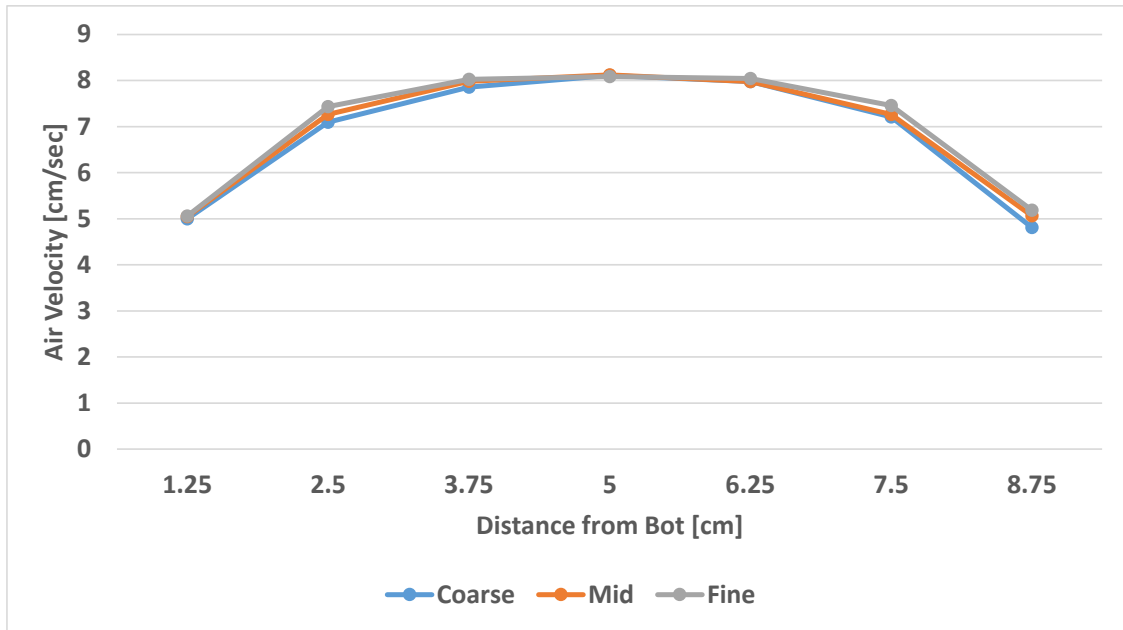


Figure 52 Velocity Profile at 5 cm before the Outlet

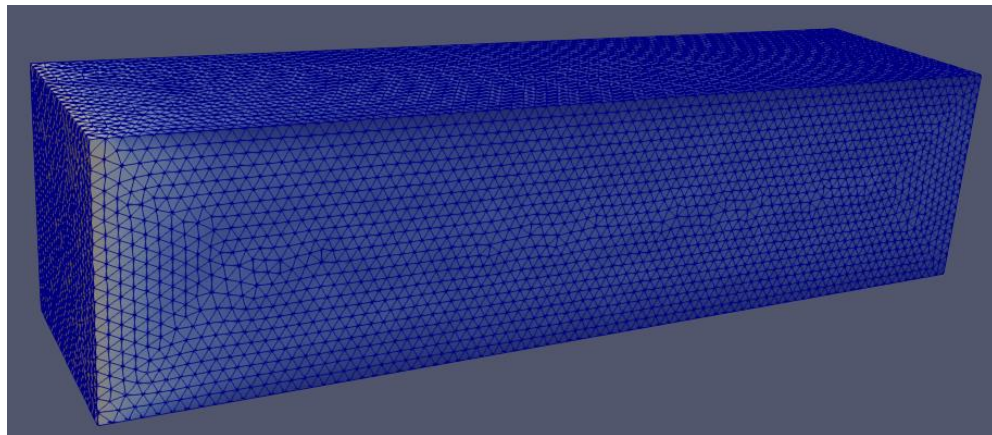


Figure 53 Selected Mesh Model

Figure 53 shows the selected mesh model with air velocity after air velocity profile was stabilized.

### 6.1.3 Base-Case of the Sensitivity Analysis

The base-case includes the following values for the four variables that were used: sound intensity, air flow, initial particle concentration, and sound frequency.

- Sound intensity: 150 dB
- Air flow: 5 cm/s
- Initial particle concentration: 250,000/cm<sup>3</sup> (for each 0.3, 0.5, 2.5, 10.0 μm particles)
- Sound frequency: 2,000 Hz

Simulations were conducted for each case, using these specified conditions. Variations were applied to only one variable per simulation. Each parcel represents 40,000 particles.

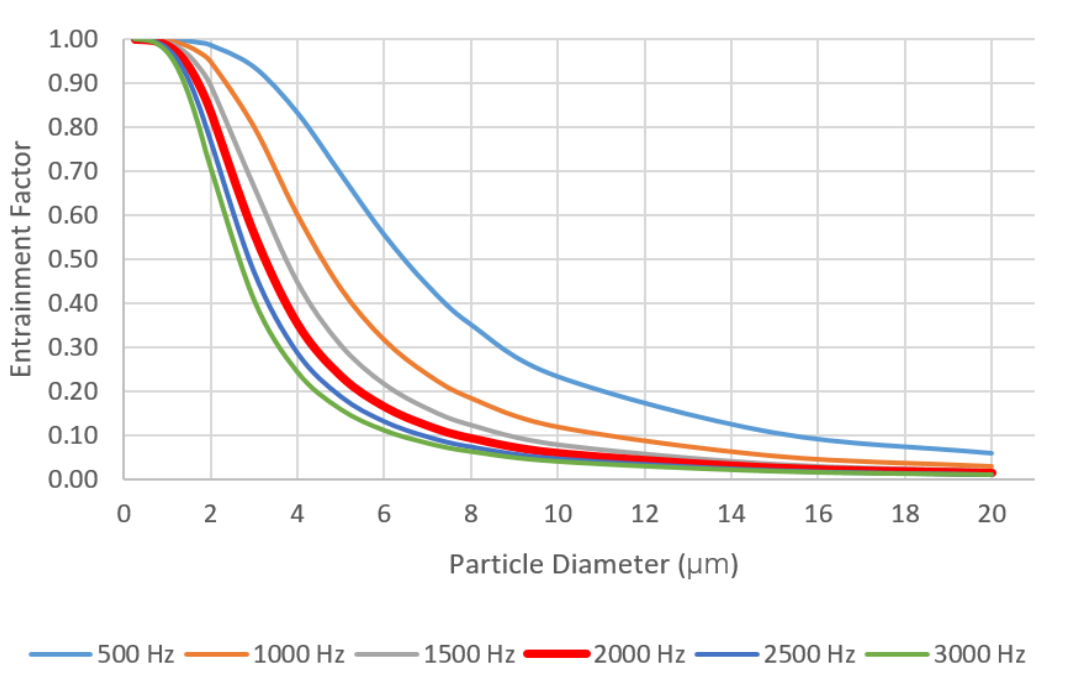


Figure 54 Entrainment Factors of the Particles Depending on Sound Frequency

### 6.1.3.1 Sound Intensity

Between the scenarios, three modes were devised with 5 dB differences and 3.2-times power differences at the center of the duct. The three simulations had sound pressure levels of 145 dB, 150 dB, and 155 dB at the center of the duct.

### 6.1.3.2 Air Flow

Four additional cases were prepared with differences of  $\pm 1\text{cm/sec}$  and  $\pm 2\text{cm/sec}$  to the base-case air velocity, which was  $5\text{ cm/sec}$ . The five simulations were conducted with volume flow rates of 0.3, 0.4, 0.5, 0.6, and 0.7 liters/sec. The following was applied for supplying particle concentration for each size of particle through the inlet surface, respectively:

- 75,000,000/sec
- 100,000,000/sec
- 125,000,000/sec
- 150,000,000/sec
- 175,000,000/sec

### 6.1.3.3 Particle Initial Concentration

In the base-case, a concentration of  $250,000 /\text{cm}^3$  was maintained and introduced into the duct. Simulations were conducted for cases corresponding to concentrations of  $200,000 /\text{cm}^3$  and  $300,000 /\text{cm}^3$ .

### 6.1.3.4 Sound Frequency

In this category of sensitivity analysis, various simulation time intervals were applied. As explained in the validation chapter, time intervals corresponding to a quarter of the sound frequency period were used. Specifically, time intervals of 0.0005, 0.00025, 0.00016666, 0.000125, 0.0001, and 0.00008333 seconds were employed for cases which stand for frequencies of 500 Hz, 1000 Hz, 1500 Hz, 2000 Hz, 2500 Hz, and 3000 Hz respectively.

### 6.1.4 Properties of the Particles

Particle Restitution Coefficient	0.01
Hamaker Constant	1.24e-19 Joule
Material Limiting Contact Pressure	0.41e+9 Pascal
Minimal Contact Distance	0.0004 $\mu\text{m}$
Particle Density	1100 $\text{kg}/\text{m}^3$

Table 22 Particle Properties for Sensitivity Analysis

The physical characteristics of the particles used in the sensitivity analysis are as shown in the Table 22.

## 6.2 Simulation Results

### 6.2.1 Results Stabilization

Based on the simulation results of the base-case, an investigation was carried out to assess result stabilization. Velocity profiles were examined at a distance of 5 cm from the outlet surface over time. Additionally, the total particle concentration within a 10 cm space from the outlet surface was analyzed to determine the point of stabilization in the particle concentration results.

### 6.2.1.1 Air Velocity

From Figure 55, stabilization was nearly achieved between approximately 8 to 10 seconds. Particles were then consistently introduced into the duct starting from the 10-second mark.

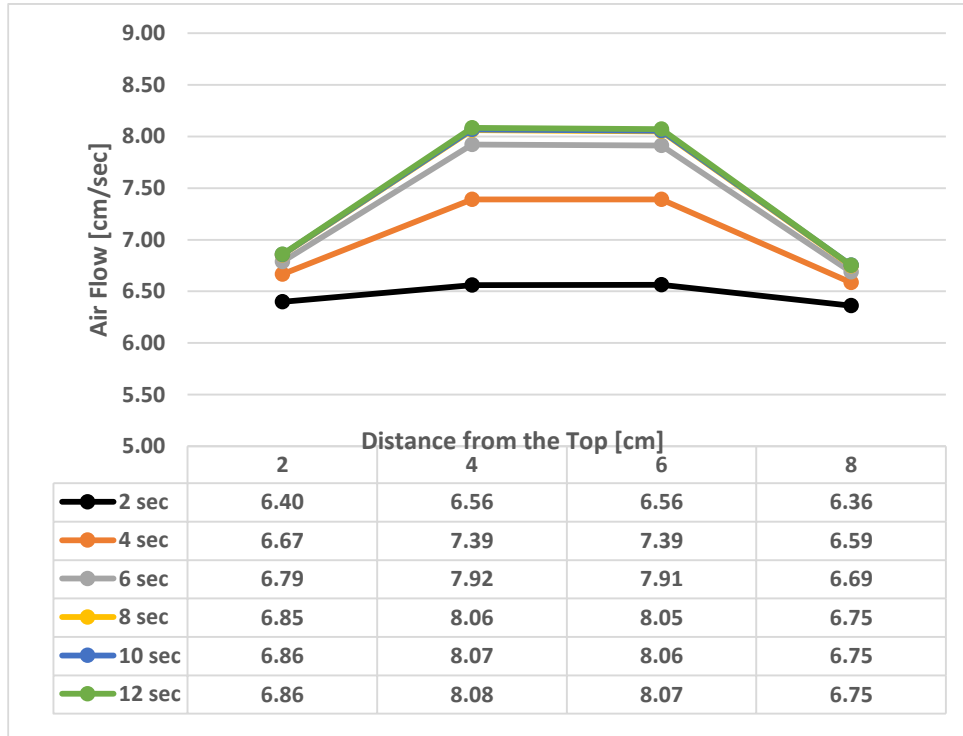


Figure 55 Air Velocity Profile over Time

### 6.2.1.2 Particle

As seen in Figure 56, particles were introduced at the 10-second mark. Within 3 seconds, they reached the center of the duct. After 5.5 seconds, the particles nearly reached the outlet surface. The particle distribution inside the duct seemed consistent between the 38-second and 40-second marks. Near the inlet surface, a uniform particle distribution was observed. In closer proximity to the outlet surface, larger particles tended to gradually move to the lower part of the duct.

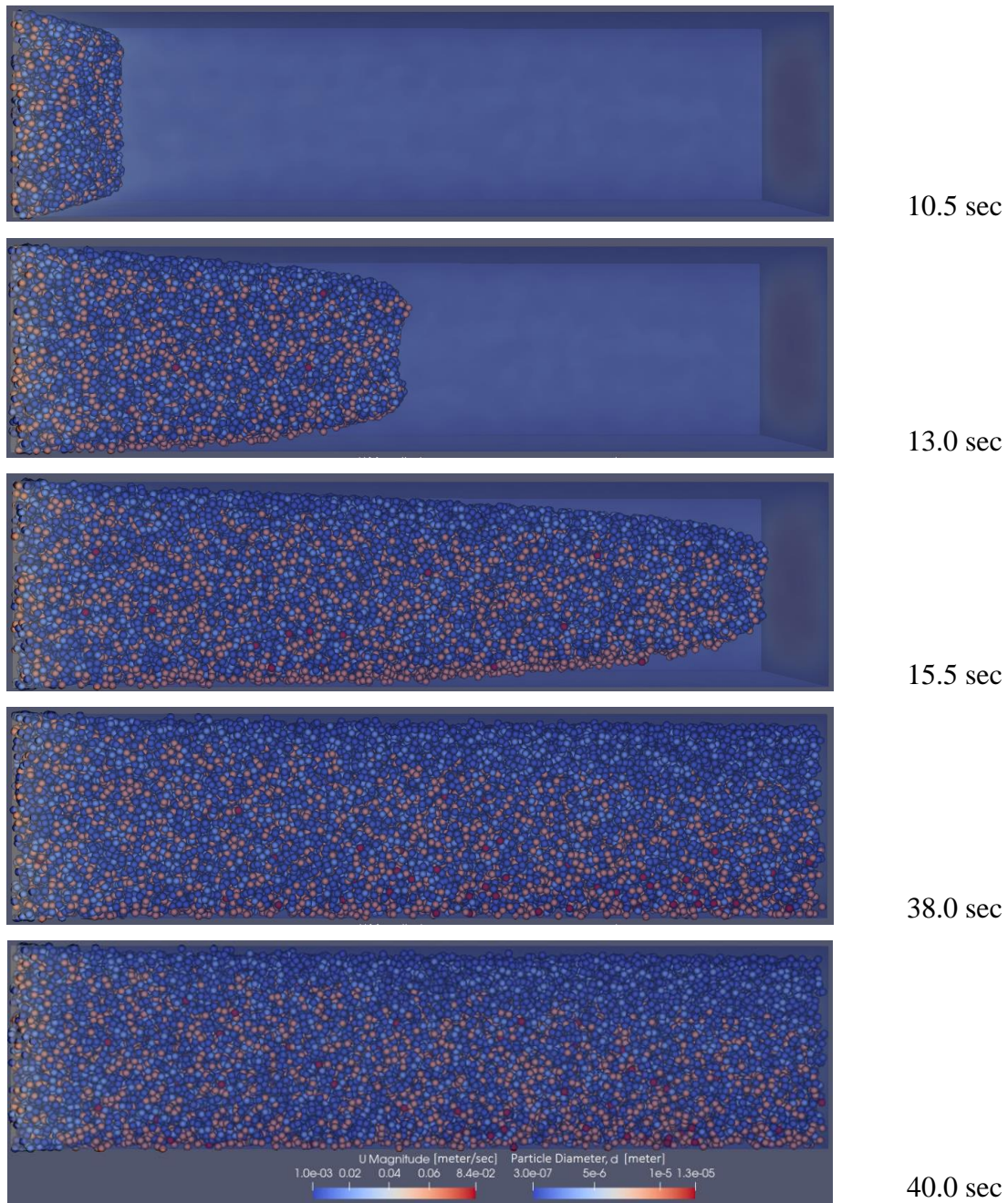


Figure 56 Particle Distribution in the Duct over Time

Based on Figure 56, two important facts were confirmed. 1) The maximum particle size increased to 13  $\mu\text{m}$ , 2) Larger particles are concentrated in the bottom part of the duct. Particles of 0.3, 0.5, 2.5, and 10  $\mu\text{m}$  were introduced through the inlet. The letter "d" in the bottom right of the figure represents the diameter of the particles. Within the simulation domain,

particles ranging from a minimum size of 0.3  $\mu\text{m}$  to a maximum of 13  $\mu\text{m}$  were present. It can be observed that the maximum particle size increased to 13  $\mu\text{m}$  due to the phenomenon of acoustic agglomeration.

From Figure 57, the total particle concentration at a distance of 10 cm from the outlet surface exhibited a consistent increase, with minor fluctuations, after 20 seconds. Starting at the 34-second mark, the graph's trend began stabilizing, and after the 38-second mark, only minor fluctuations were observed. To confirm the stability of the particle concentration results, a sensitivity analysis was conducted. The analysis uses the average particle concentration results of three time intervals, which were 39, 39.5, and 40 seconds.

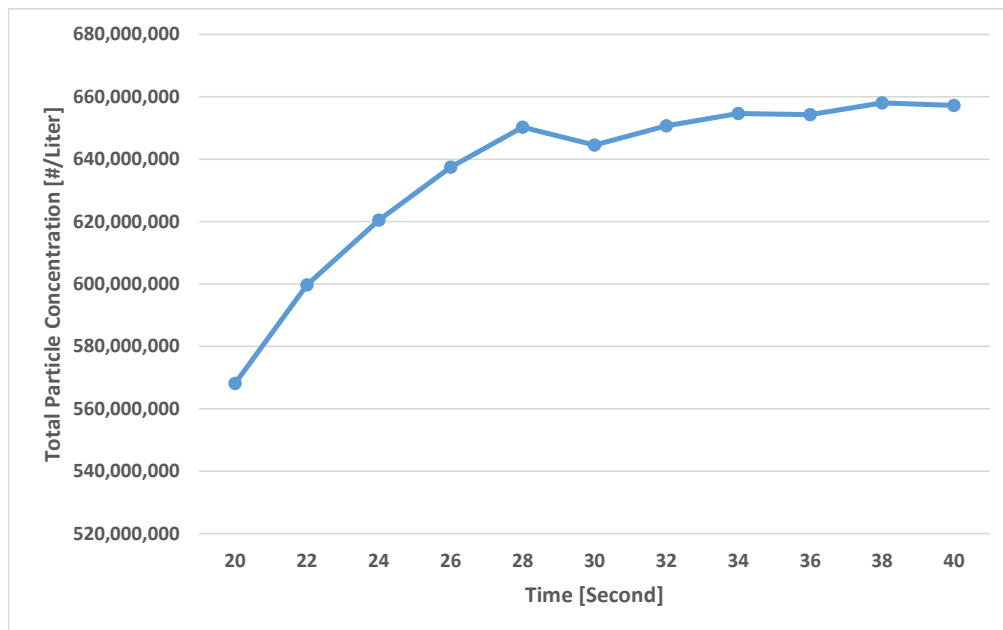


Figure 57 Total Particle Concentration over Time

### 6.2.2 Results of the Sensitivity Analysis

### 6.2.2.1 Sound Intensity

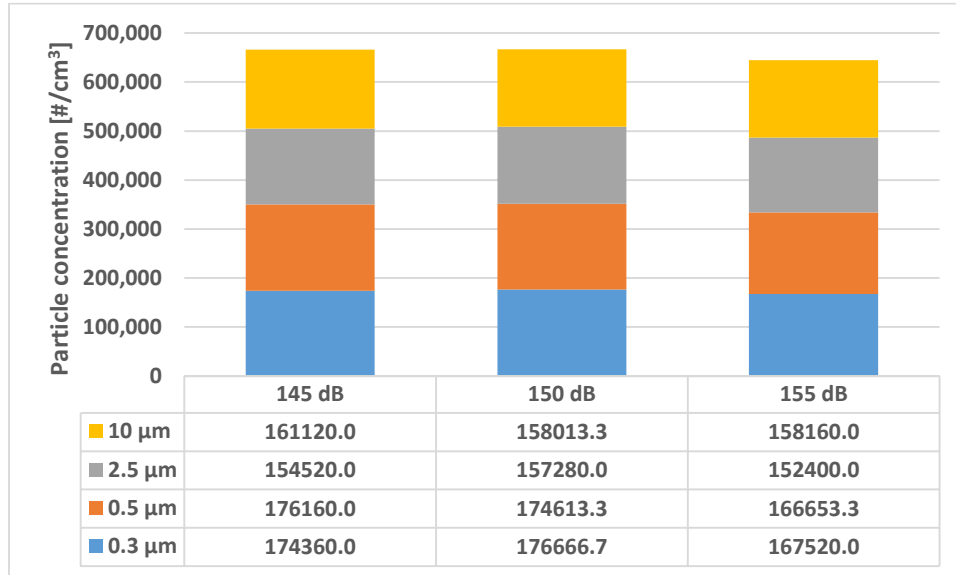


Figure 58 Particle Concentration of the Three Cases of Sound Intensity

Analyzing the particle concentration chart in Figure 58, no substantial difference in particle concentration among the three distinct sound intensity settings were observed. As depicted in the corresponding chart concerning particle removal rate, there wasn't a significant reduction in the removal rate between 145 dB and 150 dB settings. At 150 dB, the number of 0.3 μm and 2.5 μm particles increased by 0.92% and 1.1%, respectively, compared to the 145 dB scenario. These number differences are not considered to have significant meaning. Some errors may occur because the particles are randomly injected. The injection spot was not fixed in position on the inlet surface where they were introduced.

However, the use of 155 dB ultrasound showed a notable removal rate across all particle sizes, except for 10 μm particles. The sound intensity increased from 150 dB to 155 dB, resulting in a slight increase of 0.05% in the number of particles relative to the input. This increase in particle number concentrations is not considered significant. Acoustic agglomeration is a phenomenon where collector particles capture smaller particles, reducing the number of particles in the fluid stream. It is not expected that the number of 10 μm particles acting solely as collector particles would decrease due to acoustic agglomeration. There was a slight decrease of 1.2% in the input amount between 145 dB and 155 dB. This difference is also not considered significant.

However, the slight increase in particle size due to acoustic agglomeration may cause the particles to be slightly more affected by gravity and deposited onto the bottom surface and removed. While larger particles maintained a relatively consistent count, the noticeable decrease in the count of smaller particles across the three sizes strongly suggested the influence of acoustic agglomeration. The discrepancy in resonant amplitude between the 10  $\mu\text{m}$  particles and the other sizes led to direct collisions and subsequent reduction.

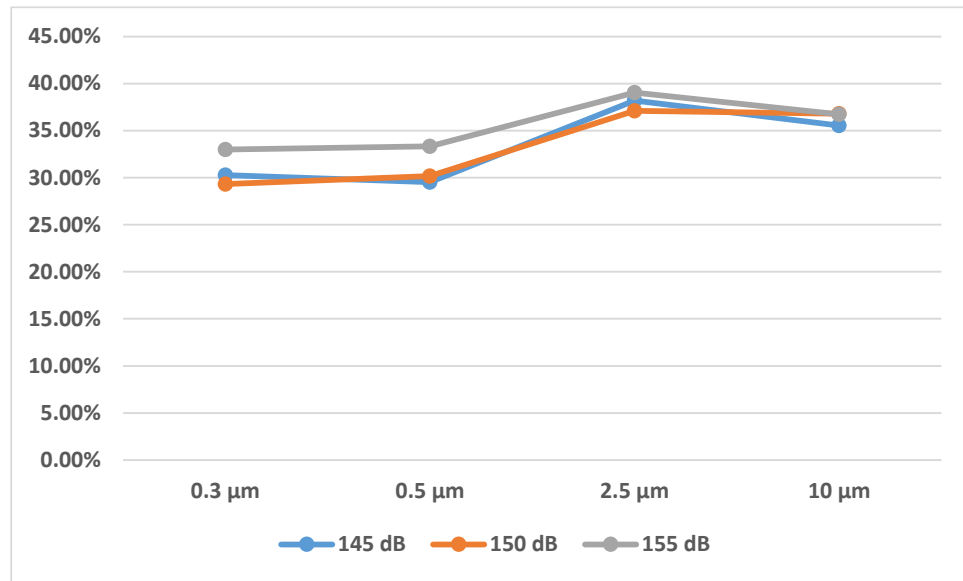


Figure 59 Percentage Reduction of the Three Cases of Sound Intensity

All other variables remained the same as in the base-case.

#### 6.2.2.2 Air Velocity

Large particles gradually moved downwards along the duct as shown in Figure 55. The largest particles, 10  $\mu\text{m}$ , served only as collector particles. Therefore, 10  $\mu\text{m}$  particles were not directly removed by acoustic agglomeration phenomena. These particles either moved towards the lower surface of the duct due to gravity and disappeared or passed through the outlet surface for removal. As the fluid velocity increased, the rate of particles reached the measuring point increased before being deposited on the lower surface of the duct due to gravity.

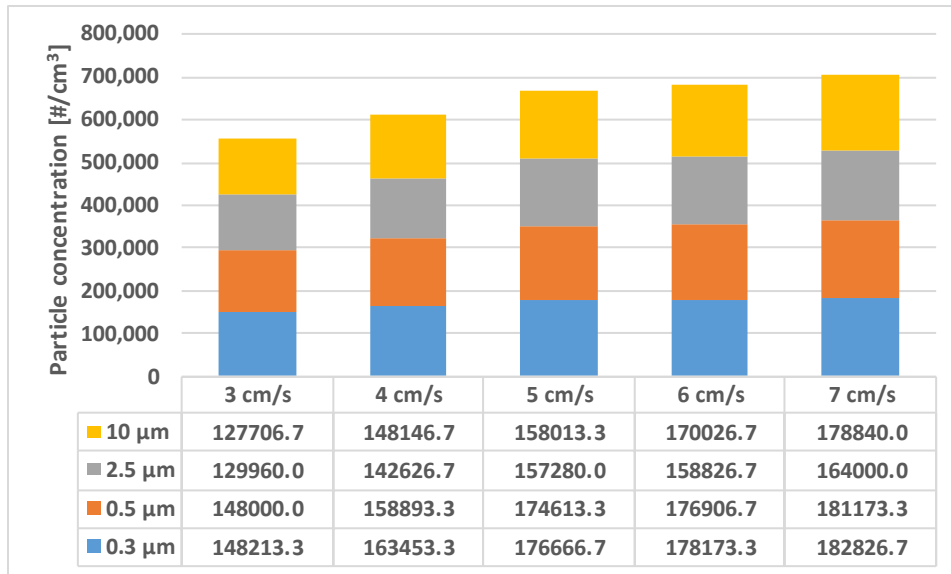


Figure 60 Particle Concentration of the Five Cases of Air Velocity

There was not a significant variation in the removal efficiency of particles targeted for capture during the transition of fluid medium velocity from 5 cm/sec to 7 cm/sec.

As the exposure time of aerosols to ultrasound increases, the removal rate also increases. As the air velocity decreases, there is an overall decrease in the number of particles for all sizes. From Figure 61, as flow velocity decreases, the particle reduction rate increases. In particular, when the flow velocity was 3 cm/sec, the particle removal rate was significantly higher compared to other cases. The removal rates of the 0.3 μm and 0.5 μm particles were approximately 40%, the 2.5 μm particles decreased by 48%, and the 10 μm particles decreased by 49%. About 10% more reduction than 5 cm/sec scenario. Generally, increasing sound intensity increased particle removal rate. Considering that in each case, 300 ml and 500 ml of fluid were processed per second by sound. It can be said that a flow velocity of 5 cm/sec is more advantageous for the reduction of 0.3 μm and 0.5 μm particles for actual particle number reduction. Examining the trends of particle reduction rates at 3 cm/sec, 5 cm/sec, and 7 cm/sec, it cannot be seen as a linear relationship. It is also necessary to establish desirable flow rate settings for efficient particle reduction relative to the amount of treated air.

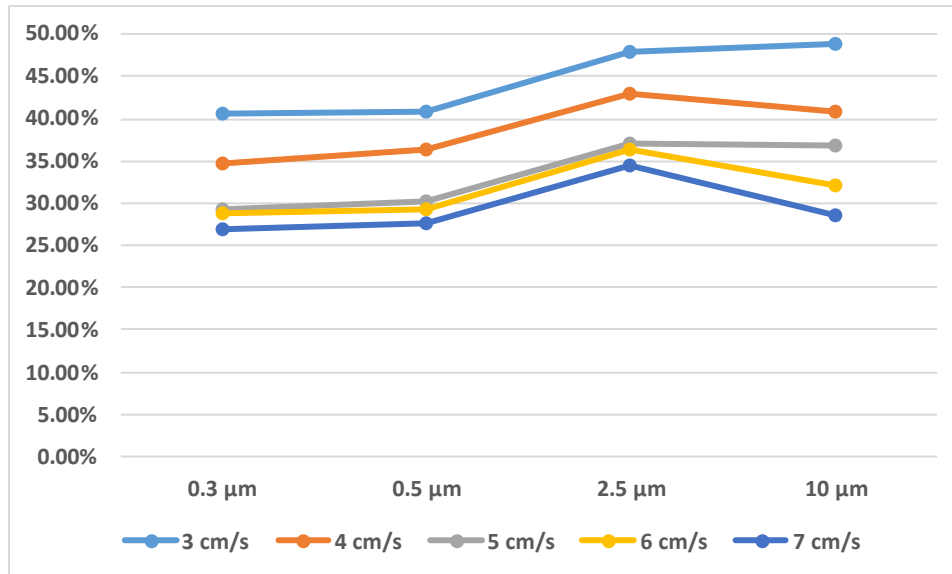


Figure 61 Particle Percentage Reduction of Five Cases with Varying Air Velocity

In the situation with a flow velocity of 7 cm/sec, a notable point is the significant weakening of the reduction rate for 10 μm particles. This can be inferred from the fact that the drag force, which is a factor affecting the movement of particles, play a larger role than gravitational force, allowing more particles to reach the point where the results are derived. This can be seen in Figure 56, where larger particles gradually concentrate in the lower region of the duct while traveling with the fluids.

All other variables remained the same as in the base-case.

### 6.2.2.3 Particle Initial Concentration

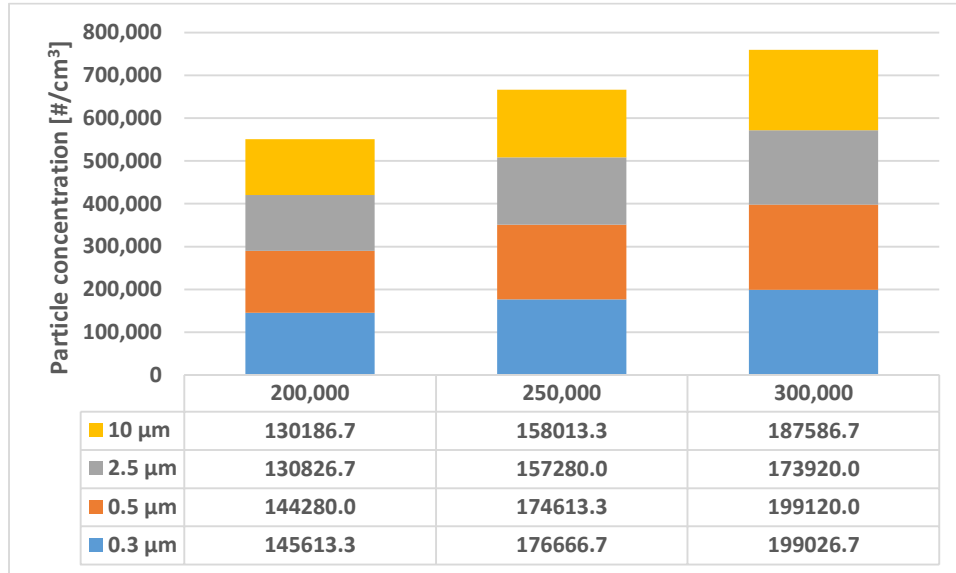


Figure 62 Particle Concentration of the Three Cases of Particle Concentration Variations

At the point of measuring the particle count from simulation results, naturally, the number of particles at the measurement point was greater when there was a larger initial input of particles. However, upon examining the number of particles at the measurement point relative to the input quantity, it is observed that a higher particle concentration at the measurement point leads to a greater removal rate compared to cases where the concentration is lower across all sections, except for 10 μm particles. The reason the removal rate of 10 μm particles is unaffected by the initial particle concentration, unlike other particles, is that these particles function as collector particles. The particles intended to capture 10 μm particles do not exist under simulation conditions and can only be removed solely by gravitational force through deposition, making them inaccessible for removal via the acoustic agglomeration mechanism.

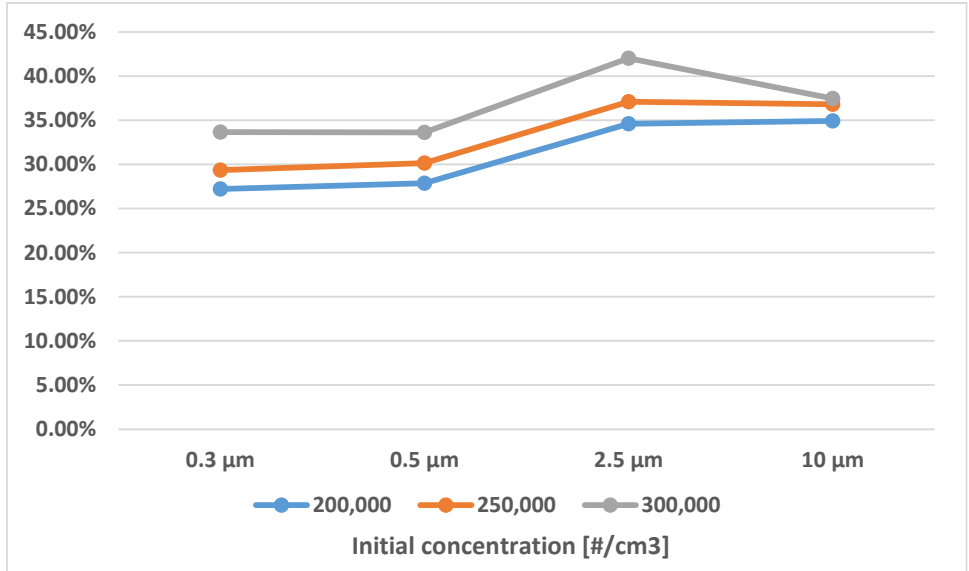


Figure 63 Particle Percentage Reduction of the Three Cases of Particle Concentration

All other variables remained the same as in the base-case.

#### 6.2.2.4 Sound Frequency

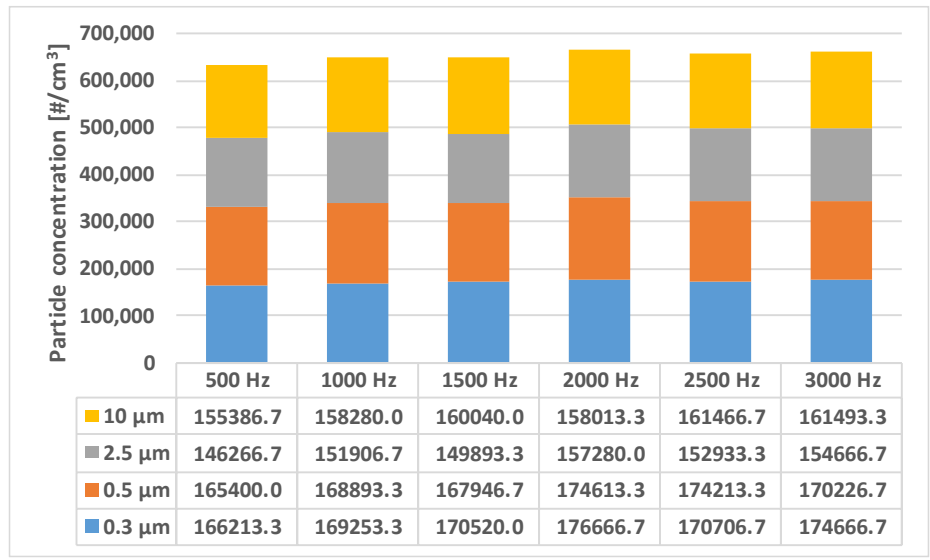


Figure 64 Particle Concentration of the Six Cases of Sound Frequency

No distinct variation in particle count due to the difference in ultrasound frequency could be observed in the chart for particle concentration.

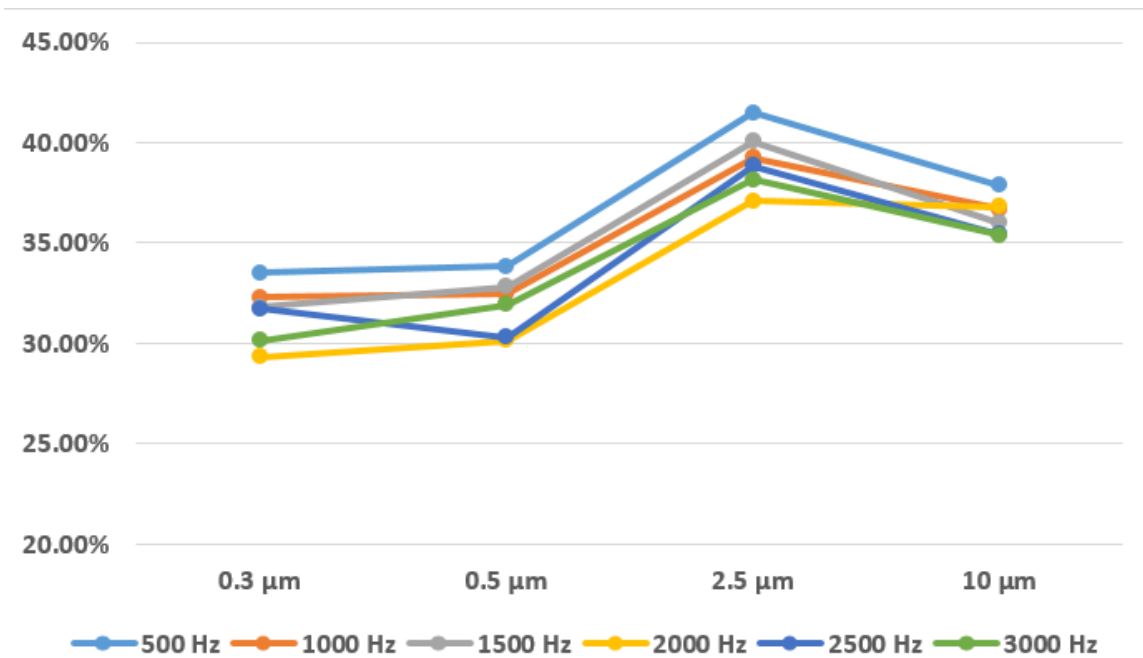


Figure 65 Particle Percentage Reduction of the Six Cases of Sound Frequency

As the sound frequency decreased, it was observed that the removal efficiency of the particles targeted for capture generally increased slightly. In the cases of 2000 Hz, 2500 Hz, and 3000 Hz, there was not a significant difference in the removal efficiency of particles due to the acoustic agglomeration phenomenon. One possible reason is that the increase in the number of vibrations per unit time may also affect particle collisions. For example, at 1 Hz there is one chance of a collision. However, at 2 Hz there are two chances of a collision. Therefore, although the probability of collisions decreases with lower amplitude, the increase in the number of possible intervals for collisions compensates, resulting in similar outcomes.

In theory, the primary cause of the acoustic agglomeration phenomenon is collisions due to the difference in resonant amplitudes, which is caused by variations in entrainment factors between particles. As seen in Figure 54, when the size of particles increases, using low-frequency sounds is necessary to increase the entrainment factor. As the size of particles for

removal increases, it is shown in Figure 54 that using low frequencies is suitable for high entrainment factors. Simultaneously, it is necessary to use lower frequencies that result in a low entrainment factor for the collector particles.

The difference in particle removal rate among cases resulting from variations in sound frequency was approximately up to 3%. This could be speculated as stemming from an insignificant alteration in the entrainment factor among particles with varying sound frequencies, as depicted in Figure 54. Generally, to anticipate acoustic agglomeration phenomena, collector particles should possess a low entrainment factor, while smaller particles should exhibit a higher entrainment factor. This disparity in particle displacement amplitude heightens the probability of collision between them. However, the resonant amplitude of the fluid under sound is higher with lower frequencies compared to higher frequencies. Consequently, to augment the chance of particle collisions, it becomes crucial to maintain meaningful contrast in the entrainment factor between collector and smaller particles, as well as using the lowest feasible sound frequency. This trend is reflected in Figure 65, where the results indicated higher removal rates with the application of 1500 Hz sound compared to the other frequencies—2000 Hz and 2500 Hz.

### 6.3 Summary

A sensitivity analysis was conducted along a duct measuring 10 cm × 10 cm × 40 cm, with mixed air containing particles influenced by a sound source located at the center-top of the duct. The variables considered for the sensitivity test of acoustic agglomeration phenomena were sound intensity, air velocity, particle concentration, and sound frequency. Air velocity was chosen as a variable for analysis to examine the relationship between particle interaction with sound waves and acoustic agglomeration.

After the sensitivity analysis was carried out with the four variables, the following findings were discovered:

- Using high sound intensity resulted in an increase in the particle reduction rate. However, the relationship between reduction rate and sound intensity was not linear, and significant

improvement in particle removal efficiency was observed only with sound intensity levels surpassing a certain threshold.

- A slower fluid flow rate led to an increase in acoustic particle removal rate. Although the volume of fluid processed per unit time decreased with slower flow velocity, a higher absolute number of particles was removed. Similar to sound intensity, a noticeable increase in particle reduction rate was observed when the flow velocity dropped below a specific threshold.
- As the initial particle concentration increased, the particle removal rate also increased. In contrast to the previous two conditions, a linear relationship was found between initial particle concentration and particle reduction rate.
- To select the frequency of the sound waves for acoustic collision, two characteristics - namely the difference in entrainment factor and vibration amplitude - must be considered simultaneously. Sound frequencies with a significant difference in entrainment factors between particles should be used to induce direct collisions. However, the vibration amplitude of the sound waves increased as the frequency decreased. Therefore, it is preferable to use low frequencies.

Commonly observed through sensitivity analysis on all the previously mentioned variables is the fact that removal of collector particles through sound waves is not possible.

## CHAPTER VII

### CONCLUSION

The background, objectives, starting point, the series of processes of the research, as well as the summary and discussion of the contents leading to the results are explored in this chapter.

In both the direct collision model and the acoustic particle collision model, if particle-to-particle collisions occur, the collision can result in agglomeration. The large particles are designed to capture the smaller particles, transforming into larger particles while the smaller particles are removed. In the particle-to-wall collision model, if a particle collides with the wall and sticks to it, it is set to be deleted. Agglomerated particles and particles attached to the wall are excluded from the simulation target, thereby reducing the simulation time cost.

#### 7.1 Summary

Different air filtering strategies have their advantages and disadvantages. To explore the possibility of an alternative to existing air filtering methods, a study on acoustic agglomeration (AA) was initiated. Through a literature review, an understanding of AA was achieved. AA can be defined as a phenomenon occurring during the resonant processes of particles due to the vibration of sound waves. AA mechanisms can be categorized into three types: orthokinetic interaction, primary refilling mechanisms, and secondary refilling mechanisms. These mechanisms all play crucial roles in AA.

Orthokinetic interaction stands out as the most essential mechanism in acoustic agglomeration. It involves direct collisions due to differences in resonant amplitude and phase angle between particles with different inertia. This interaction creates a collision space known as the agglomeration volume, which depends on the inertia of particles and various characteristics of the sound waves.

Refilling mechanisms, both primary and secondary, are mechanisms that shift particles from outside the agglomeration volume into the volume through repeated vibration caused by sound waves. These mechanisms facilitate orthokinetic interaction. Secondary refilling

mechanisms shift particle positions to locations where primary refilling mechanisms can operate, ultimately moving them into the agglomeration volume.

The theoretical study of acoustic agglomeration originated in the late 1800s, when theories based on entrainment factor and orthokinetic interaction were established. Practical research to remove fog obstructing aircraft and battleship movements began during World War II. It then continued as a means of purifying contaminated air in factories. Over time, efforts focused on enhancing particle removal efficiency through acoustic agglomeration.

Recently, significant interest has arisen in numerical research for interpreting acoustic agglomeration. Many studies using numerical methods have concentrated on small-scale acoustic agglomeration. However, substantial computation time is required for numerical interpretation of acoustic agglomeration.

Therefore, this study aimed to develop a tool for interpreting the acoustic agglomeration phenomenon by excluding ancillary factors and focusing solely on its key mechanism, orthokinetic interaction, in a relatively large space with numerous particles. Specifically, a tool using Computational Fluid Dynamics (CFD) was created for interpreting acoustic agglomeration; the particle collision analysis requires extensive simulation time.

The developed OpenFoam CFD model, pimAAFoam, comprises acoustic collision, general collision, and wall collision models. The acoustic collision model translates the principle of orthokinetic interaction, the core principle of the acoustic agglomeration phenomenon, into the CFD simulation model, pimAAFoam. It calculates the region of the virtual agglomeration volume formed due to the relationship between sound waves and particles to determine collisions. Subsequently, the result is determined as agglomeration or rebound based on the concept of critical velocity.

The general collision model compares collision velocity with critical velocity to distinguish between agglomeration and rebound when collisions occur between particles due to drag, gravity, lift force, etc. Similarly, the wall collision model compares collision velocity with critical velocity to determine agglomeration or rebound when particles collide with walls.

The pimAAFoam prototype model was developed based on the aforementioned setup. Model validations were conducted by comparing the simulation results generated using the prototype model with the experimental values obtained from two different experimental setups.

The first validation was performed through mixed air injection in a straight vertical cylinder, as discussed in the literature. The simulation results derived from the prototype model showed differences from the actual measured values. Therefore, a prototype model calibration process was carried out to obtain results closer to the actual measurements.

The second validation of pimAAFoam was conducted through mixed air injection in a straight horizontal duct test which was conducted in this study. The simulation values obtained through the calibrated model showed differences from the average measured values in the experiments. However, they fell within the range of the measured values. Additionally, the influence of each collision model on particle reduction under different experimental conditions was analyzed. Under the given experimental conditions, general collision and acoustic collision had more of an impact than wall collision on particle reduction.

Based on the two processes of model validation, it can be concluded that the OpenFOAM acoustic agglomeration model, pimAAFoam, has been proven valid. Using the validated OpenFOAM acoustic model, pimAAFoam, a sensitivity analysis was conducted. The variables related to acoustic agglomeration mechanisms included in the sensitivity analysis were as follows:

- Sound intensity
- Air velocity
- Particle initial concentration
- Sound frequency

It was found that sound intensity and initial particle concentration have a positive impact on particle removal through acoustic agglomeration. As air velocity decreased, the particle removal rate increased. Regarding sound frequency, using a lower frequency was found to be helpful for particle removal through acoustic agglomeration as long as the frequency did not produce significant changes in the entrainment factor difference between particles.

Regarding the role of the collector particle, the removal of large particles using acoustic agglomeration mechanisms was not suitable.

## 7.2 Discussion

Generally, CFD simulation requires higher simulation time costs compared to other simulations such as, building energy simulation or simulations for architectural structures. Moreover, analyzing the acoustic agglomeration phenomenon through CFD simulation demands significant simulation time costs. Therefore, when analyzing acoustic agglomeration through numerical methods, the scale of analysis, as presented in Kacianauskas et al. (2018) and Zhang et al. (2018), is often limited.

In this research, an OpenFOAM acoustic agglomeration model, pimAAFoam, was developed to analyze the acoustic agglomeration phenomenon for relatively larger scales as follows:

Simulation domain:  $10 \times 10 \times 40$  cm,

Particle initial concentration:  $1,000,000/\text{cm}^3$ .

Particles per parcel: 40,000

These conditions were used as the base-case for the sensitivity analysis. To analyze particle collision and agglomeration for 30 seconds, approximately four days of simulation time cost were required using a 6-cores, 3.7 GHz CPU. Through the model validation process, pimAAFoam has achieved reliability and offers practical simulation time costs compared to previous acoustic agglomeration analyses using numerical methods.

This study focused on the practicality of the model and excluded the application of primary and secondary refilling mechanisms. Therefore, future work will need to further develop an OpenFOAM acoustic agglomeration model that includes refilling mechanisms.

## Nomenclature

$A$	hamaker constant [J]
$A_p$	particle displacement [m]
$A_g$	fluid displacement [m]
$c$	sound velocity [ $m \text{ sec}^{-1}$ ]
$d_p$	diameter of the particle [m]
$e$	energetic restitution coefficient
$f$	frequency of sound [ $\text{sec}^{-1}$ ]
$K$	effective stokes number
$K_a$	acoustic agglomeration kernel [ $\text{sec}^{-1}$ ]
$K_{a1}$	acoustic agglomeration kernel depends on large particles [ $m^3 \text{ sec}^{-1}$ ]
$L_{AW}$	acoustic wake length [m]
$n$	particle concentration [ $m^{-3}$ ]
$P_{pl}$	material limiting contact pressure [Pa]
$\Delta P$	pressure variance at target location [Pa]
$r$	radius of particle [m]
SPL	sound pressure level [dB]
$t$	time [sec]
$u_{cr}$	critical velocity [ $m \text{ sec}^{-1}$ ]
$U_p$	particle velocity [ $m \text{ sec}^{-1}$ ]
$U_g$	acoustic velocity amplitude [ $m \text{ sec}^{-1}$ ]
$U_0$	initial velocity [ $m \text{ sec}^{-1}$ ]
$V$	volume of particle [ $m^3$ ]
$X$	distance [meter]
$z_0$	contact distance [m]
$\alpha$	refill factor
$\delta$	particle number in the parcel
$\varepsilon$	capture coefficient

$\eta$	dynamic viscosity of the fluid medium [ $kg\ m^{-1}sec^{-1}$ ]
$\varphi$	speaker sensitivity [ $dB\ watt^{-1}m^{-1}$ ]
$\mu_p$	particle entrainment factor
$\mu_{12}$	maximum relative entrainment factor of a pair of particles
$\mu_g$	degree of flow around the particle
$\nu$	collision frequency [ $sec^{-1}$ ]
$v_{ij}$	volume of the cell [ $m^3$ ]
$\rho_f$	density of fluid [ $kg\ m^{-3}$ ]
$\rho_p$	density of particle [ $kg\ m^{-3}$ ]
$\sigma$	surface tension coefficient [ $N\ m^{-1}$ ]
$\tau$	relaxation time [sec]
$\omega$	angular velocity [ $rad\ sec^{-1}$ ]

#### Subscripts

0	initial conditions
1	large particles
2	small particles

## REFERENCES

- Amy, E. V. (1934). U.S. Patent No. 1,980,171. Washington, DC: U.S. Patent and Trademark Office.
- Andrade, E. N. D. C. (1932). On the groupings and general behaviour of solid particles under the influence of air vibrations in tubes. *Philosophical Transactions of the Royal Society of London. Series A, Containing Papers of a Mathematical or Physical Character*, 230(681-693), 413-445.
- Andrade, E. D. C. (1936). The coagulation of smoke by supersonic vibrations. *Transactions of the Faraday Society*, 32, 1111-1115.
- ANSYS-Fluent. (2020). *Ansyst fluent user's guide*.
- Ariman, T., Ojalvo, M. S., & Drehmel, D. C. (1979). Novel concepts, methods and advanced technology in particulate/gas separation. *Journal of the Air Pollution Control Association*, 29(8), 818-822.
- Ariyaratne, W. H., Manjula, E. V. P. J., Ratnayake, C., & Melaaen, M. C. (2016, September). CFD approaches for modeling gas-solids multiphase flows—A review. In *9th EUROSIM & the 57th SIMS Conference, Oulu* (pp. 680-686).
- Barreras, F., Amaveda, H., & Lozano, A. (2002). Transient high-frequency ultrasonic water atomization. *Experiments in Fluids*, 33(3), 405-413.
- Brandt, O., Freund, H., & Hiedemann, E. (1936). Zur theorie der akustischen koagulation. *Kolloid-Zeitschrift*, 77, 103-115.
- Carley, M. (2001). *Some notes on acoustics*. University of Bath, UK.
- CD-adapco, S. (2017). *STAR CCM+ user guide version 12.04*. CD-Adapco: New York, NY, USA.
- Cheng, Y. S., Bechtold, W. E., Yu, C. C., & Hung, I. F. (1995). Incense smoke: characterization and dynamics in indoor environments. *Aerosol Science and Technology*, 23(3), 271-281.
- Chou, K. H., Lee, P. S., & Shaw, D. T. (1981). Aerosol agglomeration in high-intensity acoustic fields. *Journal of Colloid and Interface Science*, 83(2), 335-353.
- Clair, H. W. S. (1949). Agglomeration of smoke, fog, or dust particles by sonic waves. *Industrial & Engineering Chemistry*, 41(11), 2434-2438.

- Cohen, R., Sexton, K. G., & Yeatts, K. B. (2013). Hazard assessment of United Arab Emirates (UAE) incense smoke. *Science of the total environment*, 458, 176-186.
- Cundall, P. A., & Strack, O. D. (1979). A discrete numerical model for granular assemblies. *geotechnique*, 29(1), 47-65.
- Dianov, D. B., PODOLSKI, AA, & Turubarov, V. I. (1968). Calculation of hydrodynamic interaction of aerosol particles in a sound field under Oseen flow conditions. *Soviet Physics Acoustics-USSR*, 13(3), 314-+
- Dockery, D. W., Pope, C. A., Xu, X., Spengler, J. D., Ware, J. H., Fay, M. E., ... & Speizer, F. E. (1993). An association between air pollution and mortality in six US cities. *New England journal of medicine*, 329(24), 1753-1759.
- Dong, S., Lipkens, B., & Cameron, T. M. (2006). The effects of orthokinetic collision, acoustic wake, and gravity on acoustic agglomeration of polydisperse aerosols. *Journal of aerosol science*, 37(4), 540-553.
- Eargle, J. (2003). *Loudspeaker handbook*. Springer Science & Business Media.
- Englert, N. (2004). Fine particles and human health-a review of epidemiological studies. *Toxicology letters*, 149(1-3), 235-242.
- Flamm, R. (2017). *Acoustics in OpenFoam*. Brigham Young University-Idaho.
- Fluent, A. N. S. Y. S. (2020). *Ansys fluent theory guide*. Ansys Inc.
- Gor'kov, L. P. (1961). Forces acting on a small particle in an acoustic field within an ideal fluid. In *Doklady Akademii Nauk* (Vol. 140, No. 1, pp. 88-91). Russian Academy of Sciences.
- Hegarty, R. F., & Shannon, L. J. (1976). *Evaluation of Sonics for Fine Particle Control*. US Environmental Protection Agency, Industrial Environmental Research Laboratory.
- Ho, C. A., & Sommerfeld, M. (2002). Modelling of micro-particle agglomeration in turbulent flows. *Chemical Engineering Science*, 57(15), 3073-3084.
- Hoffmann, T. L. (1997). An extended kernel for acoustic agglomeration simulation based on the acoustic wake effect. *Journal of Aerosol Science*, 28(6), 919-936.
- Hosseini, S. M., & Sahebi, S. (2023). Evaluation of effective operation parameter on High Efficiency
- Israelachvili, J.N. (2011). Chapter 13 – Van der Waals Forces between Particles and Surfaces.

- Imani, R. J., & Robert, E. (2018). Estimation of acoustic forces on submicron aerosol particles in a standing wave field. *Aerosol Science and Technology*, 52(1), 57-68.
- Ji, X., Le Bihan, O., Ramalho, O., Mandin, C., D'Anna, B., Martinon, L., ... & Pairon, J. C. (2010). Characterization of particles emitted by incense burning in an experimental house. *Indoor Air*, 20(2), 147-158.
- Kačianauskas, R., Rimša, V., Kačeniauskas, A., Maknickas, A., Vainorius, D., & Pacevič, R. (2018). Comparative DEM-CFD study of binary interaction and acoustic agglomeration of aerosol microparticles at low frequencies. *Chemical Engineering Research and Design*, 136, 548-563.
- Kasper, R. (2017). Particle simulation with OpenFOAM® introduction, fundamentals and applications.
- King, L. V. (1934). On the acoustic radiation pressure on spheres. *Proceedings of the Royal Society of London. Series A-Mathematical and Physical Sciences*, 147(861), 212-240.
- König, W. (1891). Hydrodynamisch-akustische Untersuchungen. *Annalen der Physik*, 279(5), 43-60.
- Langmuir, I. (1948). The production of rain by a chain reaction in cumulus clouds at temperatures above freezing. *Journal of the Atmospheric Sciences*, 5(5), 175-192.
- Liu, J., Wang, J., Zhang, G., Zhou, J., & Cen, K. (2011). Frequency comparative study of coal-fired fly ash acoustic agglomeration. *Journal of Environmental Sciences*, 23(11), 1845-1851.
- Lu, M., Fang, M., He, M., Liu, S., & Luo, Z. (2019). Insights into agglomeration and separation of fly-ash particles in a sound wave field. *RSC advances*, 9(9), 5224-5233.
- Mandralis, Z. I., & Feke, D. L. (1993). Continuous suspension fractionation using acoustic and divided-flow fields. *Chemical engineering science*, 48(23), 3897-3905.
- Magill, J., Pickering, S., Fourcaudot, S., Gallego-Juarez, J. A., de Sarabia, E. R. F., & Rodriguez-Corral, G. (1989). Acoustic aerosol scavenging. *Journal of nuclear materials*, 166(1-2), 208-213.
- Mednikov, E. P. (1965). Acoustic Coagulation and Precipitation of Aerosols/Akusticheskaya Koagulyatsiya I Osazhdenie Aerozolei/Акустическая Коагуляция И Осаждение Аэрозолей. Springer.

Mizuno, A. (2000). Electrostatic precipitation. *IEEE Transactions on Dielectrics and Electrical Insulation*, 7(5), 615-624.

Montgomery, J. F., Green, S. I., Rogak, S. N., & Bartlett, K. (2012). Predicting the energy use and operation cost of HVAC air filters. *Energy and Buildings*, 47, 643-650.

Nassif, N. (2012, December). The impact of air filter pressure drop on the performance of typical air-conditioning systems. In *Building Simulation* (Vol. 5, pp. 345-350). Tsinghua Press.

Noorpoor, A. R., Sadighzadeh, A., & Habibnejad, H. (2013). Influence of acoustic waves on deposition and coagulation of fine particles.

OpenCFD Ltd., URL: <http://openfoam.com/>.

O'ROURKE, P. J. (1981). Collective drop effects on vaporizing liquid sprays (Doctoral dissertation, Princeton University).

Paiva, J., Salcedo, R., & Araujo, P. (2010). Impact of particle agglomeration in cyclones. *Chemical Engineering Journal*, 162(3), 861-876.

Parker, R. C. (1936). Experiments on coagulation by supersonic vibrations. *Transactions of the Faraday Society*, 32, 1115-1119.

Peng, R. D., Chang, H. H., Bell, M. L., McDermott, A., Zeger, S. L., Samet, J. M., & Dominici, F. (2008). Coarse particulate matter air pollution and hospital admissions for cardiovascular and respiratory diseases among Medicare patients. *Jama*, 299(18), 2172-2179.

Pethig, R., & Markx, G. H. (1997). Applications of dielectrophoresis in biotechnology. *Trends in biotechnology*, 15(10), 426-432.

Rahimi, M., Movahedirad, S., & Shahhosseini, S. (2017). CFD study of the flow pattern in an ultrasonic horn reactor: Introducing a realistic vibrating boundary condition. *Ultrasonics sonochemistry*, 35, 359-374.

de Sarabia, E. R. F., Elvira-Segura, L., Gonzalez-Gomez, I., Rodriguez-Maroto, J. J., Munoz-Bueno, R., & Dorronsoro-Areal, J. L. (2003). Investigation of the influence of humidity on the ultrasonic agglomeration of submicron particles in diesel exhausts. *Ultrasonics*, 41(4), 277-281.

Schmidt, D. P., Nouar, I., Senecal, P. K., Rutland, J., Martin, J. K., Reitz, R. D., & Hoffman, J. A. (1999). Pressure-swirl atomization in the near field. *SAE transactions*, 471-484.

Schraufnagel, D. E. (2020). The health effects of ultrafine particles. *Experimental & molecular medicine*, 52(3), 311-317.

- Shang, X., Ng, B. F., Wan, M. P., Xiong, J., & Arikrishnan, S. (2018). Numerical investigation of spatially nonhomogeneous acoustic agglomeration using sectional algorithm. *Aerosol Science and Technology*, 52(8), 872-885.
- Shaw, D. T. (Ed.). (1978). *Recent developments in aerosol science*. John Wiley & Sons.
- Shaw, D. T., & Tu, K. W. (1979). Acoustic particle agglomeration due to hydrodynamic interaction between monodisperse aerosols. *Journal of Aerosol Science*, 10(3), 317-328.
- Shi, Y., Wei, J., Bai, W., & Wang, G. (2020). Numerical investigations of acoustic agglomeration of liquid droplet using a coupled CFD-DEM model. *Advanced Powder Technology*, 31(6), 2394-2411.
- Shi, Y., Wei, J., Qiu, J., Chu, H., Bai, W., & Wang, G. (2020). Numerical study of acoustic agglomeration process of droplet aerosol using a three-dimensional CFD-DEM coupled model. *Powder Technology*, 362, 37-53.
- Sinclair, D. (1950). *Stability of aerosols and behavior of aerosol particles*. Handbook on Aerosols: Chapters from the Summary Technical Report of Division 10, National Defense Research Committee, 64.
- Song, L. (1990). *Modeling of acoustic agglomeration of fine aerosol particles*. The Pennsylvania State University.
- Tiwary, R., & Reethof, G. (1987). Numerical simulation of acoustic agglomeration and experimental verification.
- Tsuji, Y., Tanaka, T., & Ishida, T. (1992). Lagrangian numerical simulation of plug flow of cohesionless particles in a horizontal pipe. *Powder technology*, 71(3), 239-250.
- Thomas, D., Penicot, P., Contal, P., Leclerc, D., & Vendel, J. (2001). Clogging of fibrous filters by solid aerosol particles experimental and modelling study. *Chemical Engineering Science*, 56(11), 3549-3561.
- Vu, T. V., Ondracek, J., Zdimal, V., Schwarz, J., Delgado-Saborit, J. M., & Harrison, R. M. (2017). Physical properties and lung deposition of particles emitted from five major indoor sources. *Air Quality, Atmosphere & Health*, 10(1), 1-14.
- Westervelt, P. J. (1951). The theory of steady forces caused by sound waves. *The Journal of the Acoustical Society of America*, 23(3), 312-315.

- Wood, R. W., & Loomis, A. L. (1927). XXXVIII. The physical and biological effects of high-frequency sound-waves of great intensity. *The London, Edinburgh, and Dublin philosophical magazine and journal of science*, 4(22), 417-436.
- Xiang, L., Shuyan, W., Huilin, L., Goudong, L., Juhui, C., & Yikun, L. (2010). Numerical simulation of particle motion in vibrated fluidized beds. *Powder Technology*, 197(1-2), 25-35.
- Yan, J., Chen, L., & Yang, L. (2016). Combined effect of acoustic agglomeration and vapor condensation on fine particles removal. *Chemical Engineering Journal*, 290, 319-327.
- Yosioka, K., & Kawasima, Y. (1955). Acoustic radiation pressure on a compressible sphere. *Acta Acustica united with Acustica*, 5(3), 167-173.
- Yuen, W. T., Fu, S. C., Kwan, J. K., & Chao, C. Y. (2014). The use of nonlinear acoustics as an energy-efficient technique for aerosol removal. *Aerosol Science and Technology*, 48(9), 907-915.
- Zhang, G., Zhang, L., Wang, J., & Hu, E. (2017). Improving acoustic agglomeration efficiency by addition of sprayed liquid droplets. *Powder Technology*, 317, 181-188.
- Zhang, G., Zhang, L., Wang, J., & Chi, Z. (2018). A new model for the acoustic wake effect in aerosol acoustic agglomeration processes. *Applied Mathematical Modelling*, 61, 124-140.
- Zhou, D., Luo, Z., Jiang, J., Chen, H., Lu, M., & Fang, M. (2016). Experimental study on improving the efficiency of dust removers by using acoustic agglomeration as pretreatment. *Powder Technology*, 289, 52-59.